Clemson University

Biomaterials Day

"Bionanotechnology: Integrating Nanostructures into Biomaterials"

September 28-29, 2012
Madren Conference Center
Clemson, SC

Program Chair Anthony Guiseppi-Elie, Sc.D.

Organizer Frank Alexis, Ph.D.

Sponsors Society For Biomaterials and CU Bioengineering Department

Clemson's Society For Biomaterials

Biomaterials Day 2012 Program

Saturday, September 29, 2012

8:00 AM	Registration/Breakfast
8:30 AM	Keynote Speaker 1: Joel D. Bumgardner, University of Memphis, President of the Society For Biomaterials
9:00 AM	Christopher Bettinger, Carnegie Mellon
9: 15AM	Elizabeth Perpall, Clemson University Research Foundation
9:30 AM	Andrew Cannon, Hoowaki LLC
09:45AM	Joel Corbett, Poly-Med Inc
10:00AM	David Huizenga, Tao Life Sciences Inc
10:15AM	Break
10:45 AM	Michael Gara, Coulter Foundation
11:00 AM	Katina Dorton, RTP Capital Associates Inc
11:15AM	Robert L. Crutchfield, Harbert Venture Partners
11:30AM	Gregory F. Zaic, Nexus
11:45AM	Greg Hillman, SC Launch
12:00 PM	Lunch/Poster Session
2:00 PM	Keynote Speaker 2: Kazuhiko Ishihara, University of Tokyo, President of the Japanese Society for Biomaterials
2:30 PM	Undergraduate student oral presentations: S. Cole, C. Duncan, A. Farley
3:15PM	Graduate student oral presentations: O. Karunwi, G. Hilas, T. Moore
4:00 PM	Break
4:15 PM	Technology Panel Discussion
4:45 PM	Awards
5:00 PM	Adjourn

Program Chair

Anthony Guiseppi-Elie, Sc.D.
President and Scientific Director

ABTECH Scientific, Inc.

Title: An Implantable Microsystem to Change Highway Trauma Outcomes

Abstract: Trauma associated hemorrhage is the number 1 killer of persons < 50 yrs. old, is implicated in ca. 60% of battlefield deaths, and is the 5th leading cause of death overall in the US. More "work years" are lost to trauma than to cancer and heart disease combined. Trauma exerts a >$406 billion annual cost in medical care and lost productivity on the US economy. During the "golden hour" there is an abject scarcity of potentially life-saving physiologic data. There is need to initiate immediate and continuous monitoring of molecular indicators of global physiologic stress. The current state of efficacy of trauma diagnostics concerning hemorrhage and hemorrhagic shock suggests the need for monitoring of metabolic biomarkers. Base deficit has been predicative of injury severity at hospital admission. Tissue oxygen saturation has been predicative of the onset of multiple organ dysfunction syndrome. Blood potassium levels increase with onset of hemorrhagic shock. Lactate is a surrogate for tissue hypoxia and its clearance predicts mortality. Insulin resistance and attendant triage glucose measurements have been shown to be specific in predicting major injuries. On the other hand, no gross vital sign has yet to be proven effective as an independent predictor of trauma severity. Armed with an IP portfolio, an experienced management team, ABTECH is developing a fully integrated point-of-care (POC) analytical microsystem for rapid implantation into a major muscle by first responders. The system will achieve rapid, continual monitoring of glucose and lactate via dual responsive amperometric enzyme biosensors and will be expanded to include tissue acidosis via impedimetry and VO2 via voltammetry. Multi-analyte monitoring biosensors have the potential to explore areas still unexplored in the realm of trauma physiology.

Bioprofile: Anthony Guiseppi-Elie is Professor of Chemical and Biomolecular Engineering, Bioengineering, and Electrical and Computer Engineering. He is also Director of the Center for Bioelectronics, Biosensors and Biochips at Clemson University. He is Founder and Scientific Director of ABTECH Scientific, Inc., a near-patient biomedical diagnostics company. He holds the Sc.D. in materials science and engineering from MIT, the M.Sc. in chemical engineering from the University of Manchester Institute of Science and Technology (UMIST) and the B.Sc. (First Class Honors) with majors in Analytical and Applied Chemistry from the University of the West Indies (UWI). He has spent 15 years in industrial research and product development before becoming a full professor of Chemical and Life Science Engineering and of Emergency Medicine at VCU-MCV in 1998. His research interests are in engineered bioanalytical microsystems in the service of human health and medicine. He has published over 120 archival papers (2369 citations, h-factor = 26), 31 book or proceedings chapters, holds 8 patents, has given > 200 invited lectures/colloquia, and has co-organized and lead 30 national and international scientific workshops, symposia and conferences. He is an Associate Editor of Biomedical Microdevices and a member of the editorial boards of The Journal of Bioactive and Compatible Polymers, NanoBiotechnology, Applied Biochemistry and Biotechnology. Dr. Guiseppi is a Fellow of AIMBE, senior member of IEEE, a lifetime Member of AIChE and holds memberships in RSC, AAAS, ACS, MRS and BMES. At Clemson University Prof. Guiseppi teaches engineering materials, biological transport phenomena, biomolecular engineering, biosensors and bioelectronics, and nanobiotechnology.

Program Organizer

Frank Alexis, Ph.D.
Assistant Professor of Bioengineering

Laboratory of Nanomedicine

Clemson University

Abstract: Nanomedicine can provide an opportunity for improved drug development because early clinical phases often cast light on multiple side effects limiting the drug's therapeutic dose. In addition, a sharp increase over the past few years in the number of patent applications and high impact factor publications in this area highlights the level of interest in nanomedicine by both academic and industry investigators. In 2009, the NNI budget of $1.5 billion was allocated to multiple funding agencies reflecting a steady growth in addition to the $8 billion invested since 2001. To develop a common direction in the fight against cancer, the National Cancer Institute (NCI) showed a clear commitment to nanomedicine with the recent allocation of $144 million. This initiative was established with clear objectives to form academic and commercial partnerships, establish outstanding training programs, leverage additional funds, and reduce the risk of investment in new products (http://nano.cancer.gov/).

Current therapies and diagnostic systems are still lacking in precision, efficacy, sensitivity and safety. A large percentage of drug candidates (50-80%) developed by the pharmaceutical industry fail during clinical trials. In addition, efficacies of many drugs that are being approved for therapy are still limited for certain diseases leaving ample room for improvements using new technologies. Generally, therapeutic drugs have to be administered in high dose regimens because of short half-life, thereby increasing the systemic toxic side effects. Drug's physico-chemical properties such as solubility, charge, molecular size, and stability affect their systemic pharmacokinetics. In general, nanocarriers deliver drugs in the optimum dosage, increase drug's bioavailability, enhance drug's efficacy, improve patient compliance, and allow the use of drugs with a broad range of physico-chemical properties.

Bioprofile: Frank Alexis is Assistant Professor of Bioengineering and principal investigator of the Laboratory of Nanomedicine at Clemson University. He holds the Ph.D. in materials science and engineering from Nanyang Technological University in Singapore, the M.Sc. in materials science and engineering from the Technological University of Montpellier in France and the B.Sc. in chemistry from the Technological University of Montpellier in France. His research interests are in drug delivery technologies. As a postdoctoral fellow at the Brigham and Women's Hospital in the laboratory of Dr Omid Farokhzad and Research Affiliate at the Massachusetts Institute of Technology from 2006 to 2009 in the laboratory of Prof. Robert Langer, he developed multiple nanoparticle technologies. From these experiences during as postdoctoral fellow, he licensed 8 patents to BIND Biosciences and SELECTA Biosciences, both start-up companies developing nanoparticles for cancer and vaccine applications, respectively.

Keynote Speakers

Joel D Bumgardner, Ph.D.

President of the Society for Biomaterials

Professor of Biomedical Engineering, University of Memphis

Kazuhiko Ishihara, Ph.D.

Professor, Materials Engineering and Bioengineering

The University of Tokyo

Joel D Bumgardner, Ph.D.

President of the Society for Biomaterials

Professor of Biomedical Engineering, University of Memphis

Title: From Ni alloys to Chitosan – Adventures in Dental Materials

Abstract: Oral health has been cited as a major indicator of overall health and well-being. Much of my research and professional career has focused on dental materials used in crown, bridge and implant applications as well as in tissue engineering and drug delivery. Crown and bridge alloys are among the most successful biomaterials and dental implants have rapidly evolved to become an almost common place standard of care. Yet, issues still remain regarding corrosion and hypersensitivity reactions to dental casting alloys and much research is still directed towards rapid and long term maintenance of dental implant osseointegration especially in at-risk patient groups such as diabetics. Collaborations, networking and desire to promote biomaterials have contributed both to my research efforts and to shape my professional career. The impact of these interactions will be highlighted with respect to my own personal career and on-going professional development.

Biographic profile: Dr. Joel D. Bumgardner is a biomaterials researcher in the areas of dental materials, implant surface coatings and bone tissue engineering and local drug delivery systems. He is a Professor in the Biomedical Engineering Department at the University of Memphis and holds joint appointments in the School of Dentistry and School of Medicine at the University of Tennessee Health Science Center. A graduate of Florida State University (1984, B.S. with Honors, Biology) and The University of Alabama at Birmingham (1988, B.S., Materials Engineering; 1989 M.S. and 1994 Ph.D., Biomedical Engineering), Joel completed a J.W. Fulbright Fellowship (1993-1994) at the University of Umeå, Umeå, Sweden before joining the faculty at Mississippi State University in 1994. While at MS State, he was instrumental in developing many graduate and under graduate engineering programs including a Materials Engineering Certificate and a study abroad program as well as being recognized for research on chitosan materials and coatings. In 2004, Joel moved to the University of Memphis where he has been instrumental in efforts launching the undergraduate biomedical engineering degree program and has subsequently become co-director of both undergraduate and graduate academic programs in the Department of Biomedical Engineering. Joel has had over 200 presentations and invited talks on dental alloys, implants, and chitosan materials and including chitosan materials for coatings, drug delivery and bone tissue engineering applications. He is inventor/co-inventor of record on two patents and three patent applications; one patent has been licensed to a start-up company. Joel has authored over 88 peer reviewed journal articles and book chapters on dental and orthopaedic alloys, biocompatibility testing, and chitosan materials. Many of the students Joel has supervised in research have received NSF graduate research, MD/PhD fellowships and or JW Fulbright Fellowships. He is an Associate Editor for the *Journal of Biomedical Materials Research Part B (JBMR-B)*, served as co-editor of the special issue of the *Journal* on Dental & Craniofacial Materials as well as reviewer and editorial board member for many biomaterials related journals He is also regular reviewer on US National Science Foundation and National Institutes of Health panels. Joel has been a long time member of the Society for Biomaterials where as a student; he was instrumental in starting the SFB student chapters. He has held numerous leadership positions in the Society including currently serving as the 2013-2014 President of the society. He was elected as a Fellow to the American Institute for Medical and Biological Engineering in 2012.

Kazuhiko Ishihara, Ph.D.

Professor, Materials Engineering and Bioengineering

The University of Tokyo

Title: Bioinspired Phospholipid Polymers for Nanobiodevices

Abstract: Modern bioengineering requires high performance biomaterials. A special concept, introduced by our group, for preparing advanced biomaterials, "PC-polymer Surface Technology (PCST)", is one which uses phospholipids and phospholipid polymer assembly technology. Using PCST, the surface of synthetic biomaterials converts to "artificial cell membrane" surface. This new technology serves as a bridge to connect the biological field with materials engineering. PCST provides a new route for making polymer biomaterials that have good stability, processability and wide applicability and uses a methacrylate monomer with a phosphorylcholine group, 2-methacryloyloxyethyl phosphorylcholine (MPC). MPC was synthesized and purified and a sufficient amount with excellent purity could be obtained. Thus, it became possible to prepare the MPC polymer and co-polymers and their functionality was carefully evaluated. The MPC polymers are useful not only for artificial organs but also nanodevices and cell-engineering devices due to their excellent properties, for example, the biocompatibility even *in vivo* and in surface lubrication action. Among the various applications recently pursued have been; i) highly sensitive bioimaging fluorescence probe; polymer nanoparticles with embedded quantum dots were covered with an artificial cell membrane with immobilized oligopeptide as a bioaffinity moiety on the surface of the nanoparticles. ii) Biomimetic polymer nanoparticles using amphiphilic phospholipid polymer (PMBN) and water-insoluble polymers such as poly(L-lactic acid) (PLA) and polystyrene (PS) as a core material. The PMBN/PLA/QD immobilized with octaarginine (R8) was used as a model to investigate cell membrane permeation. The transfer of R8-immobilized PMBN/PLA/QD (R8-PMBN/PLA/QD) into the HeLa cells was assessed by confocal microscopy. Cytotoxicity of PMBN/PLA/QD was also evaluated. Thus we achieve preparation of polymer encapsulated QDs with excellent water-dispersion, biocompatibility and cell specificity.

Biographic profile: Dr. Kazuhiko Ishihara is Professor in the Department of Materials Engineering and Department of Bioengineering in the School of Engineering at The University of Tokyo. He received his Ph.D. in Applied Chemistry in 1984 from Waseda University, Tokyo, Japan. He has been a Research Fellow at the Sagami Chemical Research Center (1984-1986) and a Research Associate in the Institute for Medical and Dental Engineering at Tokyo Medical and Dental University (1987-1990). Prof Ishihara's research interests are in polymeric biomaterials, cell and material interactions, blood/biocompatibility of materials, tissue engineering, hydrogels, drug delivery systems, artificial organs, bioinspired chemistry, artificial cell membranes, nano/micro diagnostic systems, biosensors and biointerfaces. Professor Ishihara is the current President of the Japanese Society for Biomaterials (2012-) and is a Fellow of the American Institute for Medical and Biological Engineering (AIMBE) (2002) and a Fellow of the International Union of Societies for Biomaterials Science and Engineering (IUSBSE) (2004). He is active in the Society of Polymer Science Japan, Japanese Society of Biomaterials, Japanese Society of Artificial Organs, Japanese Society of Materials Science, American Chemical Society, and the Society for Biomaterials. Among his many notable honors and awards are the Young Investigator's Award of Japanese Society for Biomaterials, the Young Investigator's Award of Society of Polymer Science (1992), the 2009 Clemson Award, Society for Biomaterials in 2009, the 2011 High-technology Award: Award of Ministry of Economy, Trade and Industry and the 2011 Technical Progress Award of Japanese Society of Artificial

Technology Panel Speakers

Christopher John Bettinger, Ph.D.
Assistant Professor, Materials Science and Biomedical Engineering
Carnegie Mellon University

ROBERT L. CRUTCHFIELD
Venture Partner, Harbert Venture Partners

Lisa Perpall, M.S., MBA
Technology Commercialization Officer,
Clemson University Research Foundation

Andrew Cannon, Ph.D.
Research and Development Manager
Hoowaki, llc.

David E. Huizenga, Ph.D., JD
President and Chief Technology Officer
SCTAO, A Division of Tao Life Sciences, Inc.

Michael Gara, M.S., M.B.A.
Director, Research Awards
Wallace H. Coulter Foundation

Katina Dorton, JD, M.B.A.
Investment Committee
RTP Capital

Gregory Frank Zaic
General Partner
Nexus Medical & Technology Capital

Greg Hillman
SC Launch Executive Director (Interim)
SCRA Technology Ventures

Christopher John Bettinger, Ph.D.

Assistant Professor, Materials Science and Biomedical Engineering

Carnegie Mellon University

Title: Small, Soft, and Electric: The next generation of biomedical materials

Abstract: Complexity in materials and systems has permeated nearly every avenue of technology including medicine. Medical implants, for the most part, have only recently adopted advances in biomaterials including biodegradable systems, albeit with limited functionality. Biocompatible and biodegradable materials with advanced mechanical, microstructural, and electrical capabilities have the potential to serve as the centerpiece for implantable medical devices that can integrate with the human body. Our recent contributions in this area will be presented. First, I will discuss the design, synthesis, and characterization of a new class of biodegradable elastomers for use as soft tissue implants. These materials are prepared using chemistry that allow for reconfigurable networks, which confers distinct advantages in polymer processing. Next, I will describe the use of reconfigurable surfaces as a tool for deconstructing fundamental processes that are manifested by cell-topography interactions. Taken together, these results present new functionalities that will significantly advance the next-generation of medical materials.

Biographic profile: Christopher Bettinger is currently an Assistant Professor at Carnegie Mellon University in the Departments of Materials Science and Engineering and Biomedical Engineering. He directs the laboratory for Biomaterials-based Microsystems and Electronics at CMU, which is broadly interested in the design of novel materials and interfaces that promote the integration of medical devices with the human body. Chris has received many honors including the National Academy of Sciences Award for Initiatives in Research, MIT Department of Materials Science and Engineering Award for “Outstanding PhD Thesis”, the ACS AkzoNobel Award for Polymer Chemistry, the Tissue Engineering and Regenerative Medicine Society Young Investigator Award, and the MIT Tech Review TR35 Top Young Innovator. Prof. Bettinger is also a co-inventor on several patents and was a finalist in the MIT $100K Entrepreneurship Competition. Prof. Bettinger received an S.B. in Chemical Engineering, an M.Eng. in Biomedical Engineering, and a Ph.D. in Materials Science and Engineering as a Charles Stark Draper Fellow, all from the Massachusetts Institute of Technology. He completed his post-doctoral fellowship at Stanford University in the Department of Chemical Engineering as an *NIH Ruth Kirschstein* Fellow.

Lisa Perpall, M.S., MBA

Technology Commercialization Officer

Clemson University Research Foundation

Title: The management of biomedical intellectual property at Clemson University

Abstract: The Clemson University Research Foundation (CURF) is a resource both for Clemson research community seeking intellectual property protection and for industry, including established companies and **entrepreneurs, seeking innovations to drive their businesses. In this talk,** Lisa Perpall will introduce (CURF) and discuss how the organization works to promote technology commercialization activities and collaborative research partnerships related to innovative biomedical technologies originating from within Clemson University. She will provide an overview of the biomedical technology IP portfolio, highlight some examples of nanomedicine technologies within the portfolio, and feature current examples of commercialization of Clemson nanobiomaterial technology to the industry. The Clemson University Research Foundation (CURF) is a non-profit corporation that facilitates the transfer of Clemson University's intellectual property to the private sector for commercial development and societal benefit. To learn more about CURF services and to view current technologies available for license, visit www.clemson.edu/curf.

Biographic profile: Lisa Perpall is a Technology Commercialization Officer with the Clemson University Research Foundation. In this role, she manages the biomedical technology intellectual property portfolio for the University. As such, she works closely with university researchers to evaluate emerging technologies and also actively seeks industry partners, including established companies and entrepreneurs, with interest to license and commercialize Clemson University technology. She also works closely with emerging South Carolina biomedical start-up companies associated with the University. Previously, she worked for Michelin North America as an associate in the Emerging Business Ventures group and as a marketing manager for a North American Business Unit. She has an MBA and MS in Bioengineering, both awarded from Clemson University.

Andrew Cannon, Ph.D.

Research and Development Manager

Hoowaki, llc.

Title: Turning graduate research in nanotechnology into a small company

Abstract: This talk will describe my path from introduction to a technological opportunity in graduate school to turning the solution into a small company. For many decades, scientists have known that surface microstructures can affect the properties of a surface, including tribological characteristics such as coefficient of friction and wear, appearance and optical characteristics, heat transfer coefficient during boiling and condensation, and water repellency. Micromolding is a scalable route to manufacturing microstructured surfaces. The requirements for scaling micromolding tools to high volume applications are that the molding tools must be made of durable metal and be of low cost. The micromolding tool must further be of large area and of arbitrarily curved surface. Metal microstructures and nanostructures are attractive for micromanufacturing molds as they can be reused many times more than molds composed of traditional microfabrication materials such as silicon or quartz. Embossing, molding, rolling, and stamping can produce microstructures at 1/1000 the cost of conventional fabrication techniques such as silicon microfabication, micro-milling, or laser micromachining. Unlike paint, spray, or plasma-based surface finishes, micromolding can fabricate lithographically-defined and ordered three dimensional microstructures. Michelin tire company understood the opportunity and funded my graduate work to find a pragmatic solution that it could implement. When we demonstrated the robust solution, the program manager at Michelin launched Hoowaki to specialize in producing metal molds with surface microstructures that produce low cost yet highly functional replicate surfaces.

Biographic profile: Andrew Cannon earned his B.S. and M.S. degrees in Mechanical Engineering at Georgia Tech in 2003 and 2006. He earned his Ph.D. at the University of Illinois in Mechanical Engineering in 2009 while enabling Michelin tire company to mold functional engineered surface microstructures into their tire molds. The Michelin program director departed from Michelin to found Hoowaki as a surface engineering company, and Andrew joined Hoowaki in 2010 as its R&D Manager. At Hoowaki he determines how to design surface microstructures and how to integrate their manufacture into Hoowaki's clients' manufacturing processes.

David E. Huizenga, Ph.D., JD

President and Chief Technology Officer

SCTAO, A Division of Tao Life Sciences, Inc.

Title: "Nanotechnology's predictable evolution points the way for tomorrow's and opportunities"

Abstract: This talk addresses the technological challenges of nanotechnology in the context of the commercialization pressures society places on the modern expression of scientific discovery. In modern society, the relationship between science and society transforms the goal of science from mostly empirical, observational, and knowledge based to mostly directed, integrated, and product based. When under this pressure, all disciplines of science have, or are undergoing, a predictable evolution from materials based research towards "thing" or device based research, which eventually leads to integrated or systems based research. The transition zones between these three forms of research represent areas of intense problem/solution activity, and thus, areas and times of great technological and commercial opportunity. Nanotechnology has embarked on this same evolutionary path, and is currently transitioning from a materials development stage of discovery into the "thing" or device stage of discovery. Tremendous discoveries and advancements have been made in nano-materials, but nanotechnology continues to struggle to make the transition into the coming burst of device and product evolution. Systems integration of nano-materials and devices has yet to be seriously approached. The most exciting commercial and technological near term nano opportunities revolve around leaps and advances in applying the knowledge gained in nano-materials to making the coming wave of nano-based products.

Biographic profile: David Huizenga, Ph.D., J.D., is President, CTO, and Cofounder of Tao Life Sciences Inc., an early stage life sciences technology development and investment company and Managing Director of Upstream Partners Inc., a specialty IP advisory firm. Mr. Huizenga seeks to identify, and subsequently develop, life science technologies by integrating his commercial, scientific, and legal experiences and perspectives into a cohesive opportunity analysis. Mr. Huizenga has been the Chief Technology Officer of Zirus, Inc. where he was engaged in management of the Zirus patent portfolio, licensing, and competitive intelligence. Mr. Huizenga was a leader in the translation of the company's science strategy to the patent and business strategy. Mr. Huizenga was the CFO and Vice President of Venture Investment at Needle & Rosenberg, PC. Mr. Huizenga has also worked closely with small biotechnology and pharma companies in a founder's capacity. Mr. Huizenga's legal experience has focused on all aspects of biotechnology patent prosecution and intellectual property counseling as well as litigation. Mr. Huizenga obtained his Ph.D. from Harvard, in the laboratory of Jack Szostak, Nobel Laureate in Medicine. His research focused on the structure/function relationships of small molecules and functional nucleic acids, such as aptamers, and the integration of rational and irrational discovery paradigms to identify molecules having new and desired function. Mr. Huizenga obtained his Law Degree from Emory University Law School.

Michael Gara, M.S., M.B.A.

Director, Research Awards

Wallace H. Coulter Foundation

Title: Lessons from the "Valley of Death": Funding Translational Biomedical Research

Abstract: For the past eight years the Wallace Coulter Foundation has served as the primary grant making organization for translational research in the U.S. In two national programs we have given over 500 grants worth over $100M. In the Coulter Translational Research Award (formerly Early Career) we have reached out to most universities in the U.S. with substantial biomedical engineering programs. Through this effort, we have given 108 grants to a wide variety of schools including Clemson. Many of these grants have supported novel biomaterials with clinical end uses. Our second program, the Translational Partnership award has established ongoing programs at 16 universities across the U.S. This program establishes grants with 4-6 researchers per year and with the direct coaching of a full time Program Director on campus. Here we have given out over 400 grants with many in the biomaterials area. Through this effort the Foundation has been successful in seeing its investment returned 5-6 fold in follow on funding from various sources including venture capital, industry and federal SBIR, DOD and other Foundation grants. This talk will focus on the "lessons learned" in managing many of these programs over the past 8 years.

Biographic profile: Mr. Gara has been employed in the pharmaceutical and biotechnology industries for his whole career. He has held positions in the R&D, manufacturing, product development and business development functions for a number of large and small pharmaceutical companies, including Baxter Healthcare, Zeneca Pharmaceuticals, Schwarz Pharma, Bone Care International and CURx Pharma where he was a co-founder of the company. In addition, Mr. Gara was also involved in the private equity financing of biotechnology companies and university based start-ups while at Senmed Medical Ventures. Mr. Gara's last position prior to The Wallace Coulter Foundation was at the University of Chicago where he was responsible for the licensing and commercialization of medical technology and was involved in the formation of two medical start-up companies. Mr. Gara holds a B.S. and M.S. in Chemistry and an MBA from the Kellogg Graduate School of Management. His current position involves managing translational research programs in biomedical engineering at major universities across the U.S. He is the Coulter representative for the Translational Partnership Program at University of Wisconsin, Case Western, Drexel and Boston University and recently added University of Louisville, Missouri and Pittsburgh. He is also the Program Director for the Coulter Translational Research Awards, a national competition for translational biomedical research. **Specialties:** Medical technology commercialization, licensing, venture due diligence, business development.

Katina Dorton, JD, M.B.A.

Investment Committee

RTP Capital

Title: Raising Capital form Angel Investors

Abstract: This talk will introduce angel investing. Who are angel investors? What types of companies will they provide funding to: which industry sectors, stage of development and amount of funding? How does RTP Capital make investing decisions? Do angel groups work with other investors? What do you need to do to be prepared to seek angel funding? What specific issues do life sciences and biomaterials companies face when trying to obtain angel funding?

Bioprofile: Katina Dorton is a member of the Investment Committee of RTP Capital, an angel investing group based in NC's Research Triangle Park. Since moving to the Triangle about a year and a half ago, Katina has been very involved in the business and entrepreneurial community. She is currently a Partner in a small boutique investment banking firm, CoRiseCo, and a Senior Advisor to the BioPontis Alliance, a new life sciences venture fund where she is advising on fund raising and strategic partners. Katina has also been consulting for a private biotechnology company and the NC Biotechnology Center. Katina is a member of the Advisory Board of the NCSU Technology Incubator. She also serves on the Board at Evatran, a private company developing plug-less batteries for electric vehicles and at Agile Endosurgery, a medical technology company that is developing a set of articulated endoscopic surgical tools. Katina has been a Venture Mentor with the CED since the inception of its program with MIT. Katina is a senior investment banker, having spent almost 20years on Wall Street advising corporate clients and their boards of directors on fund raising, mergers and acquisitions and other strategic transactions. Katina spent 12 years of her career at Morgan Stanley, where she was a Managing Director in Investment Banking. She later was a Managing Director for the Life Sciences team at Needham & Co, a boutique investment bank. Prior to Morgan Stanley, Katina practiced law in the area of mergers and acquisitions at Sullivan & Cromwell. Katina has a BA from Duke, an MBA from George Washington University and a JD from the University of Virginia.

ROBERT L. CRUTCHFIELD

Venture Partner, Harbert Venture Partners

Harbert Management Corporation

Title: Venture investing and its possible alignment with the University's Technology Transfer Mission.

Abstract: This talk introduces Harbert; our investment thesis (early growth), our investment criteria (good management, addressable markets, customer adoption), our returns model expectations, our role post investment (BoD), and how we intersect with companies that are too early for investment, but interesting enough to begin tracking and what that means. Also, this talk will address the author's perspective on the role of universities in creating early stage companies and how they are becoming technology-based economic development engines. *"HVP seeks to identify and invest in emerging portfolio companies with high growth potential at valuations which reflect a realistic view of exit opportunities. We seek to invest with seasoned entrepreneurs building early stage growth companies with defensible positions in large and growing markets. We typically invest in the first or second institutional rounds, with initial investment amounts between $1.0 and $4.0 million. We typically seek board representation in our investments and endeavor to provide constructive, strategic, operating and networking support to our portfolio companies."*

Biographic profile: Mr. Crutchfield joined HMC in September 2008 and serves on the board of Optimal IMX, WellCentive, Inc., and RegisterPatient, Inc. He also serves as the board observer for Aldagen, Innovative Biosensors, MaxCyte, OpenQ and Control Scan. In addition to his responsibilities at Harbert, he serves as the Chairman of the Commercialization Sub-Committee for the Alabama Innovation Council Study Commission, is serving on the Steering Committee of the Alabama Obesity Institute at the University of Alabama in Birmingham, is a Venture Fellow at the University of Alabama in Tuscaloosa, is a Visiting Executive in Residence at Auburn University and is a member of the Board of Directors for the Southeast Medical Device Association, the Birmingham Venture Club, Alabama Launchpad, the Southern Capital Forum, and on the investor advisory boards for Florida Institute for the Commercialization of Public Research and the Florida High-Tech Corridor Council.

Prior to joining Harbert Venture Partners, Mr. Crutchfield served as Senior Vice President/General Manager of the Pharmacy Services Division at US Oncology, a privately held, vertically integrated cancer care provider network with cancer clinics in more than 440 sites of service and a physician network consisting of over 1000 medical oncologists and radiation oncologists. His division was responsible for approximately $2 billion of annual revenue and under his leadership the division's EBITDA grew to over $80 million.

Mr. Crutchfield was also a Senior Executive at CardinalHealth, where he served as Vice President of New Ventures. While there, he built and launched a new surgical products business unit through licensing of new technologies, acquisitions and created a new North American sales channel.

In 1995, Mr. Crutchfield founded Surgical Innovations and Services, Inc. (SIS), a surgical laser management company. Under his leadership, SIS became a leader in the emerging outsource management sector, with over 300 hospitals and surgery centers under contract with SIS for management oversight and delivery of their surgical laser programs. In 2000, SIS merged with Surgical Laser Technologies, Inc. (SLTI) a publicly traded surgical laser-manufacturing firm. Mr. Crutchfield continued as President of SIS and served as VP of Sales, Marketing and Business Development for SLTI, until he exited the company following its acquisition by publicly-traded Photomedex, Inc.,

Mr. Crutchfield has launched five successful new business ventures during his private and corporate career and has lead four merger and acquisition transactions. Mr. Crutchfield is a graduate of the University of Georgia and holds Bachelor of Science degrees in Political Science and Chemistry.

Gregory Frank Zaic
General Partner

Nexus Medical & Technology Capital

Title: The Medtech Investment Philosophy at Nexus

Abstract: Nexus has experience investing in companies in various stages of development, across sectors including medical devices, diagnostics, biotechnology, specialty pharmaceutical, drug discovery tools, software, communications and information technology and advanced materials. I will give a ~5 minute slide show describing Nexus and our medtech investment philosophy.

Bioprofile: Greg is currently a general partner of Nexus Medical & Technology Capital ("Nexus"), a private equity firm specializing in healthcare and technology investments. He has over 25 years of venture capital investment experience. He has been an active Board member of both public and private corporations, providing assistance and guidance on issues associated with business strategy, corporate expansion, corporate combinations and organizational development. He currently represents Nexus on the Boards of Sabal Medical (hospital medication tracking, recently bought by Swisslog), Zipit Wireless (smart pagers for hospitals, partnered with Verizon), Aethon Inc. (hospital-based robotic logistics), Kiyatec Inc. (3-D cell culture) and Cutanea Life Sciences (dermatological pharmaceuitcals, recently bought by Maruho Corporation, Osaka, Japan). He was responsible for Nexus' successful investment in Biodel Inc., a company developing a new formulation of insulin. He maintains offices in Greenville, SC, Ridgefield, CT and Quincy, MA.

Recent speaking engagements include: the IN3 East Investment in Innovation (Boston, 2012, 2011 and 2010), Crossroads of Ideas and Capital: Vision 2015 (New Haven, 2011), New England Venture Summit (Boston, 2010), Life Science and Healthcare Venture Summit (Boston, 2009), Health Science South Carolina (Columbia, SC, 2010), 2010 Southeast Region Angel Capital Association Meeting (Greenville, SC), 5th Annual South Carolina MedTech Conference (Greenville, SC, 2009), and the 2009 Life Sciences & Healthcare Venture Summit (New York City), Biomedix 2006 (Montreal), and the 2005 Congrès Réseau Capital (Quebec).

Prior to joining Nexus, Greg was a general partner of Prince Ventures, an independent, medically focused, venture capital partnership. His investments included PerSeptive Biosystems (bioseparations products) that was sold to Perkin Elmer for over $300 million. During the 1980s, Greg was Vice President and Special Limited Partner of the Vista Group. He was a founding investor in numerous successful companies including Focus Healthcare, an HMO that was sold to Lincoln National Insurance Company for a substantial return.

From 1972 until 1979, Greg was an executive with Baxter Laboratories. His three member team was responsible for bringing CAPD (Continuous Ambulatory Peritoneal Dialysis) into Baxter, where it became the second-most profitable product line in the company, then accounting for approximately 20% of Baxter's total profits.

Greg received a BS (*magna cum laude*) in aerospace and mechanical engineering from Princeton University; an MS in mechanical engineering from the Massachusetts Institute of Technology (MIT); and an MS from MIT's Sloan School of Management.

Greg Hillman
SC Launch Executive Director (Interim)

SCRA Technology Ventures

Title: SC Launch - The capability, capacity and credibility for making early Bio related investments

Abstract: SCRA Technology Ventures operates the flagship economic development program, SC Launch, which has invested over $13 million in South Carolina start-ups and has supported over 277 entities in South Carolina through investments and other support services. They also invest in more established companies to support commercialization and growth, facilitate the transfer of intellectual property and accelerate the transition of inventions to the marketplace. SCRA is an applied research corporation with over 29 years of experience delivering technology solutions with high returns on investment to federal and corporate clients. Multiple economic impact studies show SCRA's cumulative output on South Carolina's economy to be over $14 billion, and that the company has helped create approximately 15,000 technology-related jobs in the state, with annual wages averaging between $55,000 and $77,000.

Biographic profile: Greg Hillman and the SC Launch Team work closely with over 200 Program clients, 25% of which are early and emerging Life Sciences companies performing early drug development, medical device development and bioinformatics application systems development. SC Launch companies exist at various stages of start-up and into applied R&D and commercialization. Mr. Hillman also leads activity in preparing viable candidates in other selected technical business sectors such as advanced materials, energy and applied engineering with considerable attention commercialization. Over his five years with the Program, Greg has reviewed well over 1,000 candidate companies and continues to work with many of them as well as the 60 portfolio companies invested through SC Launch, Inc. Since inception in 2005, more than $180,000,000 of external follow-on investment has been placed into SC Launch companies.

Greg's professional background experience in technical and executive management includes positions with EDS and Computer Sciences Corporation, DuPont's Photopolymer and Electronic Materials Strategic Business Unit and with Nortel North America. As CEO and a co-founder of Integrated Business Solutions (IBS), Inc., a Memphis, TN Systems Integrator, Hillman's team pioneered digital imaging and manufacturing systems control processes and developed a series of telecom and cellular business systems applications that became industry standards. Greg applied IBS resources jointly with investor Aetna Capital Ventures, Federal Express, University of Memphis and Christian Brothers University in defining corporate mentoring programs in support of economic development efforts in Tennessee. Mr. Hillman was director with Boston based Appex LS LLC, a Greylock Venture Capital funded company where he worked the $90m acquisition of the company by Electronic Data Systems. Greg holds an MBA in Economics and Finance from the University of Utah, a BA in Business Management with Chemistry minor from Park University, KS and served in the USAF.

Undergraduate Research Oral Presentation Abstracts

Synthesis of Biodegradable Elastomeric Films for Dynamic Strain Drug Release

Scott Cole, Dr. Terry Steele

Statement of Purpose: Poly(glycerol-sebacate) (PGS) a.k.a. "biorubber" is a biodegradable elastomer whose properties have been explored for potential drug delivery applications.[1] When a drug is to be released from a material to the body, it is desirable that the effect can be triggered so that the release profile is customizable. Dynamic strain (i.e. repetitive stretching) of biorubber may be a mechanism for which drug that is infused within the polymer can be released.

In this study, the synthesized polymers were based on poly(glycerol-sebacate), using various sugars and monomer ratios. A casting technique was fabricated for the polymers, and the films' mechanical properties were characterized. Preliminary drug release studies were attempted by introducing fluorescein diacetate (FDA) into the post-cured polymers.

Methods: Polymer synthesis began by mixing sebacic acid and one of the following sugars in a 50mL test tube: glycerol, mannitol, and pentaerythritol. The mixtures were made using molar ratios of 1:1.2, 1:1, and 1.2:1 (sebacic acid: sugar). "Pre-polymers" (polymerizing monomer solutions prior to curing) were heated to 165ºC (140ºC for PGS syntheses) for 6 hours without vacuum, and then vacuum was applied until appreciable viscosity was achieved for casting.

In preparation for polymer casting, a glass petri dish was lubricated with silicon oil, and a wrinkle-free sheet of Teflon was spread onto the inside surface of the petri dish, and any air bubbles were squeezed out. The pre-polymer was poured into the middle of the petri dish and allowed to spread out. It was then placed in an oven at 140ºC until stiff.

The cured polymer films were punched into dogbone shapes using a press, and a break test was performed using a 10N load cell attached to an Instron Tester (Model 5567) and Bluehill 2 software was used for analysis. The elastic modulus (E), yield strength (δ_{ys}) and elongation-to-break (ε_b) were calculated from each stress-strain curve. Dynamic strain was performed by stretching the film at 0.5%/second with a maximum strain of 20% for 5 cycles. Drug-release studies were begun by soaking film punchouts in a high concentration of fluorescein diacetate (FDA) dissolved in dichloromethane (100mg/mL). Release was monitored by an Infinite M200 Tecan Microplate Spectrofluorometer.

Results: The mechanical properties of the synthesized films were dependent on the chemical structure of the sugar that was chosen. The pentaerythritol-based elastomer (PPS) had the greatest elastic modulus, followed by the mannitol-based elastomer (PMS), and then PGS. Unlike mannitol and glycerol, pentaerythritol contains a quaternary carbon that directly attaches to up to four polymer chains. This extra point of crosslinking resulted in the PPS polymers being the strongest (highest E and δ_{ys}) yet the most brittle (lowest ε_b) of the synthesized films. The structure of mannitol is longer than that of glycerol, which explains why the PMS films could endure more strain prior to break than the PGS films. The syntheses with a molarity imbalance in favor of the sebacic acid had the quickest synthesis times. This is because an increase in the amount of sebacic acid relative to the amount of sugar increases the potential for crosslinking. Additionally, after the films were cured, those with the most sebacic acid were the strongest but least ductile films. The samples with the most sugar were typically able to stretch the most before break because the excess sugar acts as a plasticizer.

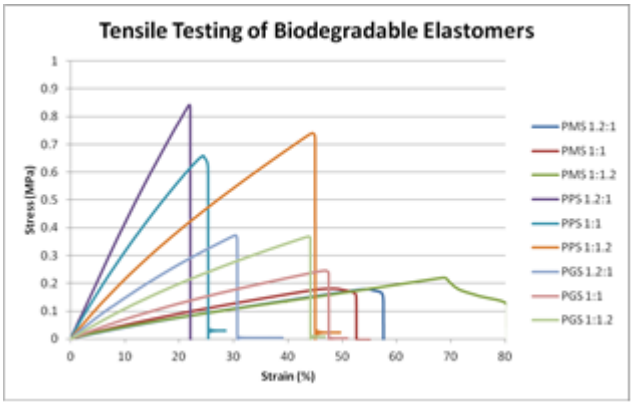

Figure 1. Stress-Strain curves for polymer break tests.

Since the plastic deformation region for all elastomers is minimal by nature, the stress-strain relationship was consistent throughout the five cycles performed in the dynamic strain study. The PMS, PGS, and PPS 1:1.2 films endured the cyclic stress without failure. In these cases, the hydroxyl crosslinking mechanism is flexible enough to maintain the films elastomeric properties' that are to be utilized for systematic drug release.

Obstacles were encountered in the planned drug release studies, and the protocol has been updated for future work.

Conclusions: Biodegradable elastomeric films were synthesized, though they were thick. A broad range of mechanical properties was achieved by exploring the use of different sugars, compared to simply adjusting molar ratios. Presumably, the degradation rate of these films will also vary and yield different drug release profiles. In general, an increase in amount of sebacic acid in synthesis increases the rate and amount of crosslinking present in the films. A centrally-connected sugar, pentaerythritol, produced the strongest films with the least ductility. On the other hand, mannitol's long structure yielded an elastomer with a relatively high elongation to break, but its strength was compromised. Ultimately, the films produced are capable of absorbing and releasing FDA, which allows for the use of a fluorometer to observer the polymers' drug release.

References:

[1]Wang Y, Ameer G, Sheppard B, Langer R. A tough biodegradable elastomer. *Nature Biotechnology*. 2002;(20): 602-606.

In Search of a Biodegradable X-ray Contrast Agent: Synthesis, Functionalization and Preliminary Characterization of Iodinated Poly(epsilon-caprolactone)

Caroline C. Duncan[1], Brooke A. Van Horn[2]

[1]Department of Biology and [2]Department of Chemistry and Biochemistry
College of Charleston, Charleston, SC, 29424.

With two of the most common processes for imaging in the human body being general X-ray radiography and computed tomography (CT) technologies, scientists today are exploring and developing exciting new choices for imaging agents and moving beyond the traditional small molecule contrast agents. A biocompatible, biodegradable polymeric macromolecule with engineered radio-opacity (X-ray and CT contrast) and reactive groups would have similar imaging utility as the traditional systems with additional means to covalently link directing groups for specific cellular targets and therapeutic agents for delivery. Our research lab at College of Charleston is interested in the fundamental design, synthesis, and characterization of such nanoscale vessels for a variety of biomedical applications.

Specifically, our lab has recently replicated the synthesis of linear polyester polymer chains with built-in ketone functional groups. This synthesis was accomplished by the ring-opening copolymerization of epsilon-caprolactone (CL) and 1,4,8-trioxaspiro[4.6]–9-undecanone (TOSUO) using benzyl alcohol as initiator and $Sn(Oct)_2$ as the ring opening catalyst. Subsequently, these polymers were deprotected using trityltetrafluoroborate to afford the ketone-bearing poly(caprolactone-*co*-2-oxepane-1,5-dione) (P(CL-*co*-OPD)) polymers. The polymer species at both stages were well characterized using proton and carbon nuclear magnetic resonance (NMR) spectroscopy for structure and number averaged molecular weight calculations and was also evaluated with gel permeation chromatography (GPC) to determine polymer sample polydispersity. Using these ketone units as a chemically reactive handle, acid-catalyzed ketoxime ether formation is possible for the reversible but covalent attachment of iodinated species, including the recently prepared *O*-(2-iodobenzyl)hydroxylamine small molecule, to impart tunable levels of radio-opacity to the polymeric material. Multiple trials with different stoichiometry were completed, with optimization of the amount of acid catalyst and molar ratio of aminooxy derivative-to-ketone to be employed for complete coupling. We will present the current state of our project in the preparation of these novel modular polymer species and highlight our plans to translate this chemistry and our preliminary results to the formation of radio-opaque water-soluble nanoparticles.

The Effect of HA and FA Microparticles on Dental Cell Differentiation

Amanda Farley, Laura Datko, Dr. Marian Kennedy, Dr. Delphine Dean
Clemson University Department of Bioengineering

Statement of Purpose: With the progression of regenerative medicine, bio-fillers are becoming a very viable option in the treatment of dental caries and the repair of cranio-facial injuries[1]. Much research in literature has been done on the possibility of using apatite minerals in bio-fillers to stimulate positive growth and differentiation in bone cells[2]. Most of the previous studies have focused on 7F2 osteoblasts cultured with micro-Hydroxyapatite (HA) particles. However, there have been mixed reports on these particles having positive or negative effects on cell differentiation. This work delves into the effects of micro-HA on BMSCs, 7F2 osteoblasts, and dental pulp stem cells (DPSCs) as well as the effects of micro-Fluorapatite (FA) on these cells.

Methods: Alkaline phosphatase (ALP) and bicinchoninic acid (BCA) assays were run for days 1, 3, 5, 7, and 14 on the three types of cells cultured in mineral particles in order to determine the protein content. Cells were cultured 2500 cells/well with 10 ul of 10 mg/ml mineral particle in 16-well plates. Antibody stains were carried out to determine osteocalcin and collagen I production over a two week period. Rabbit anti-osteocalcin and rabbit anti-collagen I were used as primary antibodies while 488 goat anti-rabbit was used as a secondary. In addition, confocal imaging was done using collagen I and osteocalcin. Separate cultures were stained with alizarin red to ascertain the presence of early calcification within two weeks. Finally, lysates were collected from cell samples and western blots are being run for osteocalcin and collagen I content.

Results and Discussion: The ALP and BCA assays yielded mixed results. Different kinds of cells reacted differently to the added mineral; most notably the DPSCs, which had almost five times the amount of ALP specific activity on day seven than did the BMSCs or osteoblasts. Generally, the control cells had higher levels of activity than those cultured with particles with the exception of osteoblasts with HA and FA, both of which had higher activity levels throughout the 14 day period. There was a spike in collagen and osteocalcin production on day 5, and a marked increase of collagen on day 5 for osteoblasts cultured with FA. The microscope images taken from micro particle cells also yielded interesting observations. Over time the cells tended to congregate closer to the HA particles in the center of the well, while FA cells moved towards the sides of the wells where small groups of them clustered around "straggler" FA particles (Fig. 1). DPSCs and osteoblasts cultured in HA grew more rapidly and were confluent by day 7 compared to those cultured in FA.

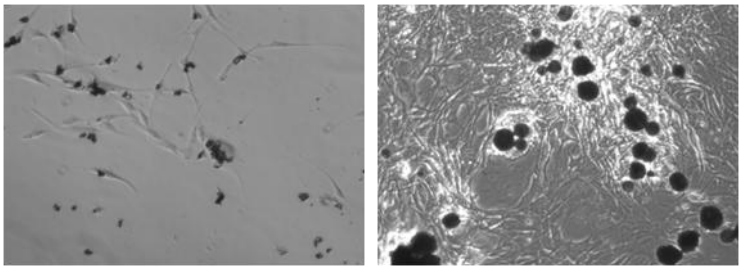

Figure 1: A dense cell population is congregated around HA particles (on the left). Conversely FA cells were more spread out, and single or paired cells were often clustered around a single FA particle (on the right). Also, HA cells were closer to confluency than FA cells at day 7.

Conclusions: The addition of apatite microparticles seems to increase osteogenic cell differentiation during the first 3-5 days. This held especially true for HA particles in ALP activity for osteoblasts and DPSCs, and FA particles in collagen production. However, the addition of microparticles proved to be more of a hindrance after 5 days. BMSCs performed much better overall without the addition of particles when compared to osteoblasts and DPSCs. In the future, different concentrations of HA and FA particles may be explored.

References: [1] Pines A, Raafat H, Lynn AH, Whittington J. Clinical trial of microcrystalline hydroxyapatite compound ('Ossopan') in the prevention of osteoporosis due to corticosteroid therapy. Curr Med Res Opin 1984;8:734–42

[2] Webster TJ, Siegel RW, Bizios R. Osteoblast adhesion on nanophase ceramics. Biomaterials 1999;20:1221–7.

Graduate Research Oral Presentation Abstracts

Single Walled Nanotube– Glucose Oxidase Conjugates via Ultrasonic Processing: Effect of Tube Length, Functionalization and Processing Time

Olukayode Karunwi[a,c] and Anthony Guiseppi-Elie[a,b,c,d,e*]

[a]Center for Bioelectronics, Biosensors and Biochips (C3B), Clemson University Advanced Materials Center, 100 Technology Drive, Anderson, South Carolina 29625, USA

[b]Department of Chemical and Biomolecular Engineering, [c]Department of Bioengineering, [d]Department of Electrical and Computer Engineering, Clemson University, Clemson, South Carolina 29634, USA

[e]ABTECH Scientific, Inc., Biotechnology Research Park, 800 East Leigh Street, Richmond, Virginia 23219, USA

Statement of Purpose: Several methods have been proposed over the years to address the issue of biotransduction devices with stable biomolecular recognition and efficient electron transfer at the biomolecule-to-solid state (bio-abio) interface. Among these are generation-1 biotransduction devices (electrochemical monitoring of reactants or products of an enzyme catalyzed reaction) and generation-2 devices (uses free or tethered redox mediators). In more recent years, generation-3 (gen-3) biosensors based on direct electron transfer that are reagentless [1] and possess long term *in vivo* stability will enable fully implantable continual monitoring of various analytes of a wide variety of physiological conditions and pathologies [2]. One of the methods for fabricating a gen-3 biotransduction mechanism is ultrasonic processing [3] to produce single walled carbon nanotube-glucose oxidase (SWNT-GOx) enzyme conjugates [4]. This was investigated as a function of sonication times, SWNT functionalities and tube length.

Materials and Methods: Aqueous suspensions of SWNT (functionalized SWNTs with –OH groups (< 1 µm-short, 1 – 5 µm-medium, 5–10 µm-long) and –COOH (1 – 5 µm-medium)) and Glucose oxidase (GOx; 1mg/ml) were ultrasonicated at 4°C (tip sonicator; 23 kHz) for 0 (control) 5 and 60 min. The resulting SWNT-GOx conjugates were collected from the supernatant following high-speed centrifugation (33,000 *g*). UV-Vis spectroscopy was used to monitor the association of the flavin adenine dinucleotide (FAD) with its apoenzyme. Circular dichroism (CD) was used to monitor changes in the structure of the enzyme within the SWNT-GOx conjugate and the activity of the enzyme was monitored by standard HRP-coupled colorimetric enzymatic assay. 2,2'-azino-bis(3-ethylbenzothiazoline-6-sulphonic acid) (ABTS) was used in place of *o*-dianisidine for more stable results. A Plackett-Burman design of experiments approach was used to optimize processing conditions for producing SWNT-GOx supramolecular conjugates with minimum loss of enzyme activity.

Results and Discussion: Three output variables studied were; i) the extent of the blue shift ($\Delta\lambda_{max}$) in the absorbance maximum of the FAD-apoenzyme at 381 and 452 nm, ii) The change in the sum of α-helix and β-sheet in the CD spectra, and iii) the change in the k_{cat}/K_M (/mM/s) and *n* of the enzyme conjugate expressed relative to the pristine GOx. UV-Vis spectra over the range of 300 to 550 nm to obtain information pertinent to the FAD bound to the native enzyme (λ_{max} at 381 and 452 nm) or the blue-shifted FAD of the denatured enzyme (λ_{max} at 377 and 448 nm) revealed that ultrasonication up to 1 h had no influence on spectral characteristics of FAD. Also, the short SWNTs (<1 µm) had little effect in the partial denaturation of the enzyme compared to the other length SWNT. CD analysis of the 2° structure showed that, for both pristine and SWNT-GOx conjugates, the "sum of the fractions" was reduced with an increase in sonication time. The short SWNTs had the least effect on the change to the secondary structure while the long SWNT had the greatest effect. **Fig. 1** shows the kinetic parameters as a function of treatment regimen. Comparing K_M, k_{cat}, k_{cat}/K_M, v_{max} and n (the Hill parameter), it is shown that increase in sonication time reduces enzyme activity although the addition of SWNT appears to stabilize the activity compared to sGOx.

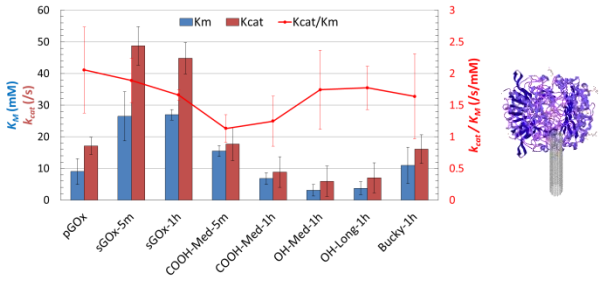

Figure 1. Enzyme kinetic parameters as a function of composition and treatment times.

Conclusions: Short SWNT appeared to support conjugate formation with no loss of FAD, medium SWNT appeared to support conjugate formation moderately while the long and non-functionalized SWNT caused partial denaturation leading to the egress of FAD. Enzyme activity was conserved for all conjugates.

Acknowledgements: The US DoD PRMRP grant DAMD17-03-1-0172 and C3B

References:

[1] Guiseppi-Elie A, Lei C, Baughman RH. Nanotechnology. 2002;13:559.

[2] Kotanen CN, Moussy FG, Carrara S, Guiseppi-Elie A. Biosens Bioelectron. 2012;35:14-26.

[3] Guiseppi-Elie A, Choi S-H, Geckeler KE. J Mol Catal B: Enzym. 2009;58:118-23.

[4] Guiseppi-Elie A, Choi S-H, Geckeler K, Sivaraman B, Latour R. Nanobiotechnology. 2008;4:9-17.

Investigation of a Multicomponent Non-Hormonal Contraceptive Device

G.T. Hilas, S.D. Nagatomi, S.W. Shalaby

Poly-Med, Inc., Anderson, SC 29625

Statement of Purpose: At present, female sterilization, oral contraceptives, and condoms are the three most widely used methods of contraception in the developed world.[1] With the exception of barrier methods, such as male or female condoms and spermicides (used in combination with condoms) and permanent contraceptive methods, such as sterilization and vasectomy, existing birth control methods primarily rely on hormones to suppress ovulation. Health risks are a growing concern among women taking hormone-based contraceptives. Studies have shown that hormones, such as progestin or estrogen, contained in these contraceptives can cause severe side effects such as an increased risk of blood clots and cervical cancer.[2] This led to the exploration of new, non-hormonal, controlled release intra-vaginal contraceptives.[3,4] It has been long known that the spermatozoa of mammalian species are highly susceptible to reactive oxygen species (ROS) induced damage due to metal-catalyzed lipid peroxidation.[5] In addition, studies have shown that ascorbic acid (AA) may increase the viscosity of cervical mucus.[4] The present study pertains to the investigation of a multicomponent intra-vaginal non-hormonal contraceptive device (Ovaprene® ring) that consists of a silicone matrix surrounding a centrally located mesh component. The silicone portion of the ring releases ferrous gluconate (FG) and AA over a period of 35 days to inhibit sperm motility and increase the viscosity of the cervical mucus while the mesh component acts as a partial physical barrier to the free movement of sperm. Therefore, the Ovaprene® ring is being considered a combination drug/device product by the Food and Drug Administration.

Methods: The knitted mesh portion of the ring is constructed from an absorbable multifilament yarn made of a segmented lactide copolymer.[6] The mesh is attached to a scaffold support made from the same multifilament yarn used to make the mesh. To prepare the ring, a two-part biomedical-grade silicone is mixed with FG, AA, and polyglycolide microparticles which function to modulate component release and control the pH of the vaginal fluid. This mixture is then injected into a stainless-steel mold that is preloaded with the reinforcing yarn/mesh construct mentioned above and heated to 80ºC until proper curing has been achieved. The mold cavities are constructed to produce a ring with an outside diameter of 55 mm and an inside diameter of 40.0 mm. Release studies to determine the quantity of FG and AA released from the device were conducted in simulated vaginal fluid (pH ~ 4.2) at 37ºC for periods up to 35 days. Eluents were collected and replaced at each day of testing. Device eluents were evaluated for FG and AA using spectrophotometric analysis testing methods as described previously[7-8]. Spermiostatic testing was conducted at the Greenville Hospital System (GHS) Reproductive Endocrinology & Infertility laboratory. Briefly, testing involved mixing 0.3 mL of device eluents, collected at various time points throughout a 35 day release study, with 0.2 mL of pooled human semen. After which, % sperm motility was evaluated at various time intervals using a MicroCell Chamber and computer-automated semen analyzer (CASA) to assess the spermiostatic potential of the device eluents.

Results: As shown in Figure 1 below, the concentration of FG ranged from 37 to 287 µg/mL over the 35 day testing period. AA concentrations ranged from 40 to 1186 µg/mL over this same period. In addition, spermiostatic testing conducted at GHS (Table I) reveals that Ovaprene® ring eluents throughout a 35 day use period are capable of inhibiting sperm motility.

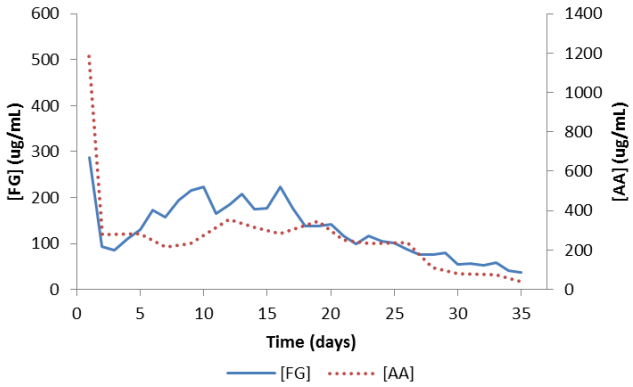

Figure 1. Concentrations of FG and AA as released from the Ovaprene® ring.

Table I. Motility of Sperm Exposed to Ovaprene® Eluents

Day	% Motility		
	0 Min.	5 Min.	24 Hrs.
Semen (control)	79	-	-
1	3	17	0
14	0	0	0
35	40	41	2

Conclusions: Results show that the non-hormonal contraceptive ring examined in this study releases concentrations of FG/AA over a 35 day period that effectively inhibit sperm motility and could lead to further advancements in non-hormonal contraception.

References:

1. Hatcher R.A. et al., *Contraceptive Technology*, 17th Ed., Ardent Media Inc., NY (1998).
2. Smith, J.S. et al., *Lancet*, 361, 1159 (2003).
3. Shalaby, S.W., U.S. Pat. Appl. 05/45,190 (2005).
4. Saxena, B.B. et al., *Contraception*, 70, 213 (2004).
5. Jones, R. et al., *Fertil Steril*, 31, 531-537 (1979).
6. Shalaby, S.W., U.S. Pat. 6,342,065 (2002).
7. Corbett, J.T. et al., *Trans. Soc. Biomater.*, 28, 644 (2005)
8. Tate, P.L. et al., *Trans. Soc. Biomater.*, 28, 645 (2005).

Delivery of Non-toxic Drugs for Enhancing Brain Cancer Therapy

Thomas L. Moore,[†] Tara L. Britton,[†] Erika K. Jelen,[†] Brandon Mattix,[†] Bruce Frankel,[§] Frank Alexis.[†]
[†]Department of Bioengineering, Clemson University, Clemson, SC 29634. [§]Department of Neurosciences, Medical University of South Carolina, Charleston, SC 296425.

Statement of Purpose: Almost 23,000 people are expected to be diagnosed with malignant brain tumors in the United States in 2012.[1] Moreover, brain cancer is the most common form of cancer in children ages 0-14 years old with a 31% mortality rate.[2] Failure to treat brain cancer patients is due to the lack of drug bioavailability, significant drug side effects in children, and significant drug resistance; therefore, there is a need to develop safe treatment to increase bioavailability, decrease drug side effects, and decrease drug resistance.[2] Nanomedicine is a field that could not only improve the therapeutic efficacy of conventional chemotherapy agents, but also offers stronger technology protection by increasing the patent life of therapeutics, allowing a portfolio of patents, and preventing generic formulations.[3]

In contrast to conventional approaches of using more cytotoxic drugs to overcome resistance, we report here a novel approach using a non-toxic drug that increases the efficacy of a chemotherapeutic toxic drug. This new treatment paradigm is expected to prevent new side effects from toxic drug combinations while overcome drug resistance. Our novel approach aims to overcome drug resistance by combining a toxic free drug and a non-toxic drug encapsulated into a nanoparticle composed of FDA-approved biodegradable polymers that can release the drug over a prolonged period of time. This will improve upon current approaches by utilizing the benefits of nanomedicine, namely by specific or passive targeting of tumors, and by mitigating the effects of drug resistance.[4,5] Our preliminary data demonstrates the feasibility of improving drug efficacy of the toxic drug using nanoparticles loaded with non-toxic drug to overcome resistance.

Methods: Nanoparticles (NP) were prepared from poly(lactide)-poly(ethylene glycol) (PLA-PEG) and loaded with the non-toxic agent via a solvent evaporation method. U-87 glioblastoma (ATCC) and U-138 glioblastoma (ATCC) cells were sub-cultured at 37 °C and 5% CO_2 in Earle's modified Eagle's medium (ATCC). Toxicity of drugs and NP was measured with a Presto Blue cell viability assay. Uptake of NP was monitored by incubating fluorescently tagged NP and quantifying uptake into human brain microvascular endothelial cells (HBMEC), U-87 and U-138 cells. Biodistribution studies of NP were performed in U-138 xenografts, nude Balb/c mice. NP were administered via tail vein injection and biodistribution was monitored with fluorescent imaging using an IVIS Lumina XR small animal imaging system.

Results: Preliminary results of nanoparticle uptake in U-138, U-87, and HBMEC shows differential uptake into brain cancer and vascular cells. Preliminary *in vitro* results demonstrated that PLA-PEG nanoparticles loaded with a non-toxic drug significantly increased the efficacy of a toxic chemotherapy drug in U-138 glioblastoma to model drug resistant brain cancer. The non-toxic drug could be released in a controlled manner from the NP. In combination, the non-toxic drug was able to improve the therapeutic efficacy of the toxic drug *in vitro*. Preliminary *in vivo* biodistribution studies of PLA-PEG nanoparticles in nude Balb/c mice with intracranial U-138 tumor xenografts showed accumulation of NP in the brain.

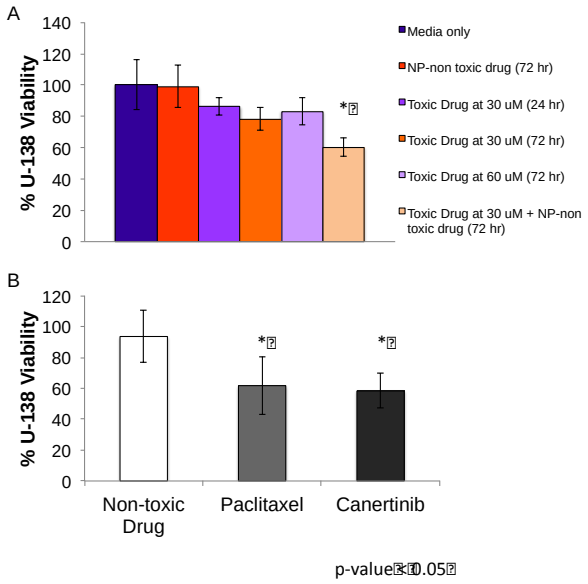

Fig. 1 Short and long term studies of toxic drug at varying concentrations confirmed drug resistance, however treatment with toxic drug and NP loaded with non-toxic drug showed significant increase in toxicity (A). Free non-toxic drug at 100 nM showed no significant toxicity (B). Paclitaxel and canertinib, two known toxic drugs, showed significant toxicity at 100 nM.

Conclusions: In summary, a controlled release drug delivery technology was developed to deliver a non-toxic drug in order to improve therapeutic efficacy in brain cancer. Preliminary *in vitro* studies verify that the non-toxic drug does not affect cell viability, however it improves the efficacy of the anti-cancer drug. Moreover, the controlled delivery NP are able to prolong the release of the non-toxic drug. *In vivo* biodistribution studies show the passive uptake of NP in brain tumor xenografts in mice. This promising drug delivery system has translational potential because of the delivery of non-toxic drugs to improve cancer therapy.

References:

1) ACS. Cancer Facts & Figures 2012.
2) Jemal A. Canc J Clin. 2003; 53: 5-26.
3) Burgess, P. et al. Nat Biotech. 2010; 28: 1267-1270.
4) Maeda H. Advan Enz Regul. 2001; 41: 189-207.
5) Heidel JD, Davis ME. Pharm Res. 2011; 28: 187-199.

Graduate & Undergraduate Research Poster Presentation Abstracts

Accurate molecular dynamics simulation of peptide adsorption to polyethylene, poly(methyl-methacrylate), and silica surfaces using dual-force-field in CHARMM

Tigran Abramyan*, James A. Snyder*, Jeremy A. Yancey*, Steven J. Stuart[#], Robert A. Latour*

*Department of Bioengineering, [#]Department of Chemistry, Clemson University, Clemson, SC

Statement of purpose: In the event of an attack by biological weapons containing toxic proteins, such as ricin, the proteins will contaminate the surrounding environment by adsorbing on exposed material surfaces. A fundamental understanding of the molecular level events accompanying protein-surface interactions (**PSIs**) is thus crucial for the design of safe and effective strategies for surface decontamination for a broad range of environmental surfaces.

All-atom molecular dynamics simulation methods hold great promise as an important tool for understanding and predicting PSIs. However, due to the complex nature of proteins, these methods have to be first properly tuned and validated before they will be able to accurately represent protein adsorption behavior on material surfaces.

Materials and Methods: We use the CHARMM molecular simulation program with available CHARMM force field parameterization to simulate the adsorption behavior for small host-guest peptides (TGTG-X-GTGT: X = N, D, G, K, F, T, W, or V) on three representative surfaces: poly(methyl methacrylate) (**PMMA**), (110) high density polyethylene (**HDPE**), and amorphous silica (**silica glass**). Then we apply advanced sampling methods (umbrella sampling and biased replica exchange molecular dynamics, biased-REMD) in order to accurately calculate adsorption free energy and compare values with experimentally measured adsorption free energies[1]. We then tune interfacial non-bonded van der Waals (vdW) parameters and partial atom charges using our *Dual force field (Dual FF) CHARMM* program[2], to match $\Delta A°_{ads}$ values with experimental values within ±1.0 kcal/mole.

Studies on HDPE surface: Umbrella sampling simulations were conducted for each host-guest peptide on HDPE (Fig. 1), and initial estimates of $\Delta A°_{ads}$ were obtained. Values were found to be deviated by up to 2.0 kcal/mole compared to experimental values. Three independent umbrella sampling simulations were performed to identify the dominant factors controlling peptide adsorption behavior: (*i*) normal CHARMM, (*ii*) vdW interactions switched on only, and (*iii)* electrostatic interactions turned on only.

PMF profiles indicated that vdW effects dominated adsorption while electrostatic contribution was minimal. Interfacial force field (IFF) parameters in *Dual FF* CHARMM were tuned to bring $\Delta A°_{ads}$ from simulation into agreement with experimental values (Fig. 3). Final biased REMD simulations with tuned IFF parameters will provide better agreement with experiment.

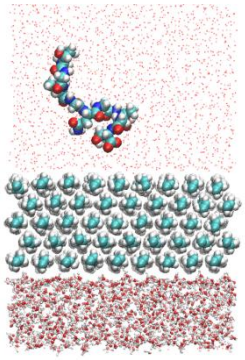

Fig. 1. Representative model for simulations with host-guest (TGTG-N-GTGT) peptide on HDPE (110)

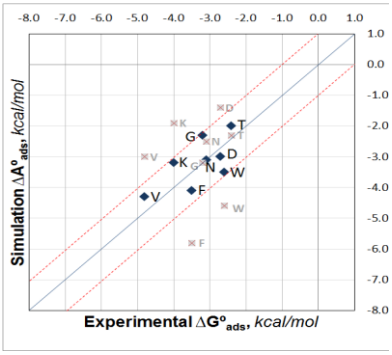

Fig. 2. Comparison of $\Delta G°_{ads}$ values from experiment and $\Delta A°_{ads}$ values from the simulations based on the initial CHARMM parameter set (grey points) and the tuned IFF parameter set

Conclusion and Future Work: Tuning IFF parameters to enable simulated peptide adsorption behavior to closely match experimental behavior using HDPE as a model system is currently in progress. Similar efforts have been in progress to obtain IFF parameters for the TGTG-X-GTGT peptides on PMMA and silica glass[3] surfaces in order to match experimental $\Delta G°_{ads}$ values. Subsequent studies are planned to apply the tuned IFF parameter set to simulate the adsorption of protein-toxin simulants (lysozyme, PDBID: 1GXV; ribonuclease A, PDBID: 5RSA) to each surface, for which synergistically matched experimental studies are also being conducted. Comparisons will be used to validate the developed simulation methods.

Acknowledgements: Research funded under DTRA grant HDTRA1-10-1-0028. Computing resources: Palmetto Linux Cluster, Clemson Univ.

References:

1. Thyparambil A.A., et al., *Langmuir*, 2012
2. Biswas P.K., et al., *J. Comput. Chem*., 2012
3. Snyder J.A., et al., *Biointerphases* (in press)

Development and Characterization of Optical Strain Gauges for Non-Destructive Evaluation of Biomaterials

Dakotah Anderson, Jonathan Heath, Melissa M. Rogalski, Jeffrey N. Anker

Remote non-destructive methods to measure strain are needed for many living systems including strain on bone, orthopedic screws, tissue, and vegetation. We designed prototype optical strain indicators to accurately measure the strain of various objects and materials nondestructively by eye or camera. Strain gauges were printed onto paper and transparencies using conventional inkjet and laser printers. The bottom paper layer of the strain gauges was composed of alternating bands of red and blue ink. The gauges appeared to change color when an overlaid "window pattern" containing transparent and opaque regions was displaced relative to the colored bands below. The strain gauges were attached to various objects/materials as they moved, stretched, or bent. The displacements and strain on the objects were measured by photographing the colored strain gauges with a high-resolution camera. The mean values for red, green, and blue that were present in the images were calculated using MATLAB. A relationship between the amount of blue or red present and displacement could be made using the collected data. The experiments showed that optical strain gauges with 500 μm line widths had a noise level of ±4 μm over a distance of 40 mm. Through the use of a force gauge, stress and strain were calculated and then plotted for a piece of neoprene rubber. Future work includes miniaturizing the alternating color lines printed on the indicators, constructing and testing a screw design, and pursuing additional tests that involve expansion and bending.

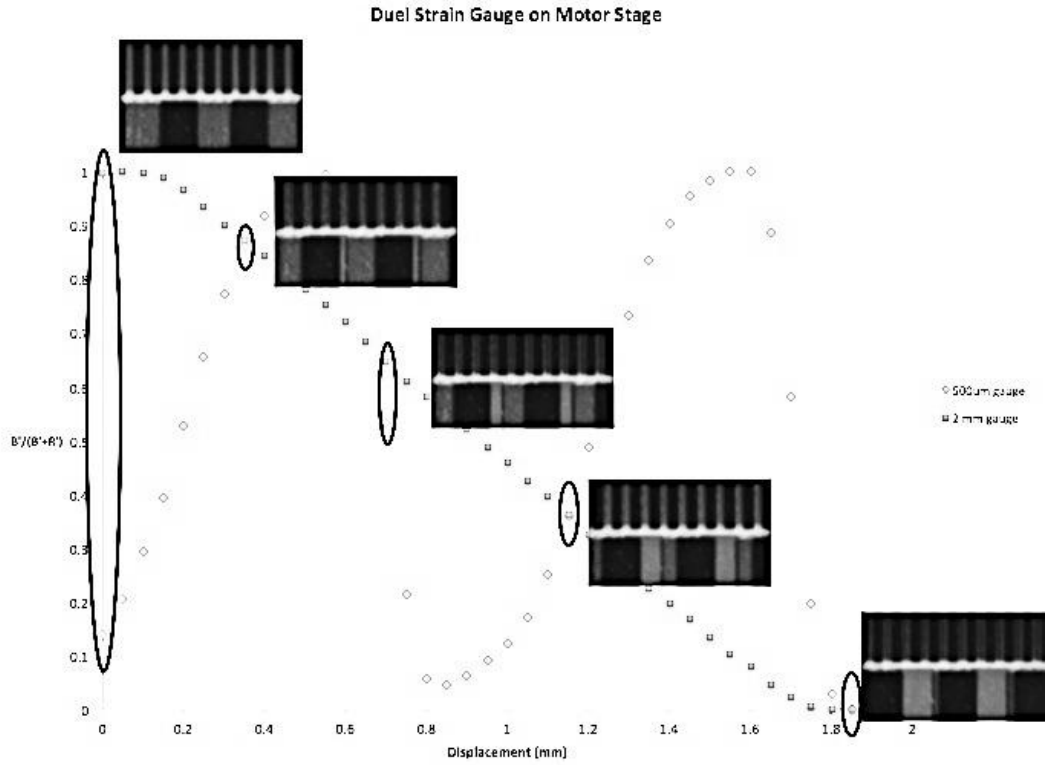

Figure 1 A duel strain gauge illustrating the color variation of the strain gauge when strain is applied to gauge.

Fundamental Synthetic Studies in the Preparation of Thiolene Functionalization of Biodegradable Poly(ε-caprolactone)

Kristin A. Arabea and Brooke A. Van Horn
Department of Chemistry and Biochemistry
College of Charleston, Charleston, SC 29424

With the growing need for improved means to deliver drugs and chemotherapy to specific tissues and cellular targets, scientists today are exploring and developing exciting nanoscale vessels and moving beyond the traditional unspecific small molecule, high dosage therapies. A biocompatible, biodegradable polymeric macromolecule with engineered immunological "stealth" character and surface-available reactive groups would potentially provide a means to covalently link directing groups for specific cellular targets and therapeutic agents to the vessel for timely and precise delivery. These modular polymers (or platform polymers) are highly desired because they afford the flexibility to production multiple functional materials from one precursor polymer system. Past work has demonstrated that linear random copolymerizations occur using allyl-caprolactone (ACL) and commercial epsilon-caprolactone (ε-CL). Functional groups and can be easily reacted with thiol-containing molecules to attach (graft) model compounds to the polymer chains. These functional units impart water solubility to the polymer chains. Our research lab at College of Charleston is interested in the fundamental design, synthesis, and characterization of such nanoscale vessels for a variety of biomedical applications.

Our project focuses synthesis of the biodegradable lactone monomer 7-allyloxepan-2-one (ACL) that is then co-polymerized with ε-CL using the organocatalyst 1,5,7-triazabicyclo[4.4.0]dec-5-ene (TBD). Using 2-allyl-cyclohexanone as the initial starting material and a Baeyer-Villiger oxidation, ACL was synthesized. After purification of the monomer using column chromatography, the final monomeric structure was confirmed using proton nuclear magnetic resonance (NMR) spectroscopy. Prior to co-polymerizations, homopolymerizations using commercial ε-CL with TBD were performed to obtain percent conversion data. Multiple trials of copolymerizations using ACL and ε-CL were performed using TBD. For example, two copolymerizations performed were placed under the same reaction conditions with the same stoichiometric balances, but the final percent conversion of monomers and isolated polymeric material characterization results were varied. Incorporation of the ACL within the final copolymer was confirmed using proton NMR. Polydispersity and average molecular weight of the copolymer were evaluated using Gel Permeation Chromatography (GPC). The final purified copolymer was placed under photo-initiated thiol-ene reactions to react with the alkene units on the copolymer to enable water solubility. These thiol-ene reactions were performed using thiol-terminated poly-(ethylene) oxide chains of varied lengths. Due to difficulties in the copolymerizations, future work will include computational modeling of the ACL-TBD polymerization using density functional theory (DFT) to learn if organocatalysis is limited to unfunctional ε-CL. Future work also includes creating a library of thiol-terminated poly-(ethylene oxide) containing copolymers to perform hydrolytic degradation studies to gather data on the proposed fate of the polymer materials under mimicked cellular conditions. We will present our project at it current state, and highlight our plans and future work.

Controlled Release of Calcium from Bioresponsive Hydrogels

Hanna Aucoin[1,2] and Anthony Guiseppi-Elie[1,2,4,5,6,*]

[1]*Center for Bioelectronics, Biosensors and Biochips (C3B), Clemson University Advanced Materials Center 100 Technology Drive, Anderson, South Carolina 29625, USA*

[2]*Department of Chemical and Biomolecular Engineering,* [4]*Department of Bioengineering,* [5]*Department of Electrical and Computer Engineering, Clemson University, Clemson, South Carolina 29634, USA*

[6]*ABTECH Scientific, Inc., Biotechnology Research Park, 800 East Leigh Street, Richmond, Virginia 23219, USA.*

Statement of Purpose: This research is currently being performed to aid in the development of an innovative product to provide treatment to those individuals suffering from chronic wounds. The goal is to create a "biosmart" hydrogel that will promote wound healing by responding to molecular biomarkers within the wound thus triggering the responsive release of an inhibitor drug from the hydrogel driving away the pro-inflammatory response towards the wound healing response. The influence of cross-linker concentration on the release of calcium ions (Ca^{++}) from within hydrogels was investigated using two approaches. Calcium ions are used as a substitute for cationic drug molecules.

Methods: Biocompatible biomimetic hydrogels of hydroxyethyl methacrylate (HEMA) were synthesized with other monomers along with various concentrations of crosslinker tetraethylene glycol diacrylate (TEGDA) using UV light. Crosslinker densities used were 1, 3, 5, 7, 9, and 12 mol% TEGDA. This synthesis occurred within a silicone mold to form discs from the monomer cocktail. The calcium ions were absorbed from solution into the pre-formed solid hydrogel discs. The release of the calcium ions into 4-(2-hydroxyethyl)-1-piperazineethanesulfonic acid (HEPES) buffer at 37 °C was monitored using a calcium ion specific electrode (ISE). Figure 1a shows the experimental set up. Triplicate runs were performed, and the data gathered were statistically analyzed to generate ISE voltage versus time-release profiles for each cross-linker concentration. These profiles were be fitted to various transport models to calculate calcium ion diffusion coefficients.

Results and Discussion: Release of calcium from hydrogels of varying cross-link density demonstrated an immediate and large burst phase release followed by a subsequently slower release regime (Figure 1b). The data were fit to the following transport release models: Higuchi, Korsemeyer-Peppas, Hixson-Crowell, and First and Second Order. The Hixon-Crowell Cube Root Law provided the best fit ($R^2 \geq 0.85$). The diffusivity was calculated to be on the order of 1.0×10^{-6} cm^2s^{-1}, which compares to 1.0×10^{-5} as reported by Kotanen, *et al*, and $2.0–2.5\times10^{-6}$ cm^2/s for Ca^{++} in buffer [1].

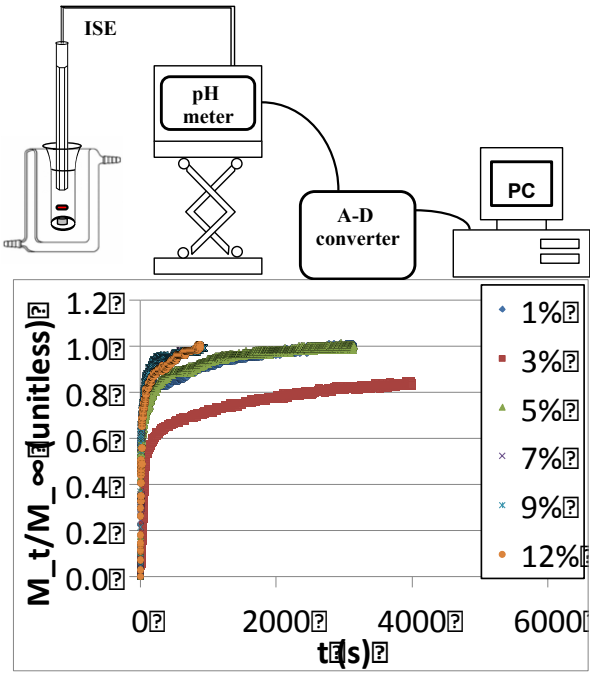

Conclusions: The release kinetics showed no correlation of the calcium release profiles with the cross-linking density. This is in sharp contrast to similar work of calcium transport through hydrogel membranes [1]. This is theorized to be a result of the low partition coefficient of calcium in the poly-HEMA based hydrogels. Continued research will be to investigate industrially available acrylate based hydrogels.

Acknowledgements: Calhoun Honors College, US DoD PRMRP grant DAMD17-03-1-0172 and the C3B.

References:

[1] Christian N. Kotanen, A. Nolan Wilson, Ann M. Wilson, Kazuhiko Ishihara and **Anthony Guiseppi-Elie** *BMMD* (**2012**) 14(3) 549-558.

The Effect of Vibratory Stimulation on Fibroblast Gene Expression

Soon Eon Bae, Jeoung Soo Lee, Jeremy L. Barth (MUSC), Ken Webb
Department of Bioengineering, MicroEnvironmental Engineering Laboratory,
Clemson University, 301 Rhodes Research Center, Clemson, SC 29634, US

Statement of Purpose: The human vocal folds are laryngeal connective tissues that develop unique structure/composition to withstand the substantial mechanical forces required for vocalization. Previous studies have shown that exposure of fibroblasts during in vitro culture to physiologically relevant vibratory stimulation significantly affects cell growth and gene expression.[1-4] However, the vibratory mechanisms responsible for the development and maintenance of vocal fold ECM remain incompletely understood. The objective of this study was to investigate the influence of variations in the three principle vibratory loading characteristics (frequency, amplitude, and duration) on the expression of fibroblast ECM-related genes.

Materials and Methods: Adult normal human dermal fibroblasts (NHDF, Lonza) were seeded on the porous Tecoflex sponges (25 mm long × 3 mm thick × 5 mm wide) at 1.2×10^6 cells/sample. Substrates (n=3/group) were incubated under static conditions for 4 days, then transferred to bioreactors constructed as previously described[1], subjected to a one-time 20% axial strain, and cultured for 6 hours under various vibratory regimes where one loading characteristic was varied while the other two were held constant. Vibratory amplitude was varied as a function of the voltage applied to the voice coil actuator (2.5, 5.0, and 7.5 V, constant 100 Hz) and frequency was varied from 25-125 Hz and constant 5.0 V. Samples were immediately lysed in Trizol and total RNA isolated from the aqueous phase using the RNeasy Mini kit (Qiagen). Two step real time RT-PCR was performed using Retroscript kit (Ambion) and Quantitect SYBR green PCR kit (Qiagen) and target-specific primers for HA synthase 2 (HAS2), fibromodulin (FMOD), TGF-β1, decorin (DECR), matrix metalloproteinase-1 (MMP1), type I collagen (COL1), connective tissue growth factor (CTGF). Relative gene expression levels were calculated using ΔΔCt method with β-2 Microglobulin (B2MG) as an internal standard.

Results: Figure 1 shows changes in expression levels of matrix-related genes in fibroblasts exposed to variable vibratory amplitude (a) and frequency (b) relative to static controls. There were significant differences in fibroblast gene expression as the parameters of vibratory stimulation were varied. In general, HAS2, MMP1, and CTGF showed the most overall sensitivity to vibration. HAS2 and CTGF were particularly affected by the amplitude of vibration, with relatively high amplitude loading (5.0 and 7.5V) stimulating significant increases in expression, while relatively low amplitude loading (2.5V) was not significantly different from the static control group. **Conclusions:** Exposure of fibroblasts to vibratory stimulation produced significant changes in matrix-related gene expression. HAS2 and CTGF exhibited sensitivity to changes in vibratory amplitude. The overall induction of HAS2 and MMP1 is consistent with the relative enrichment of glycoaminoglycans and proteoglycans relative to fibrous matrix proteins in the vocal mucosa and consistent with previous results [1,3]. The strong and consistent induction of the pro-fibrotic cytokine CTGF was unexpected. Current studies are using microarray analysis to gain further insight into the global patterns of gene expression activated in response to applied vibration.

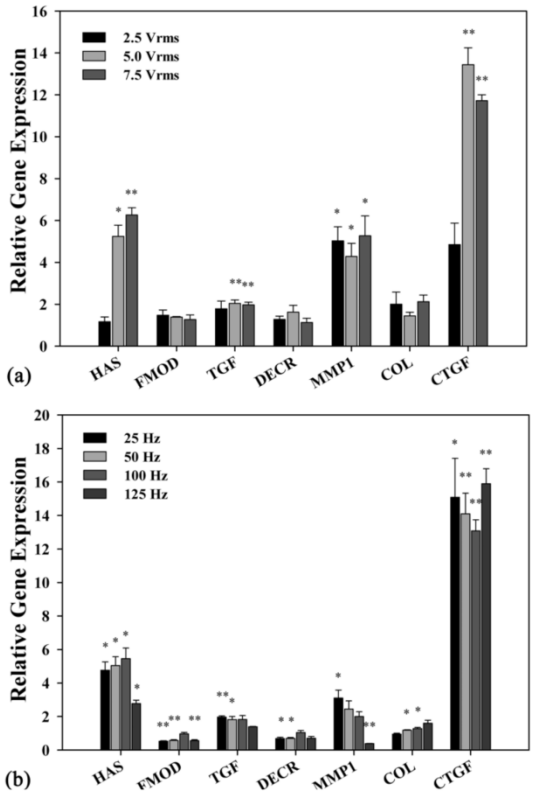

Figure 1. The effects of vibratory stimulation with variable amplitude (voltage) (a), and frequency (b) on fibroblast gene expression using real time RT-PCR.
*P < 0.05, **P<0.01 vs. control.

Acknowledgements: The authors gratefully acknowledge funding and support provided by Grants # R21EB009489, P20RR021949-03, and 8P20GM103444-04 from the National Institute of Health.

References: 1. Titze et al. J Biomech 2004;37:1521–9. 2. Wolchok et. al. Biomaterials 2009;30:327-35. 3. Kutty et al. J Tissue Eng Regen Med 2010;4:62–72. 4. Farran et al. J Tissue Eng Regen Med doi: 10.1002/term.514.

pH and Redox Dual Responsive Nanoparticle for Nuclear Targeted Drug Delivery

Remant Bahadur K.C.[1] and Peisheng Xu*

Department of Pharmaceutical and Biomedical Sciences, South Carolina College of Pharmacy, University of South Carolina, 715 Sumter Street, Columbia, South Carolina 29208, Ph. 803-777-0075, *Email: xup@sccp.sc.edu

Statement of Purpose: Smart polymeric nano-therapeutics with appropriate target-specific moieties (ligands) is evolving as alternatives of conventional (free drug) chemotherapy for the treatment of solid carcinomas (1). Ligands lead the carriers to the site of interest thereby minimize the side effects and enhance the therapeutic effects of the drugs (2). Currently, generation of endogenous stimuli sensitivity into these carriers has been evolved extremely since the synergism of two factors of a single platform can have significant effect in treatment (3). Dithiol (-S-S-) linkage is one of the most important and extensively explored endogenous stimuli generated into nano-carriers for drug delivery application because it have enough stability in extracellular compartment while liable in reducing intracellular environment (1,3). In this research, we have synthesized a functional polymer (PDS) and conjugated with cyclo(Arg-Gly-Asp-D-Phe-Cys) (cRGD) peptide for target delivery of doxorubicin (DOX) to human colorectal cancer cells (HCT-116).

Methods:

Materials: Aldrithiol-2 (from Tokyo Chemical Industry Co., LTD, Portland, OR, U.S.A.), 2-mercaptoethenol, DL-dithiothreitol (DTT), doxorubicin (DOX), thiazolyl blue tetrazolium bromide (MTT), L-glutathione (GSH), and 2, 2-azobisisobutyronitrile (AIBN) (from Sigma-Aldrich Chemical Co., St. Louis, MO, U.S.A.), PEG-SH (mPEG-SH) (MW = 5000 Da) (from Laysan Bio., Inc., Arab, AL, U.S.A.) *cyclo* (Arg-Gly-Asp-d-Phe-Cys) (cRGD) peptide (from Peptide International, Louisville, KY, U.S.A.), Dulbecco's Modified Eagle Medium (DMEM; high glucose with L-glutamine) (from Invitrogen, Grand Island, NY, U.S.A.), McCoy's 5A Modified Medium (with L-glutamine) and fetal bovine serum (FBS) (from ATCC, American Type Culture Collection, Manassas, VA, U.S.A.) were used without any further purification unless otherwise noted.

Method: Side chain functional polymer, poly(2-(pyridin-2-yldisulfanyl) (PDS) was synthesized by free radical polymerization of 2-(pyridin-2-yldisulfanyl)ethyl acrylate (PDSA) using AIBN as an initiator. Then PEG and cRGD were grafted onto the polymer by thiol-disulfide exchange reaction and then DOX was physically encapsulated. cRGD conjugation is expected to enhance the carrier selective targeting to cancer cells over expressing $\alpha_v\beta_5$ integrin and -S-S- bonding is apparently beneficial for the intracellular disassembly of the nanoparticles which is expected to prompt release of the drug. We hypothesized that these nanoparticles could be effective carriers for the delivery of DOX to $\alpha_v\beta_5$ integrin expressing tumor cells to enhance the chemotherapeutic effect with minimized side effect. Drug carrier efficiency of the nanocarriers into cancer cells was monitored through flow cytometry and confocal microscopy. Anticancer activity of the nanocarriers in cancer cells was analyzed through MTT assay.

Results: cRGD conjugation significantly improve the anticancer activity of the nanoparticles (RPDSG/DOX, IC_{50} 0.3 ± 0.015 µM, day-3) in HCT-116 cell while comparable to non-targeting nanoparticles (PDSG/DOX, IC_{50} 0.73 ± 0.15 µM, day-3) and it was comparable to free DOX (IC50 0.27 ± 0.026 µM, day-3) (Figure 1).

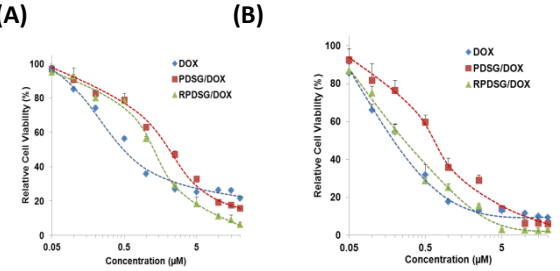

Figure 1. Anticancer activity of free DOX or DOX encapsulated nanoparticles in HCT-116. Cells were treated with different concentration of drug for 48 hr (A) and 72 hr (B). Data represent mean ± SD (*n* = 3).

The improved anticancer activity of the nanoparticles was the direct consequences of cRGD assisted endocytosis because, cRGD conjugated nanoparticles showed better *in vitro* cellular uptake while observed through confocal microscopy (Figure 2).

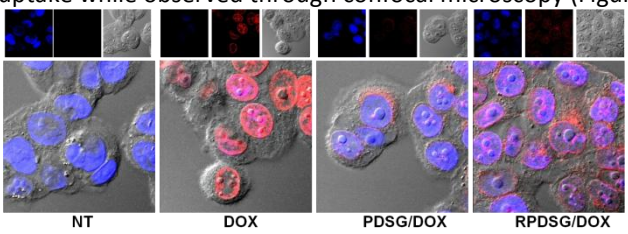

Figure 2. Confocal microscopy of HCT-116 cells treated with free DOX or DOX encapsulated nanoparticles after 3 hr. treatment. Cells treated with free DOX and RPDSG/DOX showed concentrated DOX in nucleus, whereas the cell treated with PDSG/DOX nanoparticles showed an evenly distributed DOX around nucleus. Note: nuclei stained with Hoechst 33342 (blue), intracellular DOX (red).

Conclusions: We have synthesized RPDSG by free radical polymerization of PDSA followed by grafting PEG and cRGD. cRGD conjugation enhanced the cellular uptake and nuclear localization of nanoparticles and exhibits IC_{50} close to that of free drug for HCT-116 cells. Due to duel sensitivity, RPDSG/DOX showed higher anticancer efficacy than free doxorubicin at drug concentration higher than 5 µM.

References:

1. Putnam D. Nat Mater. 2006; 5: 39-51.
2. Brannon-Peppas L., Blanchette JO, Adv Drug Deliv Rev. 2004; 56: 1649-1659.
3. Meng, F., Hennink WF., Z. Zhong Z. Biomaterials 2009; 30: 2180-2198.

Evaluating Mechanical Performance of Hydrogel-Based Adhesives for Soft Tissue Applications

Nitin Balakrishnan, Ben Fleishman, Lindsey Sanders, Ken Webb, Jiro Nagatomi.
Department of Bioengineering, Clemson University

Statement of Purpose: Accidental laceration of the bladder is the most frequent complication during hysterectomies and is generally repaired by suturing. However, suture repair method prevents proper distension of the wall tissue and necessitates drainage via catheters during healing, decreasing patient quality of life. The long-term goal of our study is to eliminate the need for suturing by creating a surgical adhesive that provides a combination of strength, compliance, and biocompatibility for application to the bladder. There are limitations with current FDA-approved surgical adhesives such as insufficient adhesion with fibrin sealants and the potential cytotoxicity in cyanoacrylates [1]. Therefore, to work toward achieving this long-term goal, we are currently exploring Tetronic (BASF Corporation), 4-arm amphiphilic AB block copolymers of polypropylene oxide (PPO) and polyethylene oxide (PEO) as a biological adhesive. Since Tetronic exhibits rapid thermal gelation at physiological temperatures, it provides an advantage over other types of hydrogels as it causes near instantaneous gelation upon contact with tissue. The overall objective of the present research is to significantly improve mechanical properties, namely the strength of Tetronic bladder adhesive by varying macromer blend ratios and concentrations.

Methods: Synthesis: Briefly, Tetronic T304, T904, and T1107 (MW 1500 Da, MW 6700 Da, and MW 15030 Da respectively) were reacted in dichloromethane and acryloyl chloride to form terminal acrylate groups using previously established methods [4]. The final synthesized product was characterized through NMR spectroscopy to determine the acrylation conversion percentage of the final product.

Mechanical Testing: Following acrylation, the Tetronic acrylate was cross-linked using dithiothreitol (DTT) as a donor of the thiol-group. The bulk strengths of various blends of the Tetronic adhesive were determined via calculating maximum tensions from end-to-end tensile adhesion tests on collagen sheets. For the end-to-end test, specimens were sectioned into ½ inch-wide strips and placed in a fixture that maintained end-to-end contact of two pieces. Then, approximately 50 µl of the Tetronic acrylate/DTT mix was applied to the joint. After thirty minutes of curing at 37˚C, the bonded specimens were subjected to uniaxial tensile tests using the MTS machine. The specimens were loaded at a speed of 5 mm/min until the bonded joints broke. The resulting data were reported as maximum tension to failure (N/cm).

Results: The use of a low molecular weight Tetronic, T304 acrylate (74% acrylation conversion; 58% product yield) blended with T1107-acrylate (93% acrylation conversion; 66% product yield) at a ratio of 75:25 at 40wt%, yielded an average maximum tension of 0.41 ± 0.06 N/cm from 6 samples and 0.45 ± 0.05 N/cm from 3 samples at a 50:50 ratio of T304/T1107 at 40wt% (Fig 1). These values were significantly greater than the maximum tensions for T904/T1107 at 40wt%: 0.15± 0.02 N/cm for 75:25 and 0.07± 0.01 N/cm for 50:50 (Fig 2). [3]

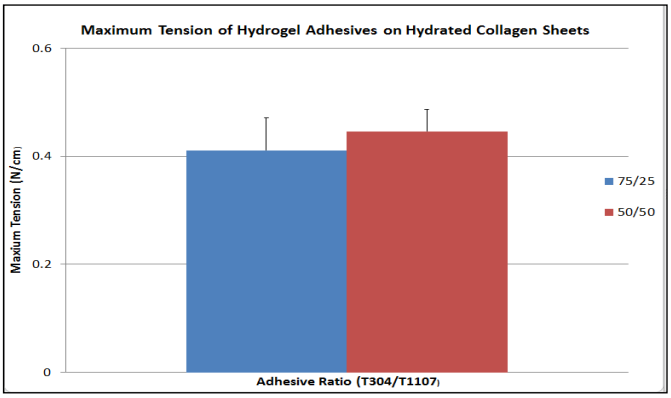

Figure 1: End-to-End Testing Mechanism for T304/T1107 ratios at 40 wt% (n=6 for 75/25, n=3 for 50/50)

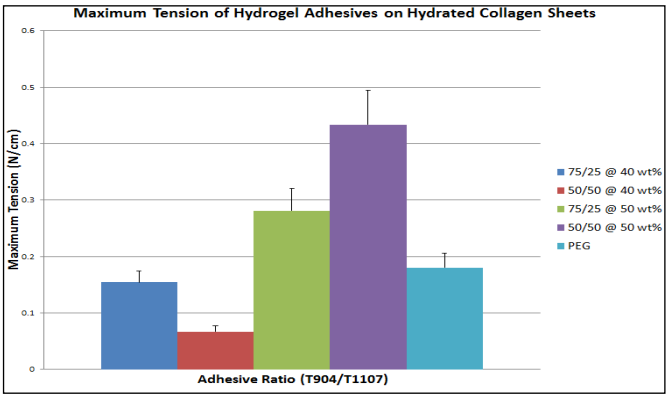

Figure 2: End-to-End Testing Mechanism for T904/T1107 ratios at 40wt%, 50wt%, and PEG control (n=9) [3]

Conclusions: The previous study by our group demonstrated that the bulk strength of the Tetronic adhesive tested was significantly lower than the maximum tension experienced by the human bladder under physiological conditions. Based on the literature report of an ultimate tensile stress of the human bladder under uniaxial tension loading, 270 kPa [2], and an approximate thickness of 2mm, the maximum tension for the human bladder would need to be around 5.4 N/cm. The results for acquired for maximum tension from the two T304/T1107 blends previously mentioned demonstrate positive strides towards that goal, but require further improvement. Future work includes, but is not limited to continuing to vary blend ratios of T304-acrylate with T1107-acrylate while simultaneously increasing the weight percentage of the hydrogel to increase bulk strength of our tissue adhesive. Moreover, rheological measurements will be acquired to characterize the viscoelastic behavior of the various Tetronic blend ratios. Finally, the tissue adhesive will be tested on bladder samples ex vivo in order to provide further insight into clinical applications.

References:

[1] Artzi N. Macrmol. Biosci. 2009; 9:754-765)
[2] Dahms SE. Brit J Urol. 1998; 82: 411-419
[3] Fleishman, B (unpublished) [4] Cribb, R and E. Cho (2009)

Sustained Release of Estrogens from PEGylated Nanoparticles for Treatment of Secondary Spinal Cord Injury

John Barry[1], Joshua Smith[2], Naren Banik[2], Alexey Vertegel[1]

[1]Clemson University, Clemson, SC; [2]Medical University of South Carolina, Charleston, SC

Introduction: Spinal Cord Injury (SCI) is a debilitating condition for many people, young and old, which causes neurological damage and can result in paralysis. Acute SCI results in an initial damage to the spinal cord, but secondary injury due to inflammation and activated biochemical pathways leading to apoptosis exacerbate the injury. β-estradiol, an estrogen, is effective at ameliorating many of events involved in secondary SCI including apoptosis. However, the therapeutic effect is limited by low retention time of the drug at the affected location. A rapid drop in local drug concentration reduces efficacy. Consistent application is undesirable due to side effects, problems with patient compliance, and a desire to limit discomfort. We propose to develop PEGylated nanoparticles with estrogen loaded for treatment of SCI. Our hypothesis is that the extended circulation time, reduced immunogenicity, and controlled release endowed by the nanocarrier will enhance the efficacy of the drug compared when with the undelivered drug.

Materials and Methods: Drug-loaded PLGA nanoparticles were prepared using nanoprecipitation method. Briefly, Poly(D,L-lactide-co-glycolide) was mixed with PEG-PLA copolymer (Mw 5,000 PEG:5,000 PLA) an estrogen or a corresponding estrogen receptor agonist in 10:2.5:1 (wt.) ratio and dissolved in acetone. This solution will be added dropwise to 20 mL of DI water in an ultrasonic water bath and sonicated for 30 minutes. The particles were then separated by centrifuging (7500 rcf), washed three times with DI water and resuspended in 2 mL of PBS buffer. Particle size will be determined using dynamic light scattering. Estrogen loading yield will be determined using UV-Vis spectroscopy following β-estradiol at 285 nm. Viability was determined using an MTT viability assay. Briefly, neuroblastoma cells were seeded onto a 24 well plate. Cells were pre-treated with drug (37 μM) for 24 hours before challenged by glutamate (17 mM). Glutamate will induce apoptosis in neuroblastoma cells and will provide a good in vitro model for apoptosis. Viability was followed at 570 nm using the MTT (thiazolyl blue tetrazolium bromide) colormetric reagent. In vitro release was determined by measuring the drug remaining in particles after dialysis with 3% bovine serum albumin in physiological PBS solution.

Results and Discussion: Using the methods described, we were able to load β-estradiol into nanoparticles with an efficiency of 56%. Before we could test the efficacy of the nanoparticle delivered estrogen, we replicated the experiments using delivery of β-estradiol by dimethyl sulfoxide (DMSO) [1]. In our results, we saw a significant difference ($P<0.05$) in viability after glutamate challenge between drug treated groups (including dissolved nanoparticles and free drug) and the untreated group. However, there was significantly lower viability in cells treated with glutamate and DMSO compared with those only treated with glutamate ($P<0.0005$), indicating that DMSO is not the ideal delivery agent. We then tested nanoparticle delivered β-estradiol and again saw a significant increase in viability ($P<0.01$) when compared to the β-estradiol untreated (Fig. 1). These results indicate

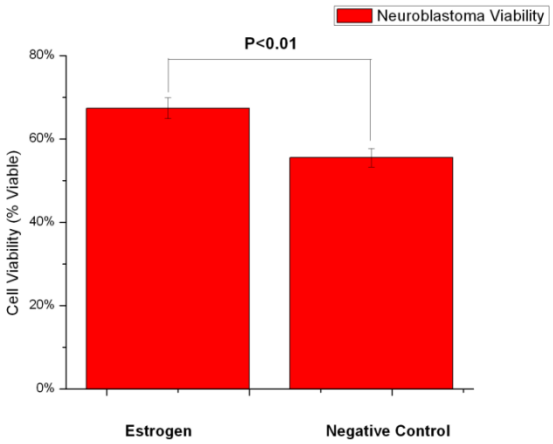

Figure 1. β-estradiol delivered by PLGA nanoparticles are effective at protecting neuroblastoma cells from apoptosis when challenged by glutamate.

that the nanoparticle delivered drug is effective at preventing apoptosis, and does not induce the toxicity present in DMSO delivered drug. In addition, the nanoparticle delivery system will offer controlled release and increased tissue residency time. Our in vitro release studies indicate that the drug is released slowly over five days. This release profile is appropriate for treatment of SCI which sees the most severe secondary effects within the first 3-4 days following injury. The dose and time of release can be customized as needed in this delivery modality. These advantages will allow for a consistent local dose, fewer treatments for the patient, and a more effective treatment than bolus dose administration.

Conclusions: Our results indicate that β-estradiol is an effective neuroprotectant. It effectively increased cell viability both when delivered by DMSO and when delivered via our nanoparticle. In addition to increased viability, our nanoparticulate delivery will enhance the efficacy of the drug through controlled release and increased tissue retention time.

Acknowledgements: This work was founded by NIH grant no. 2P20RR016461-10 and 8 P20 GM103444-04 awarded to the South Carolina Research Foundation, and NIH grant no. P20RR021949.

Reference: 1. Sribnick, E. A, et al. *J. Neurosci. Res.*, (2004) 76:688–696.

Electrofluidics at the Nanoscale

Samuel Bearden, Dr. Guigen Zhang

Statement of Purpose: Electrofluidic currents through nanopores remains a topic of interest due to applications in molecular sensing and other novel characteristics of nanoscale flow.[1,2,3,4] Ionic currents in single wall carbon nanotubes may be orders of magnitude larger than predicted by standard conductivity models.[2,3] Ionic conductivity and the concentration of the electrolyte solution are related by a characteristic power relationship.[2] Because of the small diameter of the channels (on the order of a few nanometers), the interaction between the solution and material surface may play a significant role in affecting the electrofluidic performance.[5] The purpose of this study is to demonstrate that the enhanced current observed through single wall carbon nanotubes may be satisfactorily explained by known electrochemical effects.

Methods: A numerical simulation of nanochannel fluidics consisted of simultaneously solving the Nernst-Planck, Navier-Stokes, and Poisson equations over a 2-dimensional axisymmetric geometry. The ionic distribution, electrophoresis, electroosmotic flow, as well as parameters describing the complete electrical double layer were investigated.

Results: The conductance calculated by the present model exhibited the appropriate power relationship and enhanced current. The thickness of the compact layer was found to increase with bulk solution concentration, as expected based on a physical interpretation of the structure.

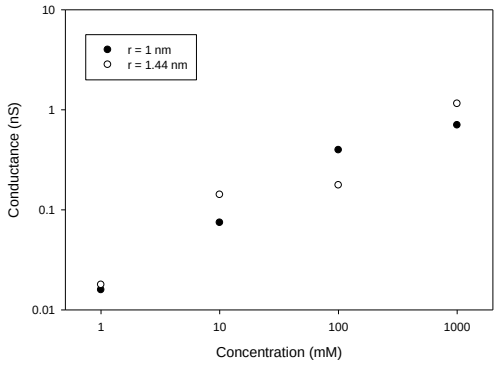

Figure 1. Variation of ionic conductance with bulk solution concentration.

Fluid flow through the nanotube was found to be proportional to the bulk fluid concentration and inversely proportional to the thickness of the compact layer. The enhanced current through the nanotube was due to electroosmosis, as previously reported.[2] A thicker compact layer effectively reduces the internal volume of the nanochannel and thus leads to a reduced fluid velocity. The reduction of electroosmotic flow at higher bulk concentrations (which correspond to thicker compact layers) is responsible for the characteristic power relationship of such nanotube devices.

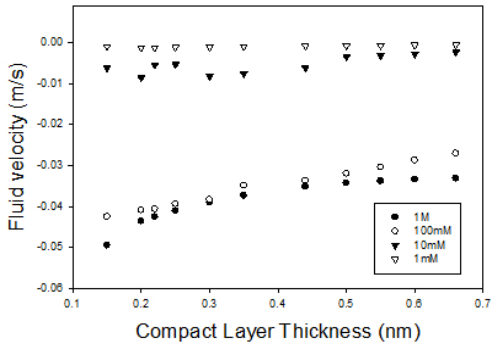

Figure 2. Fluid velocity as a function of compact layer thickness and bulk solution concentration.

Conclusion: A rigorous computational model of ionic current through a single wall carbon nanotube was created. All structures and parameters were within the commonly accepted ranges. The simulation results agree well with experimental measurements and provide insight into the unique mechanics of such devices.

References:

(1) Timp, W.; *et al. IEEE transactions on nanotechnology* **2010**, *9*, 281–294.
(2) Pang, P.; *et al. ACS nano* **2011**, *5*, 7277–83.
(3) Majumder, M.; *et al. Nature* **2005**, *438*, 43–4.
(4) Siwy, Z. S. *Advanced Functional Materials* **2006**, *16*, 735–746.
(5) Yang, X.; Zhang, G. *Nanotechnology* **2007**, *18*, 335201.

Characterization of *Nephila Clavipes* Spider Silk Structure

J. Canavan[1], B. Faugas[2], D.Dean[1], M. Kennedy[2], M. Ellision[2]
[1]Department of Bioengineering, Clemson University, Clemson, SC 29634
[2]Department of Materials Science & Engineering, Clemson University, Clemson, SC 29634

Statement of Purpose: The spider *Nephila clavipes*' dragline silk has incredible mechanical properties with a tensile strength of 1GPa, a Young's modulus of 12.7GPa, a rupture elongation of 18%, and a toughness of 80 MJ/m^3, making it stronger in these terms than Kevlar© 49 fiber[1]. Being able to create a fiber with similar properties to that of the *Nephila clavipes* dragline silk will allow for a vast number of advancements in products, as well as innovative systems. Previous research has been conducted on the properties and structure of spider silk; however minimal research has been done on the internal structure of *Nephila clavipes* dragline silk.

Methods: To expose a cross section of the dragline silk for analysis, an attempt to freeze fracture the silk on silicon wafers was made. Another approach was taken to expose a cross section as well. The standard "C" for fiber analysis was cut out of paper and super glue fastened the silk to the paper. Under liquid nitrogen, the paper was bent so as to break the silk. The fracture sites were analyzed using an Hitachi SU6600 SEM.

For the purpose of tagging negative and positive amino acids on the silk surface, gold nanoparticles were functionalized with either COOH groups or NH_2 groups that attach to positively and negatively charged amino acids, respectively. This process was created by Clemson University undergraduate student James Chow, and is described in reference[2].

In order to analyze the percent of surface area covered by negative and positive amino acids, images were taken of the silk covered with functionalized nanoparticles by Mr. Benoit Faugas. Image Pro Plus 6.3 was then used to calculate the area covered by the nanoparticles and t-tests were used to draw conclusions on various treatments tested on the silk.

Results: The two freeze fracture methods revealed a "core" and "shealth" internal structure in the silk as seen in **FIGURE 1**. Besides this, both methods for exposing a cross section proved to be inconclusive. One problem that arose with the second method described included ductile fracture sites.

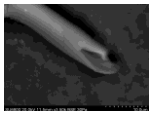

FIGURE 1: "Core" and "Sheath" Structure Apparent from Freeze Fracturing Methods

TABLE 1 depicts the results of the t-tests run on the silk coated with functionalized nanoparticles that underwent various treatments. **TABLE 2** shows the percent of area covered by the functionalized nanoparticles on silks that underwent various treatments.

TABLE 1: T-Test Results for Various Comparisons

Treatment Comparison	P-Value (α=.05)
No Treatment, + vs. - Amino Acid Areas	2.29E-05
PBS Wash vs. No Wash, - Amino Acid Area	0.506
Stretched vs. Unstretched, + Amino Acid Area	0.628
Stretched vs. Unstretched, - Amino Acid Area	2.04E-14
Stretched and Ethanol Wash vs. Unstretched and Ethanol Wash, + Amino Acid Area	0.178
Ethanol Wash vs. No Wash, + Amino Acid Area	0.053
1 PBS Wash vs. 2 PBS Wash, - Amino Acid Area	0.104

TABLE 2: Averages and Standard Deviations of Silk Surface Area Covered by Nanoparticles

Silk Treatment	Charge of Functional Group Used*	Average Relative Area on Surface (%)	Standard Deviation
none	-	1.836	2.263
none	+	4.959	2.049
stretched	-	1.615	0.811
stretched	+	19.096	4.478
ethanol wash + stretched	-	1.159	0.947
PBS wash	-	5.462	2.763

Conclusions: Future work on obtaining a clear cross section of the silk includes covering the silk in an apoxy and microtoming it.

There is a significant difference between the number of negative and positive amino acids present on the surface of the silk and it can be inferred that there are more negative amino acids on the surface than positive. Stretching the fiber increases the negative amino acids exposed to the surface, but the number of nanoparticles marking positive amino acids remains essentially unchanged. Any amount of washing with PBS does not affect the number of nanoparticles that attach to negative amino acids. However, the t-tests indicate that washing the silk with ethanol before applying the functionalized nanoparticles does slightly affect the amount that attaches onto positive amino acids.

References:

[1]Faugas, Benoit. "SURFACE CHARACTERIZATION OF NEPHILA CLAVIPES DRAGLINE SILK." MS thesis. Clemson University, 2012. Print.

[2]Zimmerman, B. "Mechanical and chemical Characterization of Biological Composite Structures", MS Thesis, Clemson University, 2009.

Spatial Control of Magnetic Nanoparticles Integrated with Cellular Spheroids as Tissue Engineered Building Blocks

Megan Casco[1], Trey Poole[1], Rick Visconti[2], Dan Simionescu[1], Agneta Simionescu[1], Brandon Mattix[1], Frank Alexis[1].
[1]Clemson University, Dept. of Bioengineering, Clemson, SC.
[2]Medical University of South Carolina, Dept. of Regenerative Medicine and Cell Biology, Charleston, SC.

Statement of Purpose: Cell aggregates, or spheroids, have gained recent attention as tissue engineered building blocks as well as *in vitro* assays that can closely mimic the natural three-dimensional *in vivo* environment. The incorporation of magnetic nanoparticles (MNPs) into cellular spheroids can allow for manipulation of spheroids into desired shapes, patterns, and three-dimensional (3D) tissues using magnetic forces. However, current strategies to incorporate MNPs often involve unintentional cellular uptake. It has been shown that internalization of MNPs into cells can induce adverse effects on cell activity, viability, and phenotype, and should therefore be avoided. Additionally, cellular spheroids have been proven to fuse together when placed within contact of each other, but a method to maintain spheroids in a set location is needed for complex tissues. We report the fabrication of a novel structure of magnetic cellular spheroids with spatial control of the MNPs to form two distinct domains: cells and MNPs, respectively. This separation of cells and MNPs to form distinct domains within the magnetic cellular spheroid has no adverse affects on long-term viability, phenotype expression of SMC markers, and allows for magnetic manipulation and fusion into controlled patterns. Ultimately, a spheroid construct possessing two segregated domains, one composed of cells and one composed of MNPs, would fully incorporate the positive benefits of using magnetic spheroids to go beyond current approaches. This spatial control of MNPs limits the contact with cells and therefore reduces uptake while still allowing for magnetic manipulation.

Methods: The majority of studies were performed using rat aortic smooth muscle cells (SMCs). Additionally, rat aortic fibroblasts and human adipose derived stem cells (ADSCs) were utilized when needed. Spheroid viability was quantified using two viability assays, MTT (Sigma-Aldrich, St. Louis, MO) and PrestoBlue (Life Technologies, Grand Island, NY), and also qualitatively confirmed using simultaneous live/dead fluorescent confocal microscopy. All experiments were performed with cellular spheroids with (IO) and without (NIO) MNPs as a control. Viability was normalized to samples without MNPs (NIO). The spatial location and orientation of MNPs and cells within the spheroid were histologically analyzed using standard paraffin fixation and staining. Magnetic cellular spheroids were aligned into a variety of patterns and allowed to fuse using commercial magnets. SMC phenotype marker expression was quantitatively and qualitatively analyzed using flow cytometry and fluorescent immunohisto-labeling for smooth muscle α-actin (SMαA), smooth muscle myosin heavy chain (SMHC), and smooth muscle 22 (SM22).

Results: Viability of magnetic cellular spheroid was maintained up to seven weeks with an iron oxide concentration of 0.3 mg/mL. Additionally, high cell viability was maintained in magnetic cellular spheroids fabricated with various collagen concentrations, cell densities, iron oxide concentrations (up to 5 mg/mL), and cell types (SMCs, fibroblasts, and ADSCs). Histological examination of magnetic cellular spheroids revealed that spheroids possessed two distinct domains: MNPs and cells, respectively. This was confirmed with multiple magnetic cellular spheroids formulations, including various MNPs and collagen concentrations. Additionally, SMC phenotype expression was confirmed for all three markers in samples with and without MNPs, with over 98.6% expression for all markers and formulations. Finally, magnetic cellular spheroids were patterned and successfully fused to form homogenous 3D tissues into multiple shapes and sizes. This strategy has been expanded to form a fused tubular tissue 5 mm in diameter composed solely of magnetic cellular spheroids.

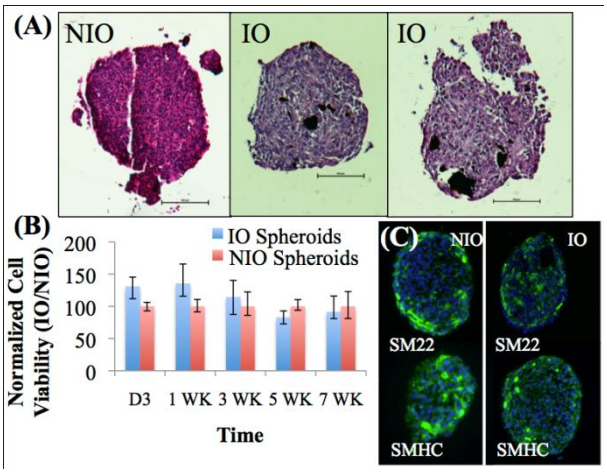

Fig 1. **(A)** H&E staining of magnetic cellular spheroids demonstrating separation of domains; **(B)** Long term viability from 3 days up to 7 weeks compared to spheroids without MNPs; and **(C)** IHC SMC phenotype marker expression (blue = nucleus, green = marker)

Conclusions: Results reveal that this novel method to incorporate MNPs into biological structures can go beyond current approaches using MNPs to engineer heterogeneous constructs composed of multiple cell lines with long term cell viability and no phenotypical affects. This allows for control of spheroid size, cell number, cell types, ECM composition, and magnetic properties to fabricate custom tissue building blocks. We have demonstrated that this technique can be used to successfully align and manipulate spheroids into controlled patterns and promote their fusion over time, a strategy that can be used to assemble larger tissue constructs through fusion of multiple cellular spheroids. Furthermore, we have demonstrated that viability is maintained up to seven weeks with MNP concentrations higher than those used by other groups that have shown adverse affects related to MNPs. The ultimate goal of this technology will be the assembly of larger tissue structures using magnetic forces.

Radioluminescent nanocapsules for controlled cancer drug release and release monitoring

Hongyu Chen, Thomas Moore, Bin Qi, Daniel C. Colvin, Erika K. Jelen, Dale A. Hitchcock, Jian He, O. Thompson Mefford, John C. Gore, Frank Alexis,* Jeffrey N. Anker*

Department of Chemistry, Department of bioengeering, Clemson, SC, 29634

It is a challenge to deliver chemotherapy agents to tumor cells while reducing systemic toxicity to non-cancerous cells. Stimuli such as pH have been studied as triggers for drug release.[1-3] They have the potential for site-selective controlled release when combined with nanoparticles because this system may allow releasing drugs into the blood only gradually, but rapidly release drugs after endocytosis in acidic tumor lysosomes and endosomes However, it is difficult to measure release *in vivo* after systemic administration. To rationally design effective chemotherapy carriers, there is a critical need to develop flexible theranostic nanocarriers that can be localized in tissues to monitor drug release at high resolution. While positron emission tomography (PET)[4-6] and single photon emission computed tomography (SPECT)[7] are the most common molecular *in vivo* imaging techniques, there is no way to distinguish encapsulated from released drug. Herein, we develop a novel radioluminescent nanocapsule with an radioluminescent spectrum that changes during drug release. The nanocapsules were fabricated with a drug loaded hollow core, a radioluminescent shell, and a pH-responsive outer polymer multilayer for controlled drug release. This approach provides an almost background-free luminescent signal for measuring drug release from particles irradiated by a narrow X-ray beam. We study *in vitro* pH triggered release rates of Doxorubicin from our nanocapsules, demonstrate that the empty particles do not affect cell viability, are good magnetic resonance imaging (MRI) T_2 contrast agents, can be observed using XEOL in a mouse model.

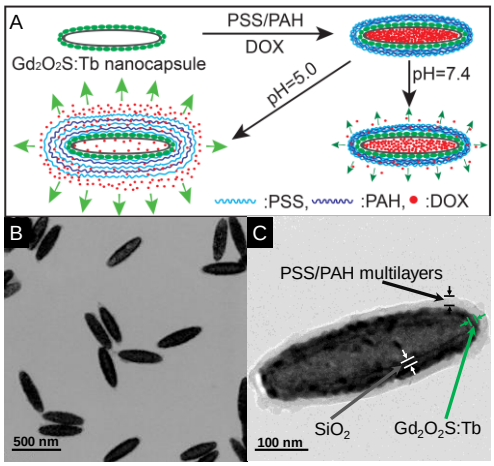

Figure 1. (A) schematic illustration of the synthesis of DOX@Gd_2O_2S:Tb@PSS/PAH and pH-responsive release of DOX. Low magnification (B) and high magnification (C) TEM image of DOX@Gd_2O_2S:Tb@PSS/PAH.

References:

[1] G. Ibarz, L. Dähne, E. Donath, H. Möhwald, *Advanced Materials* **2001**, *13*, 1324.

[2] D. G. Shchukin, G. B. Sukhorukov, H. Möhwald, *Angewandte Chemie* **2003**, *115*, 4610.

[3] G. Sukhorukov, L. Dähne, J. Hartmann, E. Donath, H. Möhwald, *Advanced Materials* **2000**, *12*, 112.

[4] H. Hong, Y. Zhang, J. Sun, W. Cai, *Nano Today* **2009**, *4*, 399.

[5] Z. Liu, W. Cai, L. He, N. Nakayama, K. Chen, X. Sun, X. Chen, H. Dai, *Nat Nano* **2007**, *2*, 47.

[6] F. Zhang, L. Zhu, G. Liu, N. Hida, G. Lu, H. S. Eden, G. Niu, X. Chen, *Theranostics* **2011**, *1*, 302.

[7] R. J. Jaszczak, R. E. Coleman, F. R. Whitehead, *Nuclear Science, IEEE Transactions on* **1981**, *28*, 69.

Mechanical properties of stem cells from different sources during vascular smooth muscle cell differentiation

Ruikai Chen, Delphine Dean
Department of Bioengineering, Clemson University, Clemson, South Carolina

Statement of Purpose: The purpose of our project is to investigate the mechanical property change during certain stem cell differentiation. Vascular smooth muscle cell (VSMC), as an essential component in human artery, plays an important role in regulating blood flow and pressure by contracting and relaxing in response to a variety of mechanical stimuli. Differentiation into smooth muscle cell by using reliable sources of stem cell introduces a potential treatment for smooth muscle repair. A completely differentiated and functional vascular smooth muscle cell should have both the ability to contract and relax in response to environmental stimuli while few researches has been done to analyze the time period it takes for different sources of stem cells to fully differentiate into VSMC. In our study, changes in the differentiating cells' mechanical properties, namely elastic modulus, were determined by using the indentation of atomic force microscope (AFM) during stem cell differentiation. Immunofluorescence and PCR were performed to determine if the expression of specific SMC markers are associated with mechanical property change. These results give us a brief view of elastic modulus change of VSMC differentiated from different stem cells and can be used to determine the optimal growth and environment required for VSMC in tissue repair and medical treatment.

Methods: MSCs isolated from human red bone marrow, were seeded at 1 X 10^4 cells/ cm^2 in Φ 35-mm dishes resuspended in MEM α, GlutaMAX (Invitrogen) supplemented with 20% FBS and 1% 100× penicillin-streptomycin. After cells were adhered to plates (1 day culture in incubator), differentiation media containing 10ng/ml TGF-β1 were added to induce differentiation to VSMC. Similar treatment was done to human adipose derived stem cells for differentiation. For AFM in vertical indentation and retraction on cells, an Asylum Research MFP-3D AFM placed on a vibration isolation table was used. Borosilicate spherical probes with a nominal spring constant of 0.06N/m were utilized to indent into cells. The AFM probe was positioned close to the cell nucleus without touch it and was carefully adjusted to avoid the edge of the cell. The AFM was set to contact mode and two indentations were performed with the loading rate of 5μm/s to determine the contact point and ensure there is enough baseline for further calculation. Then the loading rate was changed to 1μm/s to collect 5 indentation curves per cell. At each time point, 10 representative cells (smooth muscle-like if differentiated) were chosen for evaluation and their elastic modulus were then analyzed according to deflection sensitivity and spring constant. Immunofluorescence was performed on PFA fixed cells with SMC-specific markers (α-actin, SM myosin heavy chain) to assess if their expression are associated with mechanical property change. The expression of α-SMA is further quantified by PCR .

Results: Overall, the process of vascular smooth muscle cell differentiation varies if given different sources of stem cells. Mesenchymal stem cell harvest from bone marrow tends to differentiate faster to smooth-muscle like cell compared to stem cell from adipose tissue. Smooth muscle-like cell differentiated from bone marrow stem cell also exhibits a much higher elastic modulus growth during differentiation. In general, the expression of specific SMC markers matches up with AFM results. Real time PCR shows αSMA has a baseline expression for both undifferentiated mesenchymal stem cell and adipose stem cell along with a minor but constant increase over differentiation.

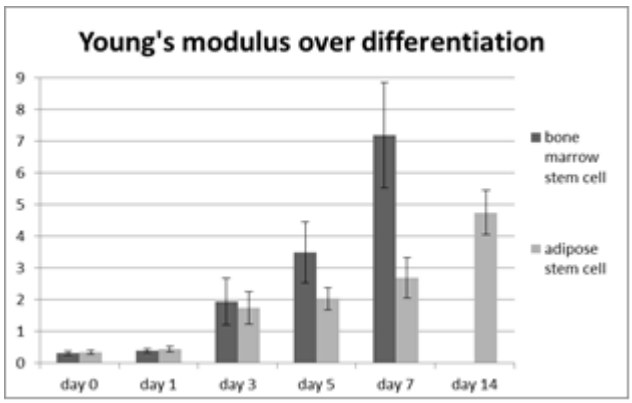

Fig. 1 Changes in Young's modulus during differentiation from day 1 to day 14 for bone marrow stem cell and adipose stem cell

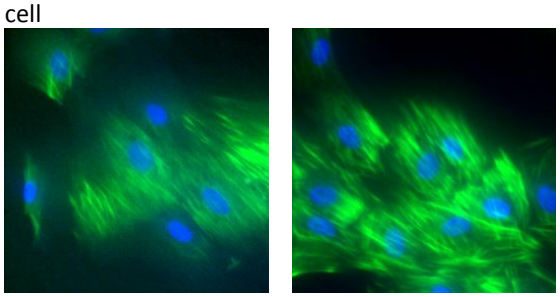

(a) (b)

Fig. 2 Expression of calponin for (a) day 7 bone marrow stem cell, (b) day 7 adipose stem cell

Conclusions: At the first stage of our research, we conducted AFM indentation on both MSCs and ADSCs during their differentiation. The result shows there is a significant difference between mechanical properties of differentiated vascular smooth muscle like cell from MSCs and ADSCs while the expression of SMC specific markers match up with AFM results. Based on these data, we find the process of vascular smooth muscle cell differentiation varies if given different sources of stem cells and further investigations are required to better determine the appropriate mechanical environment for vascular smooth muscle differentiation used in tissue engineering application.

References: 1. Wang, C., S. Yin, et al. *Tissue Engineering* Part A 16(4): 1201-1213

Glycol Chitosan Conjugated Camptothecin for active drug delivery

Bei Cheng, Bindu Thapa, Remant Bahadur K.C.,Xiaolan Luo and Peisheng Xu*

Department of Pharmaceutical and Biomedical Sciences, South Carolina College of Pharmacy, University of South Carolina, 715 Sumter Street, Columbia, South Carolina 29208, Ph. 803-777-0075*Email: xup@sccp.sc.edu

Statement of Purpose: Polymer based chemotherapeutics have been clinically proved to be effective, especially with the development of commercial available polymeric drug and polymer protein conjugates. The clinical benefits from polymer drug conjugates are 1) increasing solubility of hydrophobic drugs, 2) passive targeting by enhanced permeability and retention (EPR) effect[1].

In this study, amphiphilic glycol conjugated chitosan campotothecin (GCS-CPT) was synthesized to fabricate nanoparticles (NP). Further, PEGylated folic acid (FA) lipid was incorporated to enhance the uptake of the nanoparticles in FA over-expressing various cancer cells (including both SKOV-3 cells and KB cell). In addition, the insertion of PEGylation lipid can decrease the size of NPs, and also help to absorb hydrophobic drug via hydrophobic effects[2]. GCS-CPT nanoparticles showed high encapsulation efficacy and could be efficiently targeted to FA over-expressing cancer cells. The high potential dosing, fast intracellular releasing together with the excellent cell uptake behaviors could make the polymer CPT nanoparticles a promising tool for chemotherapy.

Materials: DL-dithiothreitol (DTT), folic acid (FA), CPT, and thiazolyl blue tetrazolium bromide (MTT) were purchased from Sigma-Aldrich Chemical Co. (St. Louis, Mo, USA). N-SuccinimidyL 3-[2-pyridyldithio]-propionate (SPDP) was purchased from ProteoChem, Inc. (Denver, CO,U.S.A).1,2-distearoyl-*sn*-glycero-3-phosphoethanolamine-N-[amino (polyethylene glycol)-2000] (ammonium salt) (DSPE-PEG(2000) Amine was purchased from Avanti Polar Lipids. CY3 NHS ester was purchased from Lumiprobe Corporation.

Method: CPT-SH was synthesized in anhydrous dichloromethane. It was coupled to the amine groups in the side chains of glycol chitosan via the bio-functional cross-linker SPDP. GCS-CPT/FA nanoparticles were prepared by simple dialysis. Briefly, GCS-CPT was dissolved in DMSO and certain amount of lipid (PEG-DSPE 2K) with predetermined composition of FA-PEG-lipid and PEG-lipid (ratio varied from 0-100%) were added in. Pre-heat the mixture to 50°C and mixed for at 1h before dialysis. Then the mixture was dialyzed extensively against DDH_2O with a molecular cutting off membrane of 6,000-8,000, consistently changing medium. After the dialysis, centrifuged at 5000×g for 10 min to remove the insoluble aggregates. Finally, 5% trehalose was then added prior to lyophilization.

Cy3-labled GCS-CPT polymer were synthesized by coupling Cy3 NHS ester to the side chain of GCS.

Result: The structure of CPT-SH, CPT-PDP and GCS-CPT were confirmed by HMNR. The colloidal properties of NPs were determined by DLS and TEM. From DLS, it has been clearly shown that the insertion of lipid to the NP system would significantly help to decrease the NP size, and even after further conjugation with FA, the size were smaller than the NPs without lipid. The average size before insertion of lipid was around 307nm, and after the insertion of lipid the size decreased by half.

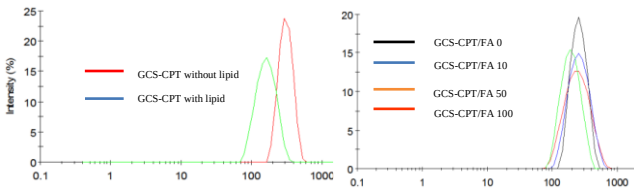

Fig 1. The hydrodynamic size was measured by dynamic light scattering (DLS) at RT in DD H_2O; (Left) Nanoparticles with or without lipid, (Right) Nanoparticles with different ratio of PEGylated FA lipid.

The release of the NPs was performed in PBS buffer (pH7.4). At first 72h, the release of drug was slow. And after adding 10mM DTT, CPT was released dramatically due to the cleavage the disulfide formed between CPT and GCS, responsible for the quick release of free drug. And the similarly mechanism could also be accomplished *in vivo* by the abundant intracellular glutathione.

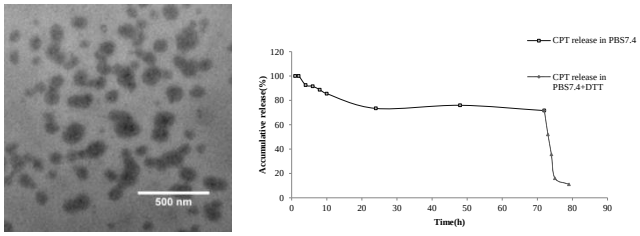

Fig 2. (Left) Representative transmission electron microscopy image of CPT loaded nanoparticles. Scale bar = 500 nm. (Right) CPT release from GCS-CPT/FA nanoparticles at PBS pH7.4(solid square), PBS pH7.4+10mM DTT (solid triangles) at 37°C.

FA was employed to act as the ligand to enhance the uptake of NPs in the FA receptor overexpressing cell. FA has been extensively used as the target ligand for many cancer therapies as they can enhance FA mediated endocytosis. In SKOV cell, both the flow cytometer results and confocal images showed the increased uptake of NP after modification of FA. Cell cytotoxicity also evidenced increased anticancer activities of GCS-CPT nanoparticles than free drug in SKOV cell and KB cell after 48h treatment of NPs.

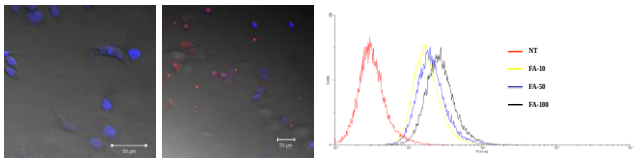

Fig 3. Cellular uptake of GCS-CPT NPs. (Left) Confocal image of blank SKOV cells, (Middle) Confocal image of GCS-CPT/FA nanoparticles in SKOV-3 cells. (Right) Flow cytometry results of SKOV-3 cells after treated with NPs at amount of FA. Note: Cells were incubated with nanoparticles for 3h. Cy3 was conjugated to the polymer, and the Cy3 amount was previously determined by fluorescent spectrometer to ensure the same amount of Cy3 (λ_{Ex}=530nm, λ_{Em}=560nm). The percentage of Cy3 positive cells were quantified by flow cytometer. Data represent mean ± SD (*n* = 3).

Conclusion: In present study, GCS-CPT conjugate was employed to overcome the limitation of low solubility and instability of CPT. FA was successfully incorporated into NP system to realize active targeting. Compared with free drug and folic acid free nanoparticles, GCs-CPT/FA nanoparticles showed significant effect in cancer cells. Therefore, the result suggested that GCs-CPT/FA active targeting system can be a powerful chemotherapy for cancer therapy.

REFERENCES:

1. Fabiana Canal. Current opinion in biotechnology. 2011, 22(6):894-900.
2. Anne-Lise Troutiera. Advances in Colloid and Interface Science. 2006, 133(1), 1-21.

Periorbital Implant for Treatment of Cytomegalovirus

Bria Dawson, Cheryl Jennings, Katherine Luffy, Even Skjervold, Dr. Terry Steele
Nanyang Technological University, 50 Nanyang Avenue, Singapore 639798
Clemson University, Sikes Hall, Clemson, SC 29634

Statement of Purpose: A variety of age-related macular degeneration (AMD) diseases exist from immune deficiency disorders such as HIV. These diseases can cause blindness at their final stages and commonly require surgery. It has been proposed that ocular implants can be used to treat these AMD diseases because of the difficult accessibility of the posterior portion of the eye. Many patients with HIV loose eyesight due to the development of cytomegalovirus (CMV) retinitis, an AMD disease. Biodegradable disks, through enzymatic reactions in the eye, can be injected and encapsulate particulate systems such as the anti-CMV drug Ganciclovir. It has been proposed that the disks should be made out of polyesters such as poly-L-lactide (PLL), polycaprolactone (PCL), or polyL-lactide-co-glycolide (PLGA) because they are most biocompatible; PCL and PLGA both degrade by the hydrolysis of their ester linkages. This biodegradable film created will then be placed on the internal limiting membrane of the eye and will disperse the drug in a unidirectional motion into the vitreous humor to concentrate the drug in the most effective way. This disk will be able to disperse drug for six months to avoid multiple reinjections and the costs of surgery**.**

Methods: pH buffer Study: Tests were performed by producing 1.0, 1.2, 1.4, 1.6, 1.8 and 2.0 pH HCl/KCl buffers. Using the highest florescence result from this test, plates were prepared to test the maximum emission and excitation wavelength. Solubility Study: Different solvents were tested with Valganciclovir and Ganciclovir: A variety of solvents were tested including DMF, DMSO, Acetone, EtOH, THF, Methanol, PBS, PBS tween 80 2%, Chloroform, Toluene, Ethyl Acetate and ACN. Film Casting: Two films were casted for each drug FDA, Ganciclovir, and Valganciclovir using a 10% incline mechanical knife caster. The flow rate was adjusted by a peristaltic pump. Gradient mixing was initiated after a few seconds to allow the solution to fill the 8cm knife caster. Two different formulations of PLGA were used in the different films, 0.2A and 0.4A. Each film made was about 100cm in length and after casting the film was left in the fume hood for 24 hours to allow DCM to evaporate. After 24 hours it was moved to a vacuum oven at 55 °C for 1 week to allow to completely dry. After drying, 5mm circular punch outs every 5cm were put into the 96-well plates for a drug release study to be performed on the films. Drug Release Study: For the FDA drug release study 200uL of PBS was put into the well plate and the plate incubated in a 37 °C oven for 1 hour. 20uL was then pulled out of that well plate and put into a “read-plate” with 180uL of 0.1M NaOH and read using the Infinite M200 Tecan Microplate reader (ex/em 490/520).Finally a 100% release was determined using new punch outs from the original film.

Results: Results were not very conclusive on how to best dissolve Ganciclovir in the PCL polymer for the film to be casted. No gain settings were able to be determined as Valganciclovir showed inconclusive results. The release of FDA showed that for two weeks the drug released very quickly but then stopped releasing any drug shortly thereafter. For the film to be inserted a short burst release of drug is fine but it needs to stabilize sooner so that it can continue to release drug for a longer period of time rather than just two weeks.

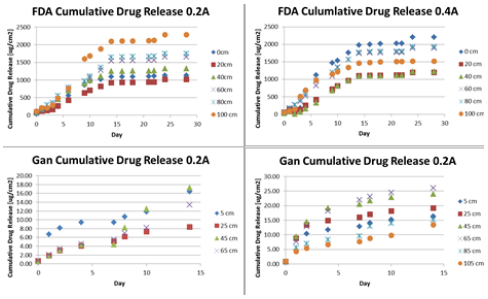

Drug	Concentration	Excitation	Emission	Gain
FDA	10-1 µg/ml	490 nm	520 nm	57
	1-0.1 µg/ml			77
	0.1-0.01 µg/ml			104
	0.01-0.001 µg/ml			118
Valganciclovir	10-1 µg/ml	270 nm	322 nm	N/A
	1-0.1 µg/ml			
	0.1-0.01 µg/ml			
Ganciclovir	10-1 µg/ml	270 nm	352 nm	105
	1-0.1 µg/ml			109
	0.1-0.01 µg/ml			125

Conclusions: It was very difficult getting both Valganciclovir and Ganciclovir into the same solvent which could also be soluble in PCL and PLGA in the films. Because there were many problems getting the drugs into solution there was not much progress with the drug release studies of Valganciclovir and Ganciclovir, however a calibration curves for FDA and complete a 1-month drug release study was completed.

Effects of Cell-Cell and Cell-Matrix Interactions on Vascular Smooth Muscle Cell Mechanical Properties under in vivo Conditions

Aesha Desai, Sandra Deitch, Delphine Dean

Department of Bioengineering, Clemson University

Statement of Purpose: Most tissue-level mechanical models assume homogeneous mechanical properties within a single cell type. However, measurements of cellular mechanical properties show large variability in whole-cell mechanical properties between cells from a single population. This heterogeneity has been observed in many cell populations and with several measurement techniques but the sources are not yet fully understood. Cell behavior is largely dependent on interactions with neighboring cells and extracellular matrix components. Results from previous studies in our lab showed that vascular smooth muscle cells (VSMCs) behave less stiff, more relaxed, and take on a more synthetic phenotype after 5 days in culture on blocking cell-cell (N-cadherin) and cell-matrix (integrin β1) interactions. To establish realistic levels of cellular heterogeneity in tissue level mechanical models, antibody-blocking experiments were replicated on more *in vivo* like conditions. For this, the experiments were carried out on collagen-coated polyacrylamide gels. Cellular media was supplemented with antibody integrin β1, which was hypothesized to reduce the heterogeneity within the cellular mechanical measures, based on the results from the previous study. The main objective of this study was to determine, if reduction in cellular mechanical heterogeneity was observed by decreasing variation in cellular adhesions under more physiologically relevant conditions.

Methods: Polyacrylamide gels with elastic moduli of approximately 10kPa, 25kPa, and 75kPa were created and deposited in a thin layer on the top of the glass slides, following the protocols by Tse et al. and Wang et al. Gels were first coated with 0.2 mg/ml of sulfo-SANPAH (cross-linker), followed by 1mg/ml collagen solution. VSMCs were isolated, passaged, and plated on the collagen-coated gels. Throughout the culture period, 3 different media conditions were used: regular VSMC media, VSMC media with 50µg/ml integrin B1 antibody, and VSMC media with 50µg/ml of a non-immune IgG (control). On day 5, AFM cytoindentation experiments were performed using a 5 µm diameter borosilicate spherical-tipped probe on a silicon-nitride cantilever. 20 cells on each sample were indented 5 times to ~1 µm depth at 1µm/sec. In addition, Western blot analysis was used to detect levels of contractile phenotype marker, alpha-actin. This will give quantitative measure for phenotypic differences for cells in the different conditions, which can be correlated with mechanical property data.

Results: Results showed increase in cellular elastic moduli measures with increase in substrate stiffness. For the no antibody control condition, cellular stiffness increased significantly from 18kPa and 28kPa to the 72kPa gel and glass coverslip samples. For IgG elastic moduli measures increased significantly from 18kPa to 72kPa. With integrin β1 sample, significant increases were observed between 18kPa gel and all the other samples. Overall, the VSMCs on the gels had elastic moduli in the range of 1.8kPa-6.9kPa, while the VSMCs on the stiffer glass substrates had moduli in the range of 4.3kPa-9.2kPa.

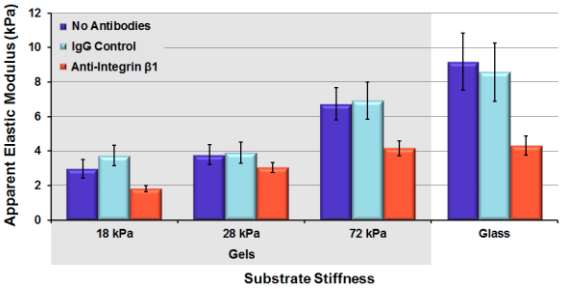

Figure 1. Apparent elastic moduli of day 5 VSMCs on substrates with varying stiffness and different media conditions. Data presented as mean ± standard error.

Conclusion: In this study, VSMCs were cultured under more *in vivo* like conditions and their overall appearance and mechanical properties were evaluated. For the gel samples, significant differences were observed in both elastic moduli and percent relaxation measures, in comparison to the stiffer glass coverslips. For all media conditions, cellular elastic moduli increased with increasing gel stiffness. The cell-to-cell COV measures for the gel samples decreased from control samples to anti-integrin β1 sample for both elastic moduli measures (70% to 43%) and percent relaxation measures (42% to 17%). This reduction in mechanical heterogeneity is very similar to the reduction that was observed on glass slides in our previous studies, indicating that VSMC most likely exhibit heterogeneous mechanical properties in vivo, especially in conditions where their cell-cell and cell-matrix interactions are highly variable.

References: [1] Jaasma, MJ. Ann Biomed Engr. 2006;34:759-768.[2] Tse, J. Current Protocols in Cell Biology, 2010. 10(16). [3] Wang, YL. Mol. Motors and the Cytoskeleton. 1998: 489-496

Potting Alignment Accuracy of Implanted Glenospheres in a Reverse Shoulder Arthroplasty Micromotion Study

Alex Devon[1], Alan Marionneaux[1], Andrew Sedler[1], Wooten Simpson[1],
Stefan Tolan[2],Andrew Bries[2], Richard Hawkins[2], John DesJardins[1]
[1]Department of Bioengineering, Clemson University, 29634
[2]Steadman Hawkins Clinic of the Carolinas, Greenville,SC, 29615

Statement of Purpose: Standard total shoulder arthroplasty has been shown to be clinically effective in patients that do not present a significant deficiency of the rotator cuff[1]. However, in patients with significant rotator cuff damage, reverse shoulder arthoplasty (RSA) implant systems have been shown to be more clinically successful[1,2,3]. Loosening of the glenoid component is one of the most common complications associated with reverse shoulder implants[2], and clinical questions regarding the link between early rehabilitation and implant-bone micromotion remains a concern. Initial fixation of the glenoid baseplate to the scapula can be affected by the baseplate screw configuration (position, size, number, direction, locking ability), central screw design and initial inclination[2]. This abstract presents the experimental design and initial surgical alignment results of implanted baseplates between three designs in a standard saw-bone model, as part of a larger RSA biomechanical study to compare the post-implantation micromotion between three RSA designs during modified ASTM 2028 testing.

Methods:A novel dynamic testing platform was designed, and the pre-testing potted alignment of three different RSA designs was investigated prior to a modified ASTM 2028 micromotion analysis. N=5 specimens from three designs (DJO Surgical (Reverse®, Austin,TX) , Exactech Inc. (Equinoxe®, Gainesville, FL), and Tornier (Aequalis®, St. Ismeir, France)) were implanted as per surgical specifications into mechanically equivalent osteopenic anatomical Sawbones scapula (4th Gen. Custom, Model 4313 Large, Pacific Labs, Vashon Island, WA). Scapulas were then potted into 5”x2” Al tubing with quick curing polymeric tray material. Potting alignment accuracy of the test specimens in three planes (anterior/posterior (A/P), superior/inferior (S/I), and glenoid version (GV) angles) between the baseplate of the glenosphere were quantified using a Matlab program. Averages and standard deviations were determined, and statistical differences in alignment bias between the three implant designs were determined using a student t-test with Dunn-Šidák correction (α=0.05).

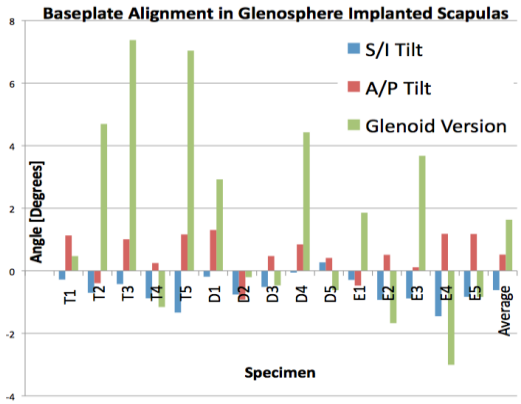

Fig. 1. Superior/inferior, anterior/posterior, and glenoid version alignment angles of the baseplate in potted scapulas implanted with RSA glenospheres for use in micromotion study

Results and Discussion: Figure 1 shows individual specimen alignment results from the developed protocol.There was average S/I baseplate tilt of -0.73°±0.41° for Tornier, -0.25°±0.40° for DJO, and –0.88°±0.41° for Exactech. Transverse A/P tilt was 0.63°+/-0.68° for Tornier, 0.42°±0.83° for DJO, and 0.50°±0.71° for Exactech. Glenoid version was 3.68°±3.86° for Tornier, 1.21°±2.32° for DJO, and 0.002°±2.72° for Exactech. Maximum variation between specimens was found to be 1.72° for S/I tilt, 2.22° for A/P tilt and 10.35° for glenoid version. No statistically significant differences were present between any of the groups for the three alignment measures.

Conclusion: Although no statistical differences were found between alignment measures, ideally all observed angles would be equal to zero. The variation observed in the resulting alignment can be taken into consideration during micromotion testing to determine any possible secondary effects on results.

References:

1. Virani, N.A, Harman, M., et al. *J Shoulder Elbow Surgery*. 2008, Vol 17: 509-521.

2. Poon PC, Chou J, Young D, et al. *British Elbow and Shoulder Society*. 2010, Vol 2: 94-99.

3. Guitierrez S, Greiwe RM, Frankle MA, Siegal S, Lee III WE. *J of Shoulder and Elbow Surgery*. 2007, May/June

Characterization of Biosensing Diacetlyene Liposomes Fabricated Via Inkjet Technology

Michael A Evans, Caroline E Hansen, Cassandra J Wright-Walker,Timothy W Hanks
Department of Chemistry, Furman University in Greenville, SC 29613

Statement of Purpose: Interest has increased in recent years over the use of nanoscale sensor systems for a variety of applications to address needs in biomedical applications, food packaging, bioterrorism and various other fields[1]. Polydiacetylene (PDA) liposomes have been shown to detect a wide variety of stimuli including temperature, pH, mechanical stress and biological entities. Once triggered, detection is relayed by a chromatic change from blue to red (See Figure 1). PDA liposomes are typically prepared via a sonication, however this results in liposomes with a broad range of sizes. Other types of liposomes have been shown to be formed when "printed" through an inkjet printer[2]. The goal of this research is to optimize the printing of PDA liposomes that indicate the presence of bacteria chromatically as well as with fluorescence. These sensors are specifically designed to identify bacterial species through use of a multifluorophore biosensing system. They could be used for detection of bacteria on wound sites among other uses.

Methods: PDA liposomes were prepared by dispersing 5mg of 10,12-pentacosadynoic acid (PCDA) in 5.0mL of ethanol. The organic solution of PCDA was placed in a HP 21 ink cartridges (17pL droplet size), then printed via stir. Once modified HP Deskjet 3915 into a vial of DI water under complete, the solution was rotoevaporated to remove the solvent and refrigerated overnight. In later trials, this method was modified slightly by replacing the 5.0 mL of ethanol with 3.3 mL of 2-propanol and heating the DI water to 60˚C. Afterwards, samples were exposed to 254 nm light to effect polymerization (t=10min).

Liposomes derivatized with amino acid liposomes (AA-PDA) and encapsulating a fluorophore were prepared similarly; 10uL of a 1M amino acid derivatized lipid (tryptophan, tyrosine, or arginine) in tetrahydrofuran (THF), 5.0mg PCDA, 50-100µL of fluorophore solution, and 5.0mL of ethanol were mixed and printed. Fluorphore solutions contained 100uL of 0.4µM BODIPY 558 (BO558) fluorophore (for tryptophan), 50uL 0.4µM BODIPY fluorophore (BOFL; tyrosine), and 50uL of 2.0µM 1-pyrenedecanoic acid (arginine).

Lipolyzed polysaccharide (LPS) from three types of bacteria were used to assess whether the AA-PDA could sense bacterial and differentiate between them. LPS from E. Coli serotype 026:B6, Salmonella enterica serotype enteritidis, and Pseudomonas aeruginosa serotype 10 were dissolved separately in a phosphate buffer of pH 7.4 (3 mg/mL). 0.5 mL AA-PDA & PDA liposome solutions were exposed to 10 µL LPS solutions for 1hr (T=25°C). An emission spectrometer (λ_{ex}=348nm) was used to analyze samples. A heated standard was also measured for normalization.

PDA liposomes were also analyzed for stability for 14 days at 25°C. Three ratios of PCDA to solvent were used for optimization (1:1, 3:2, 2:1). UV-Visible Spectrometer was used to analyze the samples & results were normalized.

Results: DLS showed average size of the AA-PDA liposome to be 94nm (PdI=0.21). Figure 1 shows the normalized spectra of Salmonella LPS exposed systems exhibited unique fluorescence at Peak 2 (corresponding to 1-pyrenedecanoic acid & arginine). Spectra for Pseudomonas and E. coli were similar. Liposomes showed a 22% shift towards red phase at Day 14. The least amount of shift was found using a 3:2 ratio (15%). It was found that heating the liposomes to 60˚C during printing helped to produce more concentrated liposome solutions than those made at room temperature. The results suggest that heating the solution causes the solubility of the PCDA solution to increase slightly which allows more of the PCDA molecules to form liposomes instead of aggregating on the top of the solution.

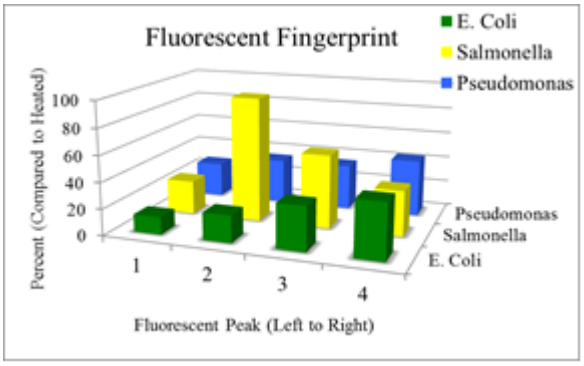

Figure 1: Fluorescent fingerprints from AA-PDA exposed to LPS solutions

Conclusions: The size of these lipids is within the reported range of 50-200nm for PDA liposomes[2]. From the fluorophore experiments, it is evident that the fluorescent fingerprint allows for distinction between Salmonella, E.Coli, and Pseudomonas. Flurophores were placed in different liposomes to provide three different detectors that could be analyzed separately, enhancing discrimination between the bacteria. The blue form of the liposome internally quenches fluorophore emission, while the red form does not, switching on the signal. The 3:2 ratio of PCDA:solvent provided the highest absorbance in addition to being the most stable. Further investigation into optimizing polymerization time and fluorophore concentrations is needed to optimize fluorophore emission and detection.

References: [1]Lasic DD. Handbook of Biological Physics 1995; 491-519. [2]Hauschild S et al. Small 2005; 1(12):1177-80.

Acknowledgements: This work was partially supported by the National Science Foundation.

The Correlation of Implant Surface Micro-Hardness and Service Lifetime for Different Retrieved Femoral Component Materials

R. Freed, E. Alvarez, C. Eljach, J.D. DesJardins

Clemson University

Introduction: The hard bearing materials used in TKR femoral components are designed to have low frictional behavior, high biocompatibility, high fatigue strength, and ease of manufacture. It is necessary for the material to have a high hardness, as this parameter determines the wear resistance of the material and can affect the amount of polyethylene wear. There is a significant amount of research being done to develop surface modifications to create harder and smoother materials for the hard bearing components of joint replacements. Such modifications include ion treatments, nitriding treatments, oxidation to create a ceramic oxide layer, and diamond like coatings. These modifications have shown promising results, yet there is still much work to be done to ensure that the surfaces will be able to withstand in-vivo conditions over extended periods of time. Changes in hardness have been observed related to the materials' vulnerability to surface damage and a resulting change in surface roughness due to in vivo function. The objective of this study was to quantify the hardness of retrieved femoral components made of different materials and to evaluate whether this property changes as a function of implantation time. Most work found in literature has only evaluated the hardness of the materials pre-implantation, and only one study has measured femoral component hardness as a function of in-vivo loading. [1,2,3]. This study provides an important link between clinical relevance and the experimental quantification of material properties of femoral TKR components.

Materials and Methods: Vickers Hardness measurements (ASTM E384) were performed on 31 retrieved TKR femoral components, including 11 OxZr retrieved after 0.5 to 6 years and 20 CoCr retrieved after 0.1 to 10.5 years. Reasons for revision included aseptic loosening, infection, and stiffening. Surface roughness was assessed using a non-contact profilometer (Wyko NT-2000, Veeco) followed by n=10 micro-hardness indentations on each specimen over ~1mmx1mm square area made with a micro-hardness tester (HVS-1000B Ebatco with applied loads of P=0.5 kgf for CoCr and P=0.3kgf for OxZr). All measurements were acquired from the non-articular flat lip of the femoral component. CoCr indentation diagonals were measured from digital images acquired with an optical microscope at 40x . OxZr diagonals were measured at 200x using a customized image analysis program (Image J, NIH) to measure diagonals using a standard calibration (3.75 pixel =1 um). Statistical relationships between the type of material and hardness were determined using single factor ANOVA and post-hoc analysis. Strength of association between material hardness and implantation time was determined using Spearman's rank order correlation. A linear regression model was used to evaluate whether there was a significant change of hardness as a function of implantation time.

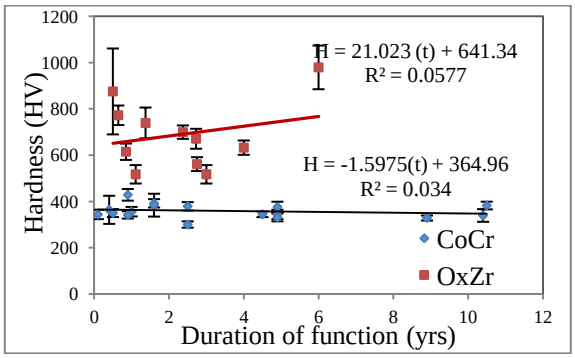

Figure 1: Microhardness measures on retrieved femoral components manufactured of different materials, CoCr and oxidized zirconium as a function of implantation time (yrs).

Results: Average surface roughness the for CoCr and OxZr groups was 55.8 + 10.8 and 51 + 6.7 nm, respectively. Vickers hardness measurements for both materials fell within the reported ranges (CoCr: 400-600 HV, oxidized zirconium: 285-1200 HV)[2,4] and are shown in figure 1. Despite a service lifetime span of up to 10 years in vivo, hardness values remained unchanged for both material groups with respect to implantation time. (CoCr group $p=0.456$, OxZr group $p=0.477$; Spearman's ratio $p>0.05$). Single factor ANOVA showed that the median hardness values for OxZr were significantly higher than the CoCr femoral components. ($p<0.001$).

Conclusions: This study successfully applied Vickers testing to quantify micro-hardness in retrieved TKR femoral components. Micro-hardness measures for both materials groups were comparable to reported pre-implantation values[4,5], and implantation time was not shown to affect CoCr or OxZr hardness. The application of this method to retrieved total joint replacement components will enable the evaluation of a wider range of bearing materials (e.g. ceramic) and implant types (e.g. hips and shoulders), and further enable the assessment of changes in bearing hardness and surface roughness within these specimens.

References: 1) Roy ME, et al. Acta Biomaterialia.2010 2) Long M, et al. 24th Annual Meeting of the Society of Biomaterials. 1998. 3) McGrory BJ, et al. The Journal of Arthroplasty 4) Galetz MC, et al. JBMR-B, 2010. 5)

Dearnley P., et al. Proc IME H J Eng Med 1999.

Characterization of Surface Roughness on Retrieved Cobalt-Chromium Femoral Heads: Dislocated vs. Non-dislocated Hips

Ryan Freed, Kevin Keith, Andrew Hodge, Melinda Harman
Clemson University

Introduction: Close reduction of the hip joint is a common treatment for hip dislocation occurring after total hip replacement (THR). However, among patients who experience an initial episode of THR dislocation, 16% to 60% go on to experience it more than once (recurrent dislocation). Contact with the metal acetabular cup is possible during each dislocation/relocation episode, resulting in the accumulation of discolored metal transfer deposited on the femoral head.[1,2] Some argue that the location of such metal transfer damage tends to be more inferior on the femoral head with potentially less influence on polyethylene wear.[3] However, systematic assessments describing the location of such damage on retrieved femoral heads have not been reported and characteristic features of this damage are still largely unknown. The purpose of this study is to characterize the location and roughness of damage on metal heads retrieved after THR dislocation compared with heads retrieved for reasons other than dislocation.

Materials and Methods: An IRB-approved archive of retrieved orthopaedic implants was queried, identifying twenty-five modular metal femoral heads retrieved during revision THR from 13 female and 12 male patients with an average age of 69±12 (range, 44-85) years. Included were 18 heads revised for hip dislocation and seven heads revised for loosening (3), polyethylene wear (2), and infection (1). These non-dislocated heads were specifically selected to have a broad range of in vivo duration and similar head diameters as the dislocated heads. The dislocated heads were retrieved after an average of 3.5±2.8 (range, 0.3 to 10) years of in vivo function and the non-dislocated heads were retrieved after an average of 11.3±5.5 (range, 4 to 18) years of in vivo function. All heads were fabricated from cobalt chrome (CoCr) with 28 mm or 32 mm diameters and articulated with polyethylene liners. Damage appearance and surface roughness were evaluated in a grid pattern of 49 zones distributed across the bearing surface of each head (ASTM F2033 and ISO 7206-2). Surface damage in each zone was evaluated using optical microscopy (7x to 30x mag)and identified using a damage mode atlas defining scratching, pitting and material transfer typical for metal implant surfaces.[5] Surface roughness for each zone also was assessed using a non-contact surface profilometer (WYKO NT2000, Veeco Corp.). Selected regions were imaged using scanning electron microscopy.

Results: Distinct regions of material transfer having a dull surface discoloration were visually evident on 16 of the 18 dislocated heads, but not on the non-dislocated heads (Figure 1). These dull discolored regions were visualized in 160 of the 882 zones evaluated (18%), of the available surface area for the dislocated heads (Table 1). Zones with dull discoloration had significantly higher surface roughness compared to zones without this damage ($p<0.001$). The high Rpm indicates considerable pile-up

Head Group	Dislocated n=18		Non-Dislocated n=7	Unused Control n=1
Damage	Dull	Not Dull	Not Dull	Not Dull
Zones	n=160	n=722	n=343	n=49
Ra (nm)	169±216 (7-1497)	41±139 (5-2423)	60±97 (10-735)	19±8 (10-59)
Rpm (nm)	1210±1048 (45-5963)	327±484 (35-6133)	515±713 (49-6343)	277±188 (59-924)

Table 1: Surface roughness (mean ± standard deviation, range) for zones with and without dull adhesive damage.

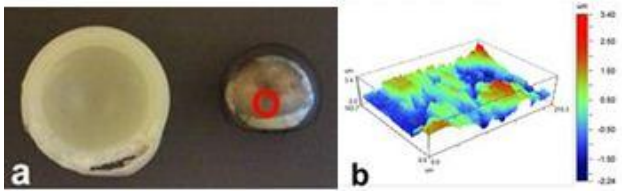

Figure 2: a) Retrieved polyethylene liner and dislocated hip head showing large region of dull surface discoloration. b) Within the red circled regions, the surface roughness shows considerable material transfer with pile-up on the bearing surface.

damage rather than polishing or wearing away of the bearing surface (Figure 1). This dull adhesive damage tended to be concentrated in regions closer to the equator rather than the apex. Mechanisms specific to hip dislocation could contribute to the different damage distribution from apex to rim. In contrast, scratches were the dominant damage mode on the non-dislocated heads and were more uniformly distributed, resulting in an overall lower surface roughness compared to the dislocated heads (Table 1).

Conclusions: While less evident than similar damage observed on ceramic heads,[2] the distinct macroscopic and microscopic features of the dull discolored damage after dislocation were associated with an approximately 3 to 4-fold increase in surface roughness compared to non-dull regions on both the dislocated and non-dislocated heads (Table 1). Computational models predict accelerated polyethylene wear when head damage occurs within 20 to 30 degrees of the superior axis,[4] corresponding to the location of rough material transfer for these dislocated heads. Materials and coatings on femoral heads that are meant to resist scratching during normal THR function need to be able to withstand the damage mechanisms that occur during THR dislocation and closed reduction, as evidenced on these retrieved metal heads.

References: 1) Ito, et al. J Arthroplasty, 2010. 2) Kim, et al. J Bone Joint Surg, 2005. 3) Bourne, et al. Clin Orthop, 2005. 4) Lundberg, et al. Clin Orthop, 2005. 5) Alvarez, et al. ORS 2012.

The Improvement of Biosensor Devices using Functionalized Nanoparticles

Melissa D. Gaillard[1,3], Matthew S. Makowski[1,2], Albena Ivanisevic[1]

[1]Department of Materials Science and Engineering, NC State University;
[2]Weldon School of Biomedical Engineering, Purdue University;
[3]Department of Biomedical Engineering, Clemson University

Statement of Purpose: Biosensors are an important tool to detect and measure analytes in a biological system. Many biosensors work as a simple transistor, taking a signal from a biomolecule and transducing it into a measureable signal. There are numerous situations in which analytes need to be detected quickly and accurately. Accordingly, the improvement of biosensing devices is critical. One such way of improving is through use of functionalized nanoparticles. In this study, the surfaces of biosensors are coated with amine, alkane, or carboxyl functionalized gold nanoparticles. The surface potential of the functionalizations electrically gate the electrons in the channel of the biosensor, changing the electrical properties of the device. By understanding these electrical properties, nanoparticle coated biosensors can be modified to have quick response, high specificity, inexpensive fabrication, reusability, multiplexing capabilities, and label-free detection.

Methods: Three separate GaN biosensor devices were coated with amine, alkane, or carboxyl functionalized gold nanoparticles. To collect values for the surface potentials of each functionalization, Kelvin Probe Force Microscopy was used. After these values were collected, UV treatment was used to strip the functionalizations off of the nanoparticles on the biosensors. To confirm that the change in surface potential was due to functionalization only, the surface potentials were measured after exposure to UV light. Statistical analysis was done on the data.

Results: The results acquired from Kelvin Probe were statistically significant, with a p-value less than 0.001. The control group had a p-value of 0.182, meaning that it had no statistical significance.

Functionalized Gold Nanoparticles	
Functionalization	Mean Surface Potential
Alkane	58 mV $\pm$ 12
Amine	-51 mV $\pm$ 20
Carboxyl	-25 mV $\pm$ 9
P-value: <0.001	

Table 1. Mean surface potentials and standard deviations for each of the functionalizations are shown. Functionalized Au NPs are used as the experimental group.

UV Treated Gold Nanoparticles	
Functionalization	Mean Surface Potential
Alkane	-21 mV $\pm$ 12
Amine	-43 mV $\pm$ 12
Carboxyl	-35 mV $\pm$ 23
P-value: 0.182	

Table 2. The functionalizations of the NPs were stripped by using UV light. Mean surface potentials and standard deviations for each of the functionalizations are shown. UV treated NPs were used as the control group.

Conclusions: Functionalized nanoparticles had statistical significance, while UV treated nanoparticles did not. Therefore, the functionalizations had an effect on the surface potentials of the nanoparticles. The UV treatment was successful in removing these functionalizations and thus their effects on surface potential. These various functionalizations can be used to program the electric properties of a biosensor, consequently improving them to have desired characteristics. Future work might include binding bioreceptors to the nanoparticles using these functionalizations, which might be more applicable for in vivo applications. Other functionalizations beyond that of just alkane, amine, and carboxyl can be analyzed to have a wider variety of choices for biosensing devices.

Development of a Low-cost Glucometer with Print On-demand Test Strips

Kayla Gainey, Joey Wilson, Kelsey Byrd, and Dr. Delphine Dean

Dep1artment of Bioengineering, Clemson University

Introduction: More than 285 million people in the world have diabetes and require daily blood glucose monitoring. As glucometers have evolved, they have become more accurate (~3% variance), but test strips can be expensive for patients, especially those without health insurance. In addition, in developing countries that rely on donated medical supplies, matching meters and strips are not always available to patients. The goal of our project is to design a low-cost meter and strip system that can be used in resource poor settings when standard meters or strips are not available. Our strategy is to create test strips that may be printed on-demand by a standard inkjet printer. This system would serve as an interim technology until more advanced systems become accessible in developing countries.

Materials and Methods: To print the enzyme, we used emptied color-ink cartridges. Glucose oxidase, horseradish peroxidase, and O-Dianisidine dihydrochloride are inserted in the printing wells of separate cartridges. These enzymes catalyze a glucose reaction whose final products elicit a color change. The enzymes are printed using a template in Microsoft Word. By varying the color in the templates, we can select the amount of each enzyme applied to the paper. Filter paper is used due to the high viscosity of blood to provide adequate flow. Once the paper has the solutions printed, it is covered with contact paper for structure and to prevent bleed-through. For proof of concept, the strips were tested using glucose solutions of varying concentrations (0-450 mg/dl). To read the strips, we designed a low-cost glucometer using LED lights, a photodetector, and an amplifier that outputs the absorbance, which is processed by an Arduino microcontroller to determine the glucose concentration based on a standard curve.

Results and Discussion: We found that the absorption measurement was able to distinguish between glucose solutions with 25 mg/dl accuracy. This provided us with a standard curve to relate absorbance to glucose concentration; it also showed that the enzyme concentrations were capable of accurately processing the necessary ranges of glucose. Due to complications with the circuit building, we have not been able to test the accuracy of the glucometer yet. After trying several test strip designs, we have a strip that will control the amount of blood the enzymes are exposed to while allowing for use of the control photodetector. Our preliminary testing has shown a definitive color change on the strips that were printed using an inkjet printer when a 450 mg/dl glucose solution was applied.

Conclusions:

The research thus far confirms that a printable test strip is feasible as a means for monitoring glucose levels. While these strips are not as accurate or as fast as current commercially available strips, they are accurate enough to provide interim support while patients await other devices. In addition, the current design of the measurement device is inexpensive and easy to build. Improvements can be made and more testing is planned. While photodetectors have been used successfully in other applications to measure absorbance, a completed circuit needs to be tested to be certain they will work in this system.

Acknowledgements:

Clemson Creative Inquiry, NIH K25 HL092228

Dental Pulp Cell Response to Micropatterned Substrates

Theresa Hafner, M. Cupelli, P. Gould, A. Patrick, D. Dean, M. Kennedy
Clemson University

Statement of Purpose: Unlike bone, teeth exhibit very poor native tissue repair mechanisms; there is very limited repair of damaged dentin by odontoblasts and almost no repair of enamel after damage. Many studies have started to focus on tissue engineering for dental restoration. Before dental pulp cells can be used for regenerative tissue strategies, more needs to be known about what factors affect their phenotype and differentiation. Our long-term goal is to understand how to engineer and design material that can push dental cells to repair damaged dentin and enamel. In our current study, we are subjecting dental pulp stem cells to different topographical substrates to analyze their migration, proliferation, and morphology.

Materials and Methods: A density of 250,000 cells was plated onto micropatterns created using lithographic techniques on a gold coated silicon wafer. Prior to cell plating, the surfaces were treated with an amine-terminated self-assembled monolayer to promote cell adhesion. There were four different types of patters: lines, circular holes, circular bumps, and hexagonal honeycomb patterns along with a control wafer. The line and circular patterns are similar to patterns used by other researchers with bone marrow cells. The hexagonal pattern was selected because it mimics the hexagonal structures found in natural dentin. Images were then taken on days 0, 1, 3, and 5 to study cell density, cell migration, and cell alignment for each of the patterns.

Results and Discussion: The cell culture studies are currently underway. Interestingly, initial results show that after a 3 day period the cell density decreased significantly over the course of a day after initial plating, perhaps due to the initial availability for cell-to-surface attachment. From qualitative analysis it appears as though cell density may continue to decrease over time, although at a much slower rate. Whether this is due to migration or cell death further information must be gathered to make a conclusive argument for either reasoning. The cells seemed to show some preference towards patterns based on their alignment on the patterns. For instance, while no cell spreading could be seen on the hexagonal or dot patterns the dental pulp cells spread across the line and hole patterns in a manner much more characteristically seen of adherent dental pulp cells when culturing them in a flask. This same behavior was observed on the control gold wafer consisting of no patterns, indicating that the pattern type does in fact play a role in the relationship between cell-surface interactions resulting in spreading

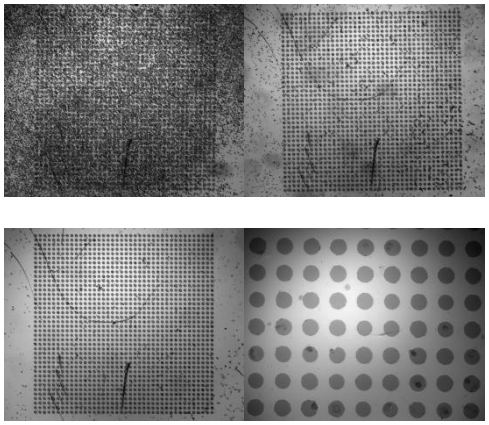

Above Figures: Dot pattern on days 0,1, and 3. Observable cell density found on the dot micropattern on days 0, 1, and 3. Close up image shows the cells retaining a round, closed shape

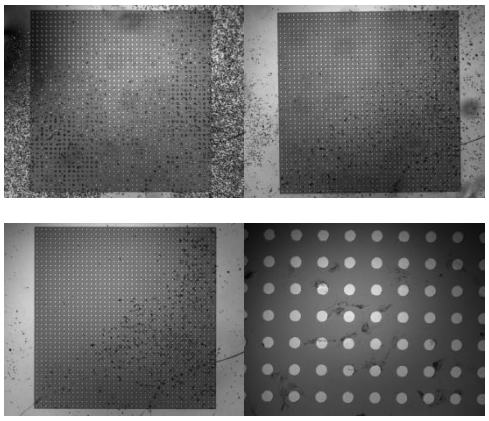

Above Figures: cell density found on the hole micropattern on days 0, 1, and 3. Close up image shows the cells stretching across the pattern

Conclusion: Successive trials are necessary in order to affirm the above findings. Particularly, an aim towards accurately quantifying future trials should be devised in order to provide statistical evidence for any conclusions. Current leads towards this end include fluorescently staining the nucleus in hopes of being able to count with an automated cell counter, and using a plasma membrane fluorescent dye in order to better study alignment. **Bibliography:**

1. Xue Chen, *Substrate Topography Design and Fabrication for Osteoblast and Dental Pulp Stem Cell Studies. 2011*
2. Laura Christine Dakto, *Effects of Microenviornment on Growth and Differentiation of Human Dental Pulp Cells. 2011*
3. Peter E. Murrary and Franklin Garcia-Godoy. *Stem Cell Responses in Tooth Regeneration.. 13: 255-262 (2004).*

Targeted delivery of doxorubicin using Herceptin functionalized glycol chitosan nanoparticle

Huacheng He[1] and Peisheng Xu*
Department of Pharmaceutical and Biomedical Sciences, South Carolina College of Pharmacy, University of South Carolina,
715 Sumter Street, Columbia, South Carolina, 29208, Ph. 803-777-0075, *Email: xup@sccp.sc.edu

Statement of Purpose: Chitosan derivatives, especially glycol chitosan (GCS), have been widely investigated as carriers for anti-cancer drug delivery due to their water-solubility, biodegradability and biocompatibility *in vivo.* [1,2] Thus we chose GCS as the substance for nanoparticle preparation. In addition, targeting ligand-modified nanoparticle has become a promising delivery system for cancer therapy because of its enhanced cellular uptake, high therapeutic efficacy and reduced toxicity and side effects to normal cells.[3] Here we expected to functionalize our nanoparticle to realize targeted drug delivery. Furthermore, intracellular and extracellular difference in some properties (e.g. pH, redox potential) can be utilized as signals to realize the controlled release of anti-cancer drugs. Also we designed the nanoparticle to take advantage of this property.

In this research study, we synthesized glycol chitosan based nanoparticles. Inside the nanoparticle, disulfide bonds (-SS-) were introduced to allow the nanoparticle response to the intracellular glutathione to release the drug since glutathione concentration is much higher inside the cell than extracellular matrix.[4] And in order to realize the targeted delivery of anti-cancer drug (e.g. doxorubicin), the surface of the nanoparticle was functionalized with Herceptin whose receptor called Human Epidermal Growth Factor Receptor 2 (Her2) is overexpressed among certain cancer cells such as breast carcinomas.[5]

Materials: Glycol Chitosan and Sephadex G-25 were purchased from Sigma-Aldrich Chemical Co. (St. Louis, MO, U.S.A). N-Succinimidyl 3-[2-pyridyldithio]-propionate SPDP was purchased from ProteoChem, Inc. (Denver, CO, U.S.A). Aldrithiol-2 was purchased from Tokyo Chemical Industry Co., LTD (Portland, OR, U.S.A). Doxorubicin was purchased AK Scientific, Inc. (Union City, CA, U.S.A). Herceptin was purchased from Roche LTD (Switzerland). Dulbecco's Modified Eagle Medium (DMEM; high glucose with L-glutamine) was purchased from Life Technologies Corporation (Grand Island, NY, U.S.A) and fetal bovine serum (FBS) was purchased from ATCC, American Type Culture Collection (Manassas, VA, U.S.A). All chemicals were used without any further purification unless otherwise noted.

Method: Glycol chitosan was firstly de-polymerized and further modified by 2-(pyridine-2-yldisulfanyl)ethyl acrylate (PDSA) by Michael Addition reaction. Later thiolated doxorubicin (DOX-SH) was conjugated to glycol chitosan by thiol-disulfide exchange reaction between PDSA and DOX-SH. The conjugation of DOX-SH will increase the hydrophobicity of glycol chitosan and thus improve the loading efficiency of anti-cancer drug in the core of nanoparticle. Free base form doxorubicin, acquired after reacting with triethylamine, was encapsulated into glycol chitosan nanoparticle after dialysis towards phosphate buffered saline (PBS). Finally, the resulting nanopaticle was functionalized on the surface with Herceptin. We expected that: a) the disulfide bond (-SS-) can lead to a rapid drug release due to the cleavage of –SS- inside the cancer cell; b) Hercetpin functionalized nanoparticle is more effective towards Her2-positive cell line (MCF-7 Her2) than nanoparticle without functionalization. Doxorubicin concentration was measured by fluorospectrophotometer. Cell viability was determined by MTT cell proliferation assay.

Result: GCS based nanoparticles with and without Herceptin functionalization are both smaller than 150nm in diameter. This size range is acceptable for drug delivery. Additionally, Herceptin functionalized nanoparticle presents improved cell toxicity towards Her2-positive cell line (MCF-7 Her2) when compared to non-functionalized nanoparticle. Both nanoparticles show almost the same toxicity towards Her2-negative cell line (MCF-7 Her2/neu).

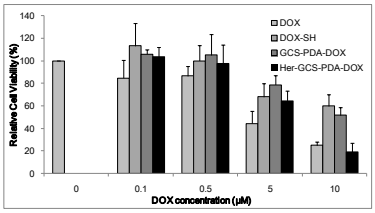

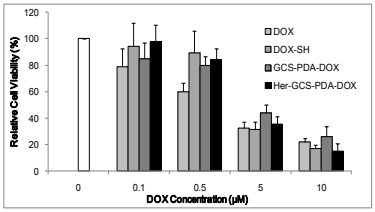

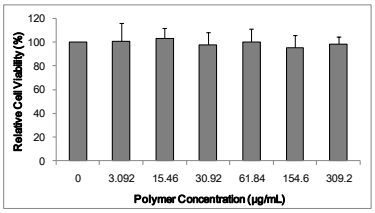

(A) (B)

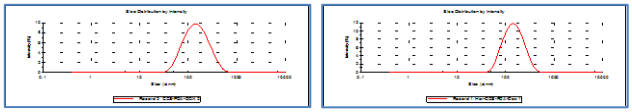

Figure 1. Size distribution of nanoparticles: (A) GCS-PDA-DOX (without Herceptin) and (B) Her-GCS-PDA-DOX (with Herceptin).

(A)

(B)

(C)

Figure 2. MTT results after 48h treatment of DOX, DOX-SH, Her-GCS-PDA-DOX (with Herceptin functionalization) and GCS-PDA-DOX (without Herceptin functionalization) nanoparticles for different cell lines. (A) Her2-positive cell line (MCF-7 Her2); (B) Her2-negative cell line (MCF-7 Her2/neu); (C) Toxicity of GCS-PDA polymer. (For

nanoparticle, it contained GCS-PDA polymer concentration is equal to 309.2ug/mL at 10uM DOX concentration).

Conclusion: We have achieved a glycol chitosan based nanoparticle. The glycol chitosan polymer itself shows no toxicity to cells, which suggests it is a safe material for drug delivery. The nanoparticle presents improved anti-cancer efficacy in Her2-positive cell lines, which is due to the interaction of targeting ligand (Herceptin) and its specific receptor expressed on the membrane of cancer cells.

References:

(1) Kim, J.-H., et al., *J. Control. Release* 2006, 111, 228-234.
(2) Sinha, V. R., et al., *Int. J. Pharm.* 2004, 274,1-33.
(3) Arya, G., et al., *Nanomedicine* 2011, 7, 859-870.
(4) Meng, F., et al., *Biomaterials* 2009, 30, 2180-2198.
(5) Hudis, C. A. *N. Engl. J. Med.* 2007, 357, 39-51.

Systematic Characterization of Specific Design Features for Retrieved Joint Prostheses

Katherine Henson, Ryan Quinn, Jacob Kuruvilla, Alison Lamb, John DesJardins, Melinda Harman
Department of Bioengineering, Clemson University

Statement of Purpose: Joint replacement, using prostheses fabricated from metal, plastic and ceramic, is a successful orthopaedic surgical procedure for treating arthritis and other degenerative joint diseases. Worldwide, more than 2.5 million joint replacement procedures are performed annually. Explant registries, sometimes referred to as "implant retrieval programs", are a promising means for quantifying the performance of joint prostheses and translating the clinical outcomes into metrics useful for biomechanical joint simulations and computational models. Explant registries aim to document comprehensive evaluations of prostheses after they have functioned in patients. However, extracting detailed information about specific prosthesis designs in a given registry is cumbersome, often requiring previous knowledge about a specific prosthesis brand or direct visualization of the explanted devices in hand. Although protocols for cataloging explanted prostheses do exist, their implementation for accurately characterizing specific design features and materials remains a challenge. The purpose of this study is to implement a standardized protocol for characterizing design features and materials for explanted knee and hip prostheses and apply it to explants that have been archived in the Clemson University Retrieval of Explants Program and Registry in Orthopaedics (CU-REPRO).

Methods: Retrieved joint prostheses obtained through an IRB-approved protocol were collected from participating hospitals and archived in CU-REPRO. The prostheses were logged and assigned a unique identification number and fixed in 10% neutral buffered formalin for a minimum of two weeks. To clean, students first used distilled water and a soft brush to remove soft tissues from the prosthesis, and then followed ASTM standards for cleaning in the ultrasonicator. Afterwards, students assessed the prostheses using an Implant Descriptor Form (Figure 1) to record physical information about the prostheses and then entered this information into the CU-REPRO database (Figure 2). The Implant Descriptor Form included design features common to hip and knee prostheses, including anatomic location, type of modularity, articular constraint, bearing and non-bearing material, fixation, relative condition, and manufacturer.

Results: To date, more than 225 explanted knee prostheses have been characterized using the standardized Implant Descriptor Form and cataloged into the CU-REPRO database. The Implant Descriptor Form proved useful for identifying key aspects of the prostheses by users with little prior knowledge of joint replacement designs. The CU-REPRO database proved useful for cataloging vital information to allow queries to narrow the number of prostheses with a given design feature. To do this, it has been important to keep recruiting and training students to maintain the database information as creditable and current. Four student users have been trained and started to record information on the Implant Descriptor Forms and input it into the CU-REPRO database. The database has been functioning correctly and the students have quickly picked up the knowledge necessary for accurate archiving of the retrieved implants.

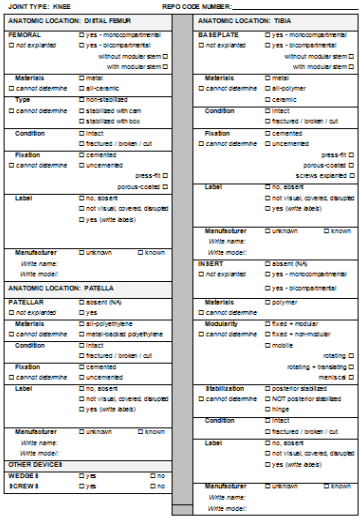

Figure 1: The Implant Descriptor Form included check-boxes to maintain uniformity among student assessors.

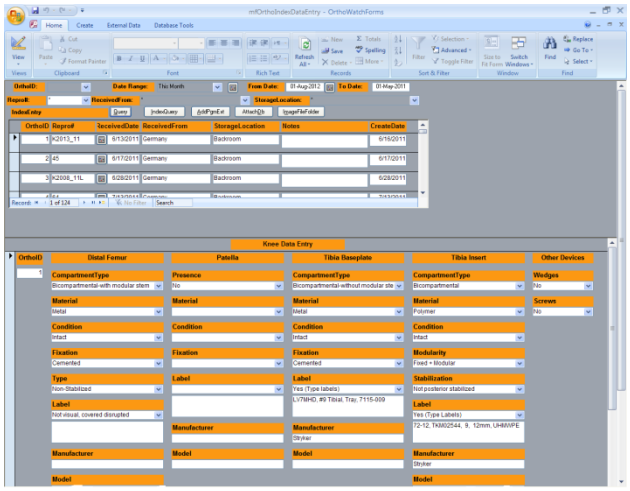

Figure 2: Dropdown menus in the database, created in Microsoft Access, duplicated the check-boxes on the Implant Descriptor Form.

Conclusions: The standardized characterization process for retrieved knee prostheses described in this paper is an easily implemented protocol for classifying joint replacement designs. Device characterization, database entry, and database searches can be performed by those with little knowledge of orthopaedics. Future work on this project involves adding a section to the Implant Descriptor Form specifically for hip prostheses to characterize the large number of explanted hip prostheses currently archived in CU-REPRO. It is intended that this database will provide a well-organized foundation of specimens suitable for research activities.

DEP Manipulation and Placement of Polystyrene Beads

Johnie Hodge and Guigen Zhang
Department of Bioengineering, Institute for Biological Interfaces of Engineering, Clemson University

Introduction: Dielectrophoresis (DEP) can be used to manipulate particles for lab-on-a-chip applications. This technique involves the movement of particles with no net charge (dielectric) when exposed to a non-uniform electric field. This differs from electrophoresis in that electrophoresis involves the movement of charged particles due to an electric field. The dielectric particles used in these studies are polystyrene beads ranging from 2µm to 10µm in diameter.

The studies described below have been designed in order to investigate the operation and efficacy of relatively low voltage dielectrophoresis for the purpose of micron-scale particle arrangement and manipulation. With this goal in mind, some work has also been done as far as attempting to characterize and quantify some of the forces involved in this process.

Methods: The principal setup used for all experiments conducted involved attaching the electrode setup to an AC function generator (0-32Vpp and 0-20MHz) and an oscilloscope to monitor the applied voltage. The electrode itself consisted of a thin titanium/gold film on a glass slide into which the pattern was laid-out and etched using photolithographic techniques. Several electrode shapes were used, all with different interdigitated geometries. Deionized water was placed on the electrode surface, above this there was a layer of insulation sheet (12µm thick) onto which the drop of polystyrene bead solution was placed. Various voltages and frequencies were then applied within the capabilities of the function generator listed above.

Results: It was found that using this setup, "pearl chains" formed readily between the interdigitated electrodes within certain frequency bands once sufficient voltage was applied (~16Vpp).

Other particle arrangements were also repeatedly induced at frequencies outside these bands. Experimental evidence also has shown that as a higher frequency is applied, a lower voltage is required in order to lift the beads off.

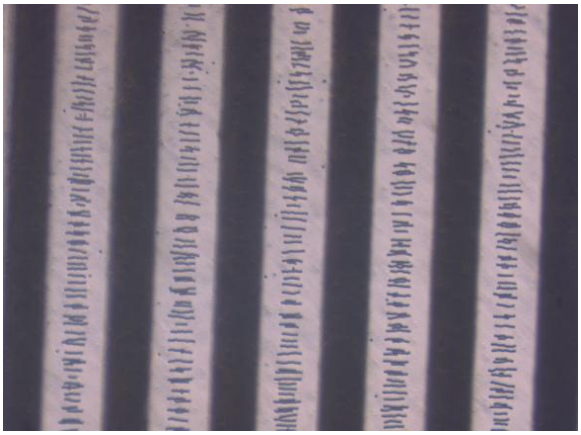

Figure 1: Pearl chains, 2µm beads

Conclusions: It has been found that it is possible to dielectrophoretically position polystyrene beads using voltages as low as 16Vpp using this setup. This voltage is significantly lower than that used by other similar studies.[1] The use of the insulation layer also allows the electrode to be reused, thus further reducing cost.

Future work will be done to achieve a more complete characterization of the vertical (lifting) component of the force due to the induced electric field. Results will be compared with analytical predictions.[2] Additional work will involve the application of these experimental conditions to cells in suspension for the purpose of patterning cells on devices for tissue engineering or other possible applications.

References:

1. Park K. Lab Chip. 2009; 9; 2224-2229.
2. Wang X –B. Biochim Biophys Acta. 1995; 1243; 185-194.

Creation of a Biodegradable Stent Utilizing Polydioxanone

James Hyde, Garret Kent, Philip Gould, Qi Guo, and Erik Hammes
Clemson University

Statement of Purpose: The purpose of this research is the creation of a biodegradable ureteral stent utilizing polydioxanone (PDO). Ureteral stents are used to maintain the flow of urine from the kidney to the bladder. They are used in treatment for urinary incontinence, kidney stones, renal transplants, and inflammation. They are implanted after almost every urological procedure to assure ureteral patency. However, current stents require a second removal surgery and are prone to encrustation. The urinary incontinence therapeutics market alone had a value of approximately 2.6 billion dollars in 2010 and is expected to double by 2018. (1) The creation of a stent that degrades safely in the ureter would prevent long-term encrustation and eliminate the need for a removal surgery. The stent must be flexible, strong, and not migrate after implantation.

Methods: The stent is made of polydioxanone, an FDA approved biodegradable polymer used in sutures. To create the stent, size 2 (.5 mm diameter) sutures are wrapped around a rod with diameter equal to the desired inner lumen in the desired shape. The material is then heated to 100^0C for 24 hours. Following the heating process, the still wrapped stent is quenched to -20^0C for 1 hour. This annealing process causes a change to the material that stiffens and strengthens it. Three areas of testing were identified to determine efficacy of the stent prototype: degradation rate, anchor strength, and flow testing. Preliminary degradation testing was carried out at 37^0C and tested under a flow rate of 5 mL/min. Anchor strength was tested by implanting the stent in a model ureter (latex tubing 4.65 mm inner wall) attached to a kidney and applying force until the stent experienced slippage. (n=5) Maximum flow rate was determined by anchoring the stent in the model ureter and then running 200 mL of water through the stent. (n=5) The time of flow through the stent was measured and the flow rate determined. Differential Scanning Calorimetry (DSC) was utilized to determine change in material properties.

Results: A ureteral stent encompassing the desired design criteria was successfully produced. The final product, including anchors, can be seen in Fig. 1. Figure 2 shows results of degradation testing. Figure 3 shows DSC data for PDO before and after processing. It was found that the average maximum force the anchor could withstand was 0.038 N. The average maximum flow rate of the implanted stent was found to be 390.5 mL/min.

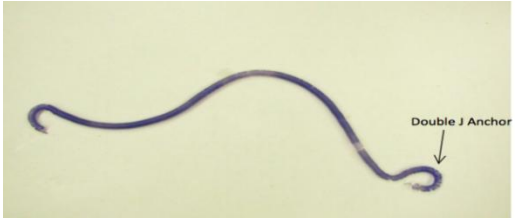

Fig. 1 Full Length Ureteral Stent with Double J Anchor

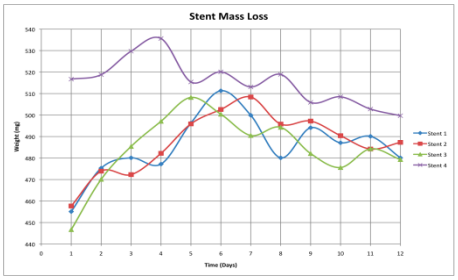

Fig. 2 Degradation Testing: Stents 2-3 are final prototype

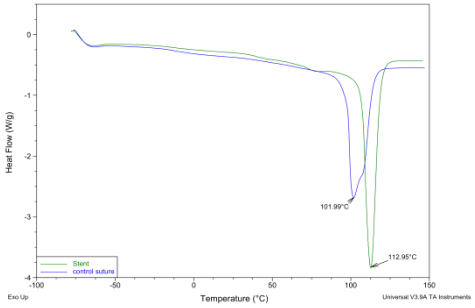

Fig. 3 DSC of PDO before and after processing

Conclusions: A working ureteral stent was created utilizing FDA approved polymers that were processed in a novel manner. It should be able to be implanted using existing methods. The stent was created with the common double J anchor type. Each bend should hook into the kidney or the bladder to prevent migration. Degradation testing showed that the polymer appeared to gain weight initially and then slowly start to lose mass. It is hypothesized that the increase in weight is due to absorption of water by the polymer. The DSC shows there is a definite change in the material after processing. However, the curve doesn't show the peak that indicates a change in crystallinity. Thus, there is not a phase change in the polymer. The change in stiffness may, instead, be a result of erasing the thermal history of the polymer. Additional testing must be done to confirm this.

References:

1. Dolcera - Patent and Market Research Services. Ureteral Stent - Market Analysis [Internet]. 2011 Jul 28. Available from: http://dolcera.com/

Special thanks to Dr. Mefford for his help running DSC.

Development of a Tissue Testing System for Three-Dimensional Biomechanical Analysis of Abdominal Aortic Aneurysm

Brad Johns, Brian Dean, Brittany York, Nitin Balakrishnan, Britton McCaskill, Jiro Nagatomi
Department of Bioengineering, Clemson University

Statement of Purpose: Abdominal aortic aneurysms (AAA) are localized, progressive dilations of the aortic wall and are the 13th most common cause of death in the United States, claiming about 15,000 lives annually. Surgery is usually recommended when the aneurysm is 5cm or larger in diameter; if the aorta bursts, severe hemorrhaging will occur, ultimately leading to death via exsanguination in 90% of cases. Because of this clinical parameter, previous studies of AAA biomechanics have utilized a one-dimensional analysis that focuses solely on changes in wall diameter and have attempted to model geometric changes with mathematical formulas, generally based on the LaPlace equation. This is not sufficient however, as the mechanical behavior of the tissue at sites of aneurysm have been documented as being nonlinear, anisotropic, and non-homogeneous. Further, since aneurysms have been found to vary in their progression, the success of such models in predicting geometric changes leading to rupture has been minimal. Therefore, an approach to quantify the 3-D changes in the wall geometry of AAA is necessary for adequate estimations of the abnormal wall stresses and strains that occur at the site of aneurysm. The overall aim of this project is to develop an ex vivo tissue testing system that will allow for 3D biomechanical analysis of aorta specimens.

Methods: To quantify the relationship between pressure and aortic wall 3D geometry, we have developed an experimental setup that allows tissue samples to be pressure loaded and imaged from multiple angles at predetermined pressure increments. The testing apparatus is composed of: (1) a stepper motor (Haydon Kerk Motion Solutions) and a set of gears to rotate an aorta specimen; (2) a syringe pump (Harvard Apparatus) which infuses physiological solution into the specimen to apply pressure loading; (3) a pressure transducer (Omega Engineering) to monitor the intraluminal pressure for feedback control of the pump; (4) a webcam (Logitech) to image the specimen from outside the tissue bath wall, and; (5) a custom LabVIEW program to control all these components and fully automate the experimental procedure as described above. The motor was calibrated so that one complete revolution of the specimen will allow acquisition of 12 images in 30° intervals of rotation. We have also developed custom MATLAB scripts to process the images and produce a 3-D representation of the specimen at each pressure interval by stitching together the acquired 2-D images. Calibration phantoms with aneurysm-like structures with known geometry were fabricated using Solidworks drawings and printed in 3-D. All models had cylindrical regions with a constant diameter, and 'bulge' regions with varying radii of curvature (2mm, 6mm, 18mm) at the fillet. These phantom structures were imaged and then processed using our code, which produced representative 3-D computer models. In order to test the accuracy of our code, several points on the surface with known principal curvatures were chosen for examination. At these points, maximum and minimum principal curvatures (κ1, κ2), as well as mean (H) and Gaussian (K) curvatures were quantified.

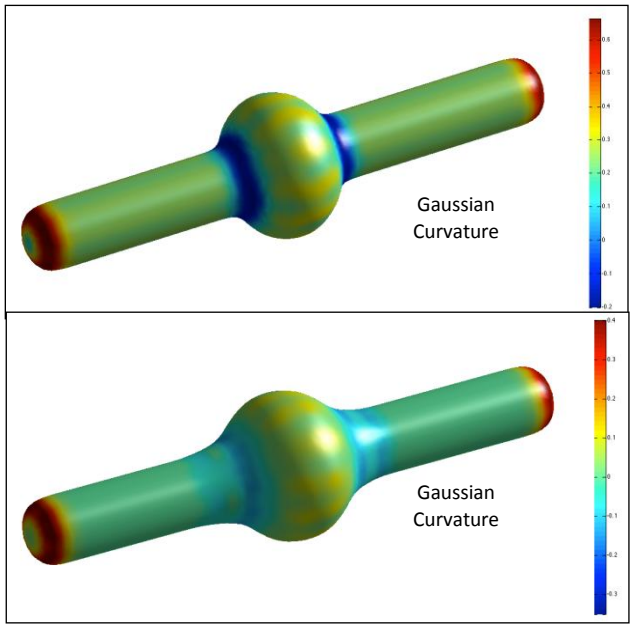

Results: The results obtained using the calibration phantoms revealed that the principal curvature calculations using our code were accurate to within 0.02 mm^{-1}. Our code also found accurate mean and Gaussian curvatures for all points on the surface of the phantom models. We have also tested the apparatus with latex rubber tubing as a phantom specimen. Results from these experiments show a steady ramping of pressure from 0 to above 180 mmHg using the syringe pump at a flow rate of 2 mL/min, with the ability to maintain the pressure at set levels to within 5 mmHg. At these pressure levels, our LabVIEW code allows for proper rotation and imaging of the test subject.

Conclusions: Upon completion of calibration, we plan to explore the efficacy of treatment possibilities for AAA using our testing apparatus and biomechanical analysis. Specifically, a rat model of AAA will be treated with experimental pharmacological agents, such as pentagalloyl glucose (PGG), and aneurysmal tissues will be compared to those of "normal" aortic tissue to see if any improvement or reversal of aneurysm characteristics has occurred. This will be accomplished by utilizing our 3-D computer models to detect changes in wall curvature as pressure is varied. Our hypothesis would be that an effective treatment should decrease not only wall diameter, but also wall curvature, resulting in an overall decrease in wall stress.

References: Vorp DA. J Biomech. 2007;40(9):1887-1902. Thirion JP. Comp Vis Img Und. 1995;61(2):190-202. Isenburg JC. Circulation. 2007;115:1729-1737. Sacks MS. Ann Biomed Engr. 1999;27:469-479.

Optimization of an Implantable Biosensor System for Continuous Monitoring during Trauma

Christian Kotanen[1], Olakayode Karunwi1 and Anthony Guiseppi-Elie[1,2]
Clemson University Bioengineering[1], Chemical and Biomolecular Engineering[2]

Statement of Purpose: Hemorrhage that accompanies trauma is the principal cause of death for persons 50 years and younger. Implantable biochips are being developed to improve trauma patient outcomes [1]. Early hyperglycemia as a result of insulin resistance is associated with excess mortality and hyperlactatemia, indicative of oxygen debt, is prognostic of trauma patient outcome. Enzymatic amperometric biosensors for glucose and lactate are capable of measuring a range of metabolite concentrations that can be useful for trauma surgeons and *intensivists*. Current generation implantable biotransducers require an ensemble of biocompatible, electroconductive and bioresponsive polymer membranes in order to successfully interface with tissues in the body [2]. The current work characterizes biotransducers fabricated using electropoymerization of pyrrole (Py) to selectively immobilize glucose oxidase (GOx), ferrocene monocarboxylic acid (FcCOOH) (a redox mediator) and carbon nanotube glucose oxidase conjugates (GOx-SWCNT) at platinum microelectrodes. Electropolymerization kinetics, electrical impedance spectroscopy, and the resulting immobilized enzyme bioanalytical parameters were studied as a function of PPy electropolymerization charge density.

Methods: Platinum microelectrodes (BASi, ϕ = 100 µm) were cleaned and seeded with a polystyrene sulfonic acid doped, nano-thin polypyrrole layer at a charge density of 10 mC/cm^2 in order to provide a stable substrate for subsequent enzyme immobilization. Biospecificity was then conferred to transducers through electropolymerization in solutions containing 0.2 M Py along with one of the following: i) 1 mg/ml GOx, ii) 1 mM FcCOOH and 1 mg/ml GOx, or iii) 1 mg/ml GOx-SWCNT conjugate. Charge densities ranging from 0.1 – 200 mC/cm^2 were explored. The polypyrrole was overoxidized prior to amperometric interrogation. The biotransducers were characterized *in vitro* using flow-injection of glucose into PBS buffer at room temperature at 0.65 V *vs.* Ag/AgCl (3M KCl) under aerated and argon sparged conditions.

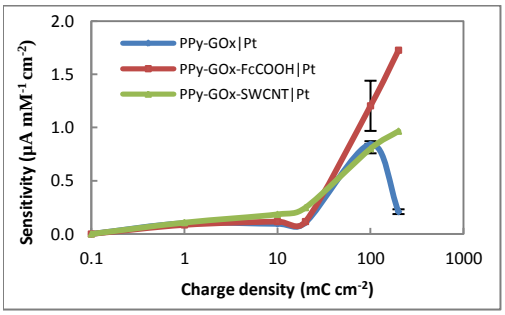

Fig. 1. The influence of electropolymerization charge density on biotransducer sensitivity.

Results: Cyclic voltammograms showed a maximum biosensor response to glucose at potentials beginning ca. 650 mV vs. Ag/AgCl for both aerated and sparged solutions. Polymerization kinetics was fastest for FcCOOH-GOx doped polypyrrole and slowest when solely GOx was used as a dopant. Biosensor sensitivity was shown to increase as polypyrrole charge density was increased, **Fig 1**. The greatest increase in sensitivity was observed at 100 mC/cm^2 for all biosensor types. Impedance profiles show that overoxidation occurs during the polymerization process. Electrochemical discharge of hydrogen peroxide was the dominant mechanism of biosensor response to glucose for all three biosensor types.

Conclusions: Biosensors fabricated using electropolymerization of polypyrrole are capable of generating adequate amperometric response to target *in vivo* concentrations of analytes. Incorporation of a mediator, FcCOOH or single wall carbon nanotubes as GOx conjugates did not change the oxygen dependence of the biosensor system. Polymerization efficiency was greater for FcCOOH and SWCNT-GOx systems while maintaining high sensitivity.

Acknowledgements: US DoD PRMRP grant DAMD17-03-1-0172 and the C3B.

References: [1] Kotanen, C.N. and A. Guiseppi-Elie, *ASGSB Bull* 2010. **23**(2): p. 55-63. [2] Kotanen, C., C. Tlili, and A. Guiseppi-Elie, *Appl Biochem Biotech*, 2012. **166**(4): p. 878-888.

Low Dose L1 Optimizes the Living Condition of Chick Embryonic Forebrain-Neuron Culture

Yan Kuang[1], Lina Wei[2], Atanu Sen[1], Tingfei Xi[2], Ken Webb[1], Mark Kindy[3], and Bruce Z. Gao[1]
[1]Department of Bioengineering, Clemson University, Clemson, SC
[2]Center for Biomedical Materials and Tissue Engineering Peking University, Beijing, China
[3]Medical University of South Carolina, Charleston, SC

Statement of Purpose: In exploration of the etiology and mechanisms of the recent rapid increase in the preveilence of Autism Spectrum Disorders (ASD), the imbalance of excitation/inhibition in the cortical neuronal network has been proposed to underpin the pathophysiological changes of ASD and supported by increasing research data. To study the proposed imbalance at the cellular and neuronal network level, morphological and immunohistochemical classifications of the cortical excitatory projection neurons (glutamatergic) and the inhibitory interneurons (GABAergic) is essential, which requires an evenly non-clustered distribution of the seeded neurons in a proper density in our chick-forebrain-neuron (FBN) culture. However, cultured chick FBNs sometimes aggregate to form clusters in the wells pre-coated with poly-L-lysine (PLL), particularly in the presence of glials. This clustering interferes with the morphological and immunohistochemical classifications of FBNs and further study on the imbalance of cortical excitation/inhibition. To optimize the chick FBN culture, L1 was selected to solve the cell clustering problem and to promote the neuronal network formation due to its positive effect on neurite outgrowth and its inhibitory effect on the glial attachment in the chick FBN culture [1]. L1 is a natural cell adhesive protein expressed dominantly on the surface of neurons in nervous system. The objective of this study was to test whether a desired, non-clustered, evenly distributed, purer and healthier neuronal network could be achieved in chick FBN culture to facilitate cortical neuron classification and the study on the imbalance of excitation/inhibition.

Methods: E6-8 chick FBNs were dissociated and plated randomly on various cell culture wells. Purified recombinant insect cell-derived L1 was obtained from Professor Webb's Lab in the Department of Bioengineering at Clemson University[2]. Control wells were pre-coated with PLL (0.1 mg/ml, Sigma) only. L1 effect was examined in three experimental conditions: a) pre-coating L1 only, b) pre-coating L1 mixed with PLL, and c) one-time administration of soluble L1 after cells attached on PLL pre-coated substrate (24 hrs after seeding). A wide dose range of L1 was used in condition a) and b). Cell attachment, neurite outgrowth, and the neuron distribution in culture were observed, documented, and photographed every other day. **Results:** 1) The ability of L1 to promote neurite growth increased dose-dependently over a wide range from 2.5 μg/ml to 100 μg/ml. 2) FBNs in control group grew more but thin neurites, whereas in the presence of L1, neurons grew less but thicker neurites as shown in Fig. 1.

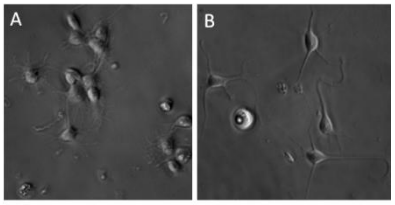

Figure 1. FBNs 1 day in cultures: A) control cells on PLL coating; B) cells on L1 coating.

3) Cells in PLL + L1 group distributed most evenly in comparison with the control and the L1 only group. This desired effect was more favorable in a low dose of L1 ranging from 10 μg/ml to 25 μg/ml. 4) The one-time administration of 10 μg/ml soluble L1 at 24 hrs after seeding prevented FBNs from degeneration in comparison with the control neurons shown in Fig 2.

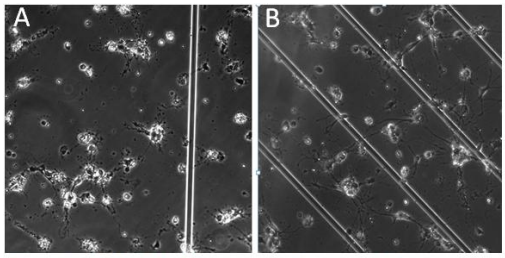

Figure 2. FBNs 7 days in cultures after a one-time administration of soluble L1 (10 μg/ml) at 24 hrs after dissociated FBNs were plated on chambers of micro-electrode arrays pre-coated with PLL: A) Control; B) soluble L1 treated.

Conclusions: Low dose L1 facilitates even distribution of FBNs in culture and prevents FBNs from degeneration. **References:**

[1] Webb, K. et. al., Biomaterials. 2001; 22:1017- 1028

[2] Cribb, R.C et. al., Protein Expression and Purification. 2008; 57:172–17

Cellular remodeling in different network compositions of PEG diacrylate/hyaluronic acid semi-IPNs

Ho-Joon Lee, Atanu Sen, Jeoung Soo Lee, Ken Webb
Department of Bioengineering, Clemson University, Clemson, SC 29634

Statement of Purpose: Hybrid hydrogels are designed to integrate the precise control of composition/properties provided by synthetic networks with the bioactivity of naturally-derived materials. PEG derivatives crosslinked with MMP-sensitive peptides are a prominent example and have been widely used for *in vitro* culture models and *in vivo* tissue engineering. Alternatively, the use of intact, naturally-derived macromolecules offers several benefits including substantially lower cost and preservation of native structure supporting higher rates of enzymatic degradation. Previously, we have shown that incorporation of native hyaluronic acid (HA) into photocrosslinked networks of hydrolytically degradable PEG diacrylates (PEGdA) creates semi-interpenetrating networks (semi-IPNs) that support increased cell spreading and proliferation relative to fully synthetic networks that is dependent on cellular hyaluronidase activity. The objective of this study was to systematically examine the effects of PEGdA/HA semi-IPN composition on cellular activity.

Methods: Three different types of PEGdAs with varying susceptibility to hydrolytic degradation were synthesized by a two-step process. First, PEG (Fluka, MW 4000) was reacted with chloroacetyl chloride, 2-chloropropionyl chloride, or 4-chlorobutyryl chloride and then the resulting intermediate products were reacted with sodium acrylate to obtain PEG-bis-AA, PEG-bis-AP, or PEG-bis-AB [2]. Human fibroblasts (NHDF, Lonza) were encapsulated (5 million cells/mL) in photocrosslinked PEG-dA/HA (Lifecore) semi-IPNs containing 1□mol/mL of acrylate-PEG-GRGDS peptide. 6% w/v PEG-bis-AP with 6% w/w (HA/PEGdA, 1500 kDa HA) was used as a baseline composition. Experimental variables and their ranges included: HA concentration (0-15% w/w), HA molecular weight (MW-100, 700, 1000, 1500 kDa), PEGdA chemistry (PEG-bis-AA, PEG-bis-AP, PEG-bis-AB), and PEG-bis-AP concentration (4, 5, 6, 8, and 10% w/v). After 3, 7, and 14 days in culture, hydrogel samples were fixed and stained with Alexa Fluor 647 phalloidin (Invitrogen) for confocal microscopy (Nikon Ti Eclipse). Cell morphology at 200 □m inside the gel was compared. Different ratios of PEGdA blends were polymerized for long-term degradation study. Samples were lyophilized and weighed for mass loss at certain time points: day 3, 7, 10, 14, 18, 22, and 36.

Results: Cell spreading was supported at all HA concentrations with limited variability among groups. No spreading was observed in the absence of HA or in full IPNs formed from PEGdA and methacrylated HA, indicating that the observed capacity for cellular remodeling is unique to the semi-IPN network structure. Gels prepared using HA ranging in MW from 700-1500 kDa all supported cell spreading, while 100 kDa HA was completely ineffective and comparable to controls without HA. Within 3 days, gels formed from all 3 PEGdA chemical compositions supported cell spreading. The presence of cell spreading in PEG-bis-AB gels that exhibit negligible mass loss at this time point demonstrates that the inclusion of HA is sufficient to support initial cell spreading in the absence of hydrolytic degradation. On the other hand, cells spread most extensively in the PEG-bis-AA gels that have the highest rate of hydrolytic degradation, suggesting the most efficient cell remodeling can be achieved by simultaneous hydrolytic and enzymatic degradation. Cell spreading decreased with increased PEGdA concentration and was completely eliminated at 10%. A representative confocal montage of cell spreading at varying depths within 6% PEG-bis-AP / 6% 1500 kDa HA semi-IPNs is shown in Figure 1. Different ratio of PEGdA blend combinations could achieve prolonged hydrolytic degradation up to day 35 with increased linearity.

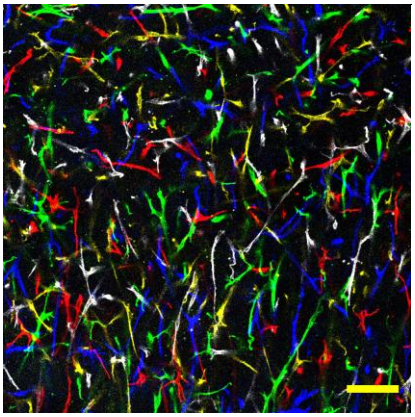

Figure 1. NHDF spreading in semi-IPNs at 14 days, pseudo-colored as a function of depth. Red=100, green=200,blue=300,white=400, yellow=500 μm. Scale=100 μm.

Conclusions: Collectively, we interpret the above results to suggest that the bioactivity of PEGdA/HA semi-IPNs derives from phase separation between the two components occurring during photocrosslinking that creates HA-enriched zones within the networks susceptible to enzymatic degradation. This is consistent with the reduction in cell spreading observed in response to lower molecular weight HA, higher PEGdA concentration, and co-polymerization of methacrylated HA, all of which would be expected to reduce phase separation. Currently, we are investigating changes in network structure using SEM and evaluating longer-term cell behavior in networks prepared from blends of the 3 PEGdAs that exhibit more linear and prolonged hydrolytic degradation

References: [1] Kutty JK. Biomaterials 2007;28:4928-38. [2] Cho EH. J Biomed Mater Res. 2009;90A:1073-82.

Vascular calcification can be reversed by chelating agents in vitro

Yang Lei[a], Arjun Grover[b], Naren Vyavahare*[a]

[a]501 Rhodes Hall, Department of Bioengineering, Clemson University, Clemson, SC, US, 29634. Tel: 864 656 5558; E-mail: narenv@clemson.edu; [b]1819 Six Mile Hwy, D. W. Daniel High School, Central, SC, US, 29630

Introduction: Vascular calcification is a ubiquitous feature of aging and is associated with a number of common pathologies including atherosclerosis, renal failure, and diabetes[1]. Chelation therapy most often involves the injection of disodium ethylene diamine tetraacetic acid (EDTA), a chemical that binds, or chelate ionic calcium, trace elements and other divalent cations[2]. We hypothesize that chelating agents, such as EDTA, diethylene triamine pentaacetic acid (DTPA) and sodium thiosulfate (STS) might work by directly removing calcium(Ca) from precipitated minerals into soluble calcium complex so as to reverse vascular calcification. The objective of current study is to compare the chelation efficiency of three types of chelating agents-EDTA, DTPA and STS to remove calcium from calcified porcine elastin and calcified human aorta.

Materials & Methods: Calcified porcine elastin was prepared by implanting pure porcine elastin subdermally in rats as described previously[3]. Calcified human aorta was from Greenville Hospital System, SC. Hydroxyapatite, disodium ethylene diamine tetraacetic acid, diethylene triamine pentaacetic acid and sodium thiosulfate are all from Sigma Aldrich. 10 mg of Calcified porcine elastin and 10 mg of calcified human aorta were soaking in 30 ml chelating solutions(5 mg/ml of STS, EDTA, and DTPA, n=3) respectively. The control group was soaking in distilled and deionized (DD) water. At frequent intervals, 1 ml of chelation solution were withdrown for Ca assay. Calcium content was measured by atomic absorption spectroscopy (Perkin-Elmer Model 3030, Norwalk, CT). Dahl's alizarin red stain was used for the qualitative analysis of calcium.

Results & Discussion: Initial results show that all three types of chelating agent could remove Ca from hydroxyapatite(data not shown). The kinetic extraction of Ca from calcified porcine elastin was shown in Fig.1. Both EDTA and DTPA could effectively remove Ca from calcified porcine elastin while STS is not so effective. Fig. 2 showed kinetic extration of Ca from calcified human aorta after soaking in chelating agents for 48 hours, which is consistent with the calcified porcine elastin. Dahl's alizarin red stain (Fig.3) for the human aorta after 4 hours of treatment of DD water, STS, EDTA and DTPA clearly showed that EDTA and DTPA tratment group greatly remove the Ca.

Conclusion: Both EDTA and DTPA could effectively remove calcium from calcified porcine elastin and calcified human aorta, while STS is not so effective. Vascular calcification could be reversed by chelating agents in vitro. We propose to site-specifically deliver these chelating agents intrapped microparticles to the site of calcification to reverse vascular calcificaton.

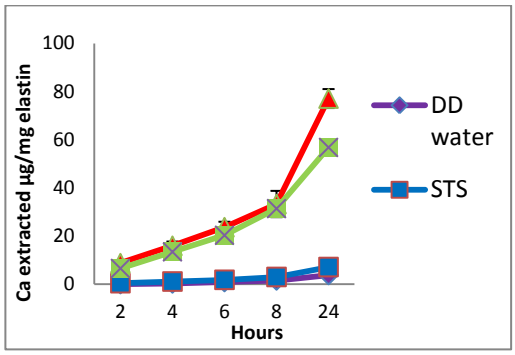

Fig.1. Kinetic demineralziaion study of calcified porcine elastin.

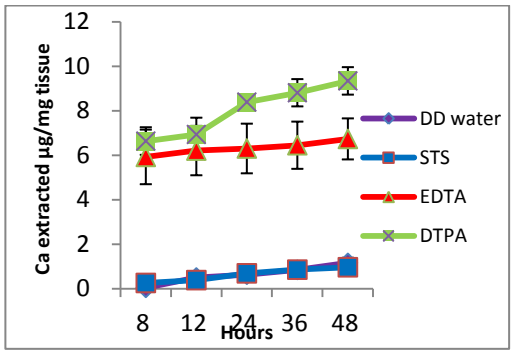

Fig.2. Kinetic demineralziaion study of calcified human aorta.

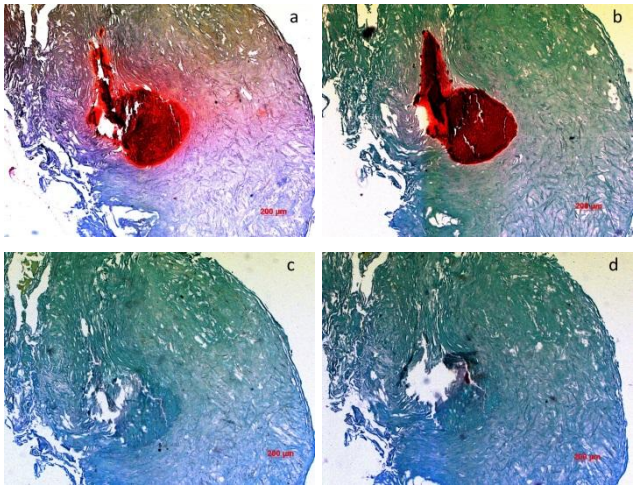

Fig.3. Dahl's alizarin red stain for human aorta. A) DD water. B) STS. C) EDTA. D) DTPA.Magnification-25X.

References:

1 A. Kapustin. and C. M. Shanahan, *Current Opinion in Pharmacology* ,2009, . 9(2): 84-89.

2 G. A. Lamas, and S. J. Hussein, *Complement Ther Clin Pract*, 2006. 12(3): 213-215.

3 J. S. Lee, D. M. Basalyga, N. Vyavahre, *The American journal of pathology*, 2006, 168(2): 490-498

Synthesis of Luminescent Hydroxyapatite Nanoparticles

W. David Locklair, Dakotah Anderson, Hongyu Chen, Jeffrey N. Anker
Department of Chemistry and Center for Optical Materials Research and Engineering Technology (COMSET), Clemson University, Clemson, South Carolina, 29634, USA.

ABSTRACT: Developing biocompatible labels that can be optically observed through thick tissue is an important challenge for biomedical imaging. To address this issue, hydroxyapatite nanoparticles doped with Eu^{3+}, $Ca_{10}(PO_4)_6(OH)_2$:Eu^{3+}, were synthesized and their luminescence spectra were studied under blue light excitation and X-ray irradiation. Narrow emission peaks were observed for both excitations. The emission peaks are most intense around 620 nm, accounting for the orange emission. Radioluminescence images were essentially background free, while blue and UV excitation can excite sample auto fluorescence.

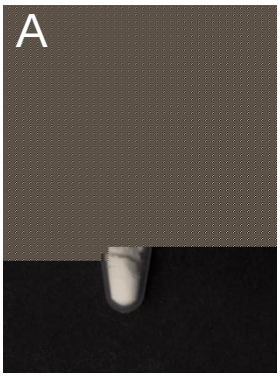

Luminescent hydroxyapatite particles doped with Eu in a 1.5 mL centrifuge tube viewed under (A) Room Light (B) UV excitation (C) X-ray excitation

Graphene Coated Technology for Biomedical Implants

Thomas Moore,[1] Ramakrishna Podila,[2,3] Apparao Rao,[3] Frank Alexis.[1]
[1] Department of Bioengineering, Clemson University, Clemson, South Carolina 29634. [2] Department of Pharmacology and Toxicology, Brody School of Medicine, East Carolina University, Greenville, North Carolina 27858. [3] Department of Physics, Clemson University, Clemson, South Carolina 29634.

Patent Submitted: *Graphene Coated Substrate for Biomedical Implants (CURF #2011-117)*. CURF Contact: Elizabeth Perpall

Statement of Purpose: Heart disease is the number one cause of death in the United States and in 2008 approximately 405,000 people died from coronary heart disease.[1] Vascular stents are a means of increasing blood vessel patency with a small, often metallic, mesh tubes implanted endovascularly. While metallic alloys such as nitinol (NiTi) or stainless steel are often chosen for their superior mechanical properties, stents still fail at rates as high as 12% due to deployment complications, stent geometry, material properties, and surface coatings.[2,3]

In this study we developed a fundamental materials approach to reduce material thrombogenicity and improve hemocompatibility. Carbon-based coatings have been previously used to improve implant properties, however many are still limited in their efficacy as a functional stent material.[4,5] NiTi substrates were coated with an atomically smooth graphene layer in order to improve physiological response by 1) reducing protein adsorption on the surface. 2) Reducing the relative amount of fibrinogen adsorption, a protein involved in thrombus formation, compared to albumin, a serum protein. 3) Decreasing charge transfer from adsorbed proteins to the substrate, a physical process indicating protein conformational change. 4) Improving cell viability and morphology on the substrate. Thus, the new graphene-coated NiTi (NiTi-Gr) offers potential as a successful stent material.

Methods: NiTi was coated with graphene using a chemical vapor deposition technique. NiTi-Gr was characterized with micro-Raman spectroscopy and scanning electron microscopy (SEM). Protein adsorption studies were performed with SDS-PAGE of adsorbed proteins and SYPRO red protein staining. Protein adsorption was qualitatively observed with SEM. Rat aortic smooth muscle cells were grown in Dulbecco's modified Eagle's medium (ATCC) on substrates and cell viability was measured by the conversion of 3-(4,5-dimethylthiazol-2-yl)-2,5-diphenyltetrazolium bromide (MTT) to purple formazan in cells grown on substrates normalized by cells grown in untreated culture. Cell morphology was observed qualitatively using confocal microscopy.

Results: SEM results show that qualitatively, protein adsorption on pristine NiTi is higher than on NiTi-Gr. Further studies quantifying the ratio of fibrinogen to serum albumin (Fib/Alb) show that the Fib/Alb ratio decreases by two-fold. Micro-Raman measurements of fibrinogen adsorbed on NiTi-Gr showed that there was not shift in Raman spectrum, indicating no charge transfer from the fibrinogen to the substrate.

In vitro cell viability results show that cells maintained viability over a one week period on all substrates, however confocal microscopy studies show that NiTi-Gr maintained cell morphology similar to controls grown in untreated culture compared to pristine NiTi substrates.

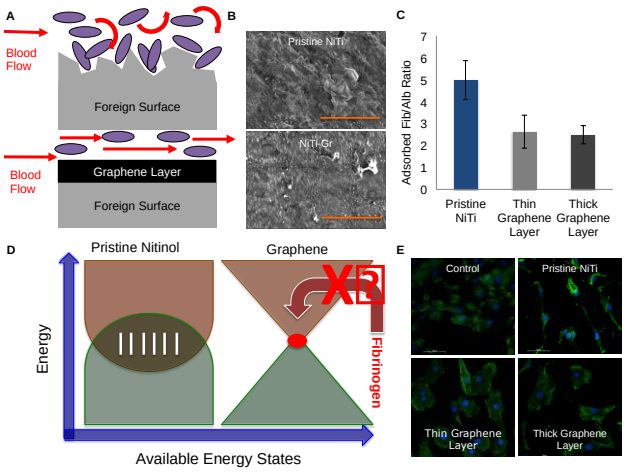

Figure 1. (A) Representative illustration of how an atomically smooth surface helps reduce protein adsorption. (B) SEM images of fibrinogen adsorbed on pristine Niti (top) compared to NiTi-Gr (bottom) qualitatively shows less adsorption on the graphene coated substrate. (C) Adsorption studies of albumin and fibrinogen binding show that the ratio of Fib/Alb for NiTi-Gr samples are significantly lower than for pristine NiTi. (D) Illustration of how a graphene coating reduces the charge transfer from adsorbed proteins to the metallic substrate. Graphene only has a single energy state to which electrons can be transferred. (E) Confocal microscopy shows that rat aortic smooth muscle cells grown on NiTi-Gr more closely resemble the morphology of control cells grown on a slide than cells grown on pristine NiTi.

Conclusions: Our preliminary results indicate that graphene-coated NiTi substrates are a viable material for stent applications due to decreased the relative adsorption of fibrinogen to albumin, decreased transfer of charge from adsorbed fibrinogen, and improved cell viability and adhesion. Future work includes *in vitro* studies of platelet adhesion on NiTi-Gr. *In vivo* work studying the inflammatory response and eventually a functional NiTi-Gr stent model are necessary to fully realize NiTi-Gr as a potential stent material.

References:

1) Miniño AM, et al. Nat Vit Stat Reports. 2011; 59: 1-52.

2) Baran KW, et al. Am J Cardiol. 2008; 102: 541-545.

3) Kolandaivelu K, et al. Circul. 2011; 123: 1400-1409.

4) Gutensohn K, et al. Thromb Res. 2000; 99: 577-585.

5) Airoldi F, et al. Am J Cardiol. 2004; 93: 474-477.

Modulus of Elasticity of Electroconductive Hydrogels

Ben Murphy and Anthony Guiseppi-Elie
Center for Bioelectronics, Biosensors and Biochips (C3B)
Clemson University

Introduction and Background: Bioactive hydrogels are being developed for use as coatings for implantable bioanalytical biochips. Biochips are being designed and fabricated for the continual measurement of glucose and lactate with the potential to save human lives of persons suffering from hemorrhage-associated trauma. Physical trauma is the leading cause of death for people under the age of 44[1]. In order for these biochips to function properly over the extended period of implantation, they must be coated with a suitable polymer that matches the elastic modulus of the tissue bed within which they are implanted. Accordingly, the elastic modulus of the coating should be compatible with muscle for intramuscular implantation. This approach addresses one potential source of the foreign body response; elastic modulus mismatch of the implant with the host tissue. This study aims to determine the modulus of elasticity of polyacrylamide hydrogels both with and without absorbed aniline or pyrrole monomers and both before and after their oxidative polymerization. The approach is to measure the coefficient of restitution (CoR) from simple drop tests and to calculate the modulus of elasticity from the CoR. Values of elasticity of human muscle ranges from 21.6kPa to 44.8kPa[2].

Methods: Cross linked polyacrylamide spherical gel beads (Deco beads (JRM Chemical, Inc., 4881 NEO Parkway, Cleveland, OH)) were soaked overnight in solutions of either; DI water, PBS, 0.4M aniline/DI water, 0.4M aniline/PBS, 0.4M pyrrole/DI water, 0.4M pyrrole/PBS. P-Toluenesulfonic acid monohydrate, a dopant, was added to the pyrrole solutions (0.04M).

Coefficient of Restitution: Swollen hydrogel spheres were videotaped while being dropped to record bounce back height. Additionally, the weights and diameters of the hydrated gels were measured using an electronic balance and an electronic pair of calipers respectively. Subsequently, the hydrated gels were soaked in 5.0mM ammonium persulfate, an oxidant, for 90 minutes; initiating polymerization of the aniline and pyrrole within the swollen hydrogel. The bounce test was then repeated and the mass and diameters were also re-measured. These measurements allow for calculations of the CoR.

$$e_{th} = \sqrt{\frac{h}{H}} \qquad \text{(eq.1)}$$

Where e_{th} is the coefficient of restitution, h is the bounce back height, and H is the drop height. For each sample there were three technical replicates and each was measured in triplicate. The changes in coefficient of restitution under the different solution conditions and the effect of oxidative polymerization were compared. The moduli of elasticity were calculated based on the model of two colliding spheres where the bounce surface was considered rigid or non-elastic and a sphere of infinite radius.

$$e_{Th} = \left\{\left(\frac{6\sqrt{3}}{5}\right)\left[1-\frac{1}{6}\left(\frac{v_Y}{v_{in}}\right)^2\right]\right\}^{1/2}\left\{\left(\frac{v_Y}{v_{in}}\right)\left[\left(\frac{v_Y}{v_{in}}\right)+2\sqrt{1.2-.2\left(\frac{v_Y}{v_{in}}\right)^2}\right]^{-1}\right\}^{1/4} \qquad \text{(eq. 2)}$$

Where v_y is the yield velocity and v_{in} is contact velocity. Solving for v_y we then solve for the modulus of elasticity.

$$v_Y = 3.149\left(\frac{(\sigma_Y)_{Th}{}^5 (R^*)^3}{(E^*)^4 m^*}\right)^{1/2} \qquad \text{(eq. 3)}$$

Where $(\sigma_Y)_{Th}$ is the contact yield stress, R^* is the equivalent radius, E^* is the equivalent modulus of elasticity, and m^* is the equivalent mass. A yield stress of 10 kPa was used in these calculations[3].

Results and Discussion: The modulus of elasticity of the 12 different sample types were calculated using (eq. 2) from the coefficient of restitution (eq.1). The elasticity of the various hydrogels ranged from 45,432Pa for aniline/PBS to 53,745Pa for PBS soaked in the oxidizing initiator solution.

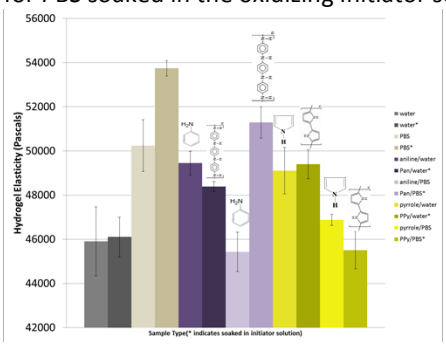

Figure 2. Average and standard deviation of the modulus of elasticity of the several hydrogel formulations studied.

Conclusions: Adding a monomer to the hydrogel within PBS solution tends to decrease elasticity whereas when in water this tends to increase elasticity. The polymerized and un-polymerized hydrogels seem to have an effect when the solvent is PBS but not when the solvent is water. Size and CoR did not seem to correlate with elasticity. Future studies should include testing how similar two material's elasticity need to be in order for them to be compatible alongside each other. Additional studies should implant hydrogel composites into the muscle of lab rats to study the foreign body response.

References:

1. CDC and Prevention, National Center for Injury Prevention and Control. Web-based Injury Statistics Query and Reporting System (WISQARS) [online] (2007) Available from URL: http://www.cdc.gov/injury/wisqars
2. Nordez, A. and F. Hug. J Appl Physiol 2010; 108(5): 1389-1394.)
3. Goodrich, K., A. Yoshimura, et al. J Rheo 1989; 33: 317

3T3 Fibroblasts Solving Mazes in Response to Growth Factor Concentration

A. Nguyen, E. Mappus, T. Harvey, B. Peterson, M. O'Kelly, E. Hammes, D. Dean
Department of Bioengineering, Clemson University

Statement of Purpose: In wound healing, fibroblasts migrate to the site of injury and serve an integral role in repairing and healing the wound. As tissue engineering develops into a potential tool for regenerating damaged and diseased tissue, understanding of the fibroblast migration mechanism and the effects of fibroblast growth factor is vital. Cellular navigation through the extracellular matrix in vivo requires recognition and avoidance of obstacles. Directed cell migration through chemotactic signaling offers one explanation for how cells arrive at their intended destination; however, this explanation cannot predict the behavior of cells when presented by 3 dimensional objects with additional signaling.

Methods: In order to study the fibroblast migration mechanism, we examined the process of wound healing interrupted by a physical barrier when two leading edges of fibroblasts are separated by a maze of polydimethylsiloxane (PDMS). To construct the microfluidic mazes, we laser printed maze patterns onto Shrinky Dink plastic. The Shrinky Dink is then heated to produce plastic molds with raised maze patterns. The molds were then used to cast the PDMS mazes. The PDMS cellular maze was attached to the bottom of a cell culture dish and 3T3 fibroblasts were plated on both sides of the access points. After the cells grew to confluence outside of the maze, the maze was opened with a surgical blade allowing entrance to the maze. Observation of the growth of the fibroblasts occurred for 48 hours after opening of the entrance to the maze.

A second study of alternative fabrication procedures has been started in an attempt to create a permanent and reusable maze for a standardized testing platform. The maze pattern was cut into sheets of clear acrylic using a laser cutter. Three separate layers were cut out of the plastic. The bottom layer was a solid square of plastic, which covered the entire maze area to provide a surface for the cells to grow on, the middle layer contained the maze cut-out, and the top layer contained wells above the maze entrances in order to plate cells. The three layers were then stacked together using acetone, screws, or a combination of the two in order to create a self contained, reusable maze. Cells could then be plated in the maze and observation studies of the cells' traversal of the maze could be performed as previously described.

Results: During observation studies, the PDMS mazes failed to adhere to the surface in many cases. However, in the cases in which full or partial adhesion occurred, cell growth did not appear to be negatively affected by the PDMS and growth into the maze channel was observed.

The study of alternate fabrication techniques arose impart as a way to combat the adhesion problem. Prototype mazes using this technique have held fluid well, with only
minor leakage problems due to individual defects. The next step will be to perform the observation studies using the new, more robust mazes.

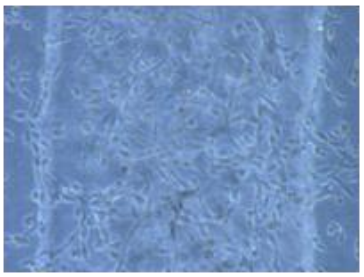

Figure 1. Fibroblasts inside a channel of a maze created using PDMS. Note that the cells are able to leave the channel due to poor adhesion of the PDMS to underlying the substrate.

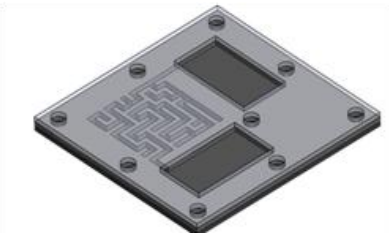

Figure 2. Schematic of maze fabricated from laser cutting acrylic sheets. Acrylic maze is a self-contained system developed for characterization of fibroblast migration studies.

Conclusions:
The results of these studies will be compared to mathematical models of cell growth in response to chemical soluble factors. The long-term goal of the project is to build a model to predict cell growth and migration in 3D that can be used to help design novel wound healing therapies. These initial studies are focused on fibroblast growing in response to 2D confinement and guidance; our next step will be to design a well-characterized patterned maze system for the cells to grow in a 3D environment.

References:
Thampatty B P and Wang, J H-C. Cell Motility and the Cytoskeleton. 2007; 64: 1–5.
Nakagaki, T. Research in Microbiology. 2001; 152: 767-770.
Grimes, A. Lab on a Chip. 2008; 8: 170-172.

Treatment of Osteolytic Defects with Bone Graft in Total Knee Replacement

Leah Nunez, Dr. Brandon Broome, Dr. Thomas Pace, Dr. Melinda Harman
Clemson University
Greenville Hospital System

Introduction: Accepted treatment for osteolysis of the acetabulum in total hip replacement includes polyethylene liner exchange and retroacetabular bone grafting of lesion sites. Traditionally osteolysis around total knee replacements (TKR) is treated with complete revision but due to decreasing survivorship associated with complete revision and increasingly younger patients, polyethylene liner exchange and bone grafting may be applicable in some subsets. This retrospective study reports surgical technique and clinical outcomes for selective bone grafting in osteolytic patients without complete revision of TKR.

Methods: Ten TKR (9 patients, 66.5 ± 6.1 years old) presenting with radiographic osteolysis evidence revised after 8.7 ± 1.9 years of in vivo function of an uncemented prosthesis and modular polyethylene insert with anteroposterior articular constraint (Ultracongruent, Natural Knee II, Sulzer). The decision not to revise the metal components in these patients was based on absence of radiolucent lines prior to revision surgery and firm fixation of components during intra-operative manual assessment. Osteolytic lesions were treated by opening a small window, removing necrotic bone tissue, and filling the osteolytic defect with bone graft materials. Polyethylene insert exchanged to a modular standard congruent prior to closure.

Results: Patients have not exhibited any further complications associated with osteolysis after 4.6±2.4 years. Radiographic exams show complete incorporation of graft material into the defect in all patients and no radiolucent lines adjacent to the prostheses. There were 2 small (<2cm), 4 medium (2-4 cm), 3 large (>4 cm) tibial lesions and 2 medium, 4 large femoral lesions of all patients pre-revision. Axial alignment was within 3° of neutral for all patients.

Conclusions: In some osteolytic TKR in which the components are firmly fixed, removal of necrotic tissue through a small window in the anterior medial tibial cortex and defect filling with bone graft materials can be a viable solution. This study shows complete osteolysis resolution in all patients without complications.

AC Dielectrophoresis and the Effects of Frequency and Electrode Dimension

Vandana Pandian, Dr. Guigen Zhang (Advisor)
Department of Bioengineering, Institute for Biological Interfaces of Engineering
Clemson University

Statement of Purpose: It is a well-known fact that particles in a non-uniform electric field experience a dielectrophoretic (DEP) force which manipulates them. The conventional DEP force is proportional to the in-phase component of the induced dipole moment in a non-uniform AC electric field. The purpose of this study was to evaluate the forces acting on the particles and the factors affecting the forces through analytical and computational studies.

Methods: Analytical development for the conventional dielectrophoretic (DEP) forces was done to show the dependence of Clausius-Mossotti factor (CM factor) upon the frequency of the applied electric filed along with the permittivity and conductivity of the particle and the medium. With the in-phase component of the CM factor, the time averaged magnitude of the conventional DEP force was determined. On the computational modeling side, a time dependent study was performed using COMSOL Multiphysics 4.2. Four electrodes, made of Gold and separated by alumina, were considered as shown in Figure 1. The electrodes were supplied with sinusoidal voltage inputs with the adjacent electrodes having 90° $(or\ \pi/2)$ phase delay. The model was made completely parametric to make it very versatile.

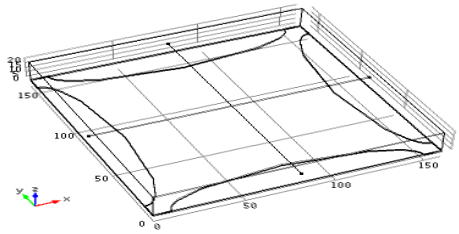

Figure 1: Model used for the analysis

The particles considered were polystyrene beads. Water was used as the medium carrying the particles. The conventional DEP forces were determined at various different frequencies, electric potentials and electrode dimensions (width of the electrode).

Results: Figure 2 shows that the DEP force determined from the modeling is the same as the time averaged analytic result. Figure 3 shows how the force varies with different factors: the magnitude of the DEP force changes as the frequency, electric potential and width of electrodes change.

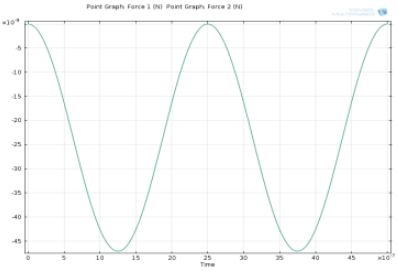

Figure 2: Plot for both the forces against time

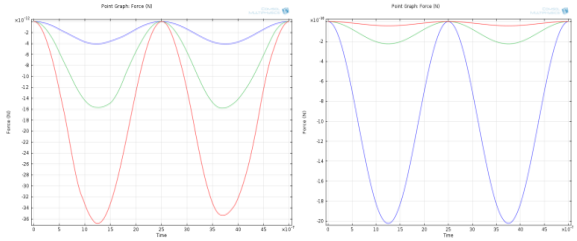

Figure 3: Shift in curve with different factors

Discussion: The electric condition, electrode geometry and the frequency of the electric field all play an important role in affecting the magnitude of the DEP force. With further optimization of the model, we will determine which of the values of these factors would produce maximum force necessary to move biological particles and cells for biofabrication purpose.

Reference: X-B. Wang, Biochim. Biophys. Acta 1243 (1995) 185-194. Holzel, R. (1992) Biochim. Biophys. Acta 1104, 195-200. Huang, Y. (1991) Meas. Sci. Technol. 2, 1142-1146.

Protein Adhesion to Various Monomer Blends

Matthew Rusin, Ying Mei, Delpine Dean
Clemson University

Statement of Purpose: Finding appropriate materials for medical devices, especially implantable devices, is an issue that has plagued doctors for years. One way to insure that a material is suitable for implantation is to see the types of proteins that adhere to the surface. In order to get good tissue integration it is imperative that the surface has a high attraction to ECM proteins. This would enable tissue integration to occur much sooner after implantation and potentially decrease the inflammation response from the body. In order to test this, 96 polymers were created by combining 70% of one monomer (called the major monomer) and 30% of another (called the minor monomer) from a group of 24 monomers. Each polymer was deposited as a nanoliter dot on a standard glass slide, and then imaged using atomic force microscopy (AFM).

Methods: Polymer dots were imaged using a Veeco Dimension 3100 AFM and gold coated cantilevers. The cantilevers were functionalized with 11-amino-1-undecanethiol and sulfo-NHS and rinsed with PBS. Vitronectin was then added drop-wise to the cantilevers and allowed to bind for 2 hours. Imaging was done in PBS at room temperature. 100 force measurements were taken for each polymer dot, which were converted and analyzed using custom MatLab scripts.

Results: It was observed that the differences in adhesion force between each polymer dot were pretty significant, even if the monomers involved had a similar structure. Shown in Figure 1 is a sample of 18 polymers that use monomers 2, 3, and 4 as their major monomer. Each of these monomers is relatively similar, with monomers 2 and 3 being the closest; however it is observed that the addition of certain minor monomers causes a large difference in the adhesion force between the polymer and vitronectin. Minor monomer 10 is a great example of how that addition creates a large difference in adhesion force. However, when we look at minor monomer 12, which has a similar structure to monomer 10, the differences in adhesion force are very small.

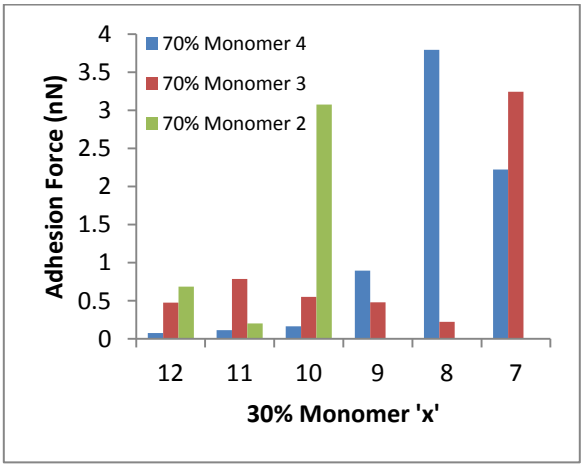

Figure 3: Adhesion force for 18 different polymers is shown.

Conclusions: Of the 3 major monomers tested, it is clear that monomer 4 has the best adhesion properties with vitronectin. Monomer 4 had the most minor monomer combinations that had significantly higher adhesion force over major monomers 2 and 3. This would signify that that monomer combination could be a good candidate for an implantable material. Further study should be done to determine how much adhesion is too much, though. There is a point where the polymer is so sticky that the protein denatures in order to adhere as much as possible. So, a point of further study would be to determine what the optimum adhesive level the polymer should have.

References: Anderson DG. Nature Biotech. 2004; 22; 863-866.

Evaluating Performance of Hydrogel-Based Adhesives for Soft Tissue Applications

Lindsey Sanders, Nitin Balakrishnan, Roland Stone, Ben Fleishman, O. Thompson Mefford, PhD, Ken Webb, PhD, and Jiro Nagatomi, PhD

Department of Bioengineering, Clemson University; Clemson, SC 29634

Statement of Purpose: Approximately 600,000 hysterectomies are performed annually in the United States, which means that approximately 20 million U.S. women have had a hysterectomy to date[1]. One of the most common complications during these surgeries is accidental laceration to the bladder. Current treatments for the bladder injuries are limited to sutures, which prevents proper distention of the bladder wall during filling and necessitates use of a catheter and a bag during recovery. Although a number of tissue adhesives and sealants approved by the FDA for surgical use are currently available on the market, none of them are suitable for application to the bladder because of their inadequate strength, compliance, or biocompatibility. Therefore, the goal of this project is to develop a novel, hydrogel-based tissue adhesive that provides proper mechanical properties for bladder application. Tetronic (BASF), a PEO-PPO block co-polymer was chosen for the base material of the adhesive due to its reversible thermo-gelation characteristics. More specifically, we are currently investigating the synthesis process for bi-functionalization of Tetronic with 3,4-Dihydroxphenyl (DOPA) and acryloyl chloride to achieve a balance between bulk and adhesive strengths of the hydrogel suitable for bladder application. Since DOPA has water-resistant and rapid curing abilities this process should, in theory, increase the adhesive strength to the tissue with DOPA while taking advantage of the thermal gelation property and bulk strength of thiol-crosslinked T1107-acrylate.

Methods: Adhesives were prepared from blends of 50% (2 of 4 arms) acrylate terminated T1107 and acrylate:DOPA, 50:50, terminated T1107. Fifty percent (2 arms) acrylation was performed in dicholormethane using published methods[2]. Synthesis of T1107 (MW: 15,000) with Triethlyamine (TEA) and acryloyl chloride was stirred for 24 hours. Triethlyammonium precipitate was filtered out and the product was neutralized to pH 7.0, then washed with ethyl either. In the 50:50 terminated T1107 the two additional arms were modified with DOPA in a three step process: reaction of (1) T1107-OH, 4-Dimethylaminopyridine (DMAP), Succinic Anhyride and TEA in Tetrahydrofuran (THF) for 12 hours, (2) T1107-COOH, N-Hydroxysuccinminide (NHS) and Dicyclohexylcarbodimide (DCC) in THF for 4 hours, and (3) T1107-NHS and DOPA in Dimethylformamide (DMF) for 6 hours. Crosslinking was achieved by the addition of dithiothreitol (DTT).

Five blend ratios (100:0, 75:25, 50:50, 25:75, 0:100) of T1107-acrylate and T1107-acrylate-DOPA respectively, were prepared, and shear adherence testing on collagen sheets was performed to quantify bonding strength of the adhesive. Briefly, a 0.2 inch diameter circular defect was created at one end of ¾ inch strips and then placed over ½ inch strip and approximately 50 µl of adhesive was applied into the circular defect. Adhesives were cured under hydrated conditions in PBS at 37° C for 30 min before mechanical testing. The bonded specimens were subjected to uniaxial tensile loading and force of failure was measured using a MTS machine. Data were plotted as adherence stress (MPa) versus strain (mm/mm) and the maximum stress values were reported as the bond strengths.

Results: Acrylation percent and product yield for T1107-acrylate were 65% and 66.3%, respectively. Some of this product was then used for the DOPA modification resulting approximately 5% DOPA conversion rate and 42.2% product yield.

Shear adherence testing with collagen sheets demonstrated that the bond strength was greatest for 25:75 T1107-acrylate:T1107-acrylate-DOPA, 0.75 MPa, when compared to the other blends tested (Figure 1).

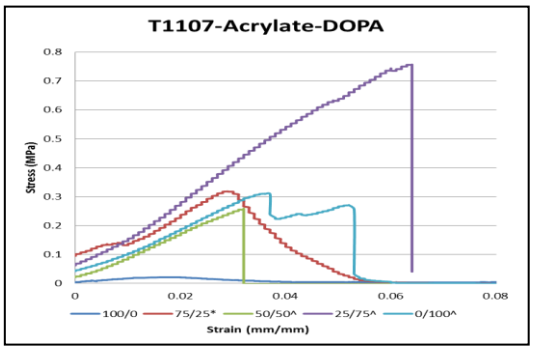

Figure 1. Stress-strain curve obtained from shear adherence testing of Tetronic-DOPA hydrogel adhesive with collagen casing.

The blend containing no DOPA (100:0) failed at the lowest stress with having very little bonding between the adhesive and casings. Moreover, the blend with the highest DOPA content (0:100) exhibited approximately a thirty-fold increase in bond strength compared to the previously published data on Tetronic-based tissue adhesives[2].

Conclusions: The results of the present preliminary study suggest that DOPA can significantly improve Tetronic-based adhesive's bond strength to biological materials. However, the adhesive needs further improvement by tuning the amount of acrylate and DOPA end group modifications of Tetronic to achieve proper balance between bulk and adhesive strengths required for bladder applications.

References: [1]Centers for Disease Control and Prevention (2012) [2]Cho, et al., Acta, 2012.8:p.2223-2232.

Fiber scaffolds for CNS regeneration

Atanu Sen[1,2], Jeoung Soo Lee[1,2], Phillip J. Brown[2], Kathryn Stevens[2], Ken Webb[1,2]
Microenvironmental Engineering Laboratory[1], Department of Bioengineering[2], Material Science and Engineering[3], Clemson University, Clemson, SC 29634

Statement of Purpose: Regeneration of neurons upon spinal cord injury (SCI) requires directed growth of axons in a specific direction to obviate unwanted sprouting. Aligned fibrous scaffolds are known to provide such axonal growth by contact guidance [1]. Such topographic support can be provided by capillary channel polymer fibers (CCP) which also allow increased surface area. This topographic support can be coupled with trophic support to enhance axonal growth via biochemical pathways in the growth cone. L1 neural cell adhesion molecule is one such biomolecule expressed at the growth cone that enables axonal elongation and migration by contact mediated attraction [2]. Our goal was to immobilize L1 on these CCP fibers to develop a neuroregenerative biomaterial which synergizes the topographic and trophic benefits of the fiber design and the biomolecule.

Methods: Effect of L1 concentration on rat cerebellar neurite extension was studied by adsorbing varying concentrations on polystyrene well plate. Poly-l-lactide (PLLA) was used to fabricate CCP fibers of various groove dimensions by melt extrusion technique. Chicken Forebrain Neurons (CFNs) and Dorsal Root ganglion neurons (DRGs) were isolated from E8-9 chicken embryos and seeded onto L1-coated (10µg/ml) fibers in 24 well plates. The neurons were fixed in 4% paraformaldehyde after 24 hours of seeding and stained for β-III Tubulin. Neurite lengths were measured using ImagePro software.

Results: Increase in neurite lengths was observed with increasing L1 concentrations from 0.1-50µg/ml concentration on polystyrene 96 well plate (Fig.1).

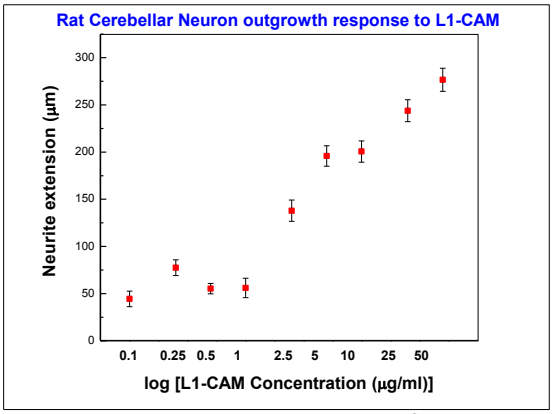

Fig.1. Dose dependent response of L1 on neurite extension

Various groove sized CCP fibers were obtained by varying extrusion conditions (Fig. 2). The PLLA melt was extruded through a spinneret shaped to result in two major and 4 minor channels in the fiber and the rotor speed can be varied to obtain various groove sizes.

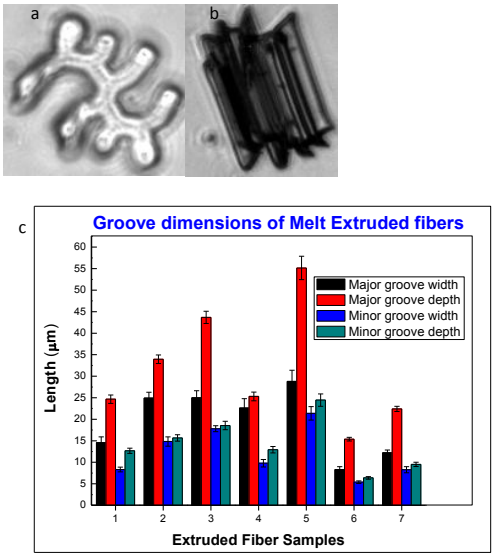

Fig.2. (a).Cross-section of PLLA CCP fiber, (b). Longitudinal view of a CCP fiber staple, (c). Various groove sized CCP fibers obtained by varying extrusion conditions.

Dissociated CFN and DRG explants were seeded onto L1coated CCP fibers and aligned growth of axons was observed in the grooves of CCP fibers (Fig.3)

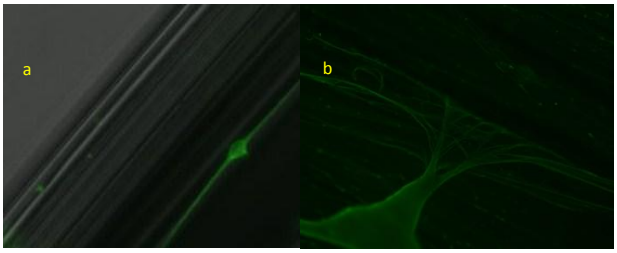

Fig.3. (a). CFN aligned growth on CCP fiber, (b). Neurons from DRG explant aligning to the CCP fibers.

Conclusions: L1 coated CCP fibers promote directional contact guidance of neurons and offer a basis for stimulating and directing axonal regeneration following spinal cord injury (SCI).

References:

1. Yang, F., et al., *Electrospinning of nano/micro scale poly (L-lactic acid) aligned fibers and their potential in neural tissue engineering.* Biomaterials, 2005. **26**(15): p. 2603-2610.
2. Kamiguchi, H., *The role of cell adhesion molecules in axon growth and guidance.* Axon growth and guidance, 2007: p. 95-102.

Acknowledgments: SC Center of Biomaterials for Tissue Regeneration and NIH grant #P20RR021949.

Tetronic hydrogel based scaffolds for urinary bladder tissue engineering

Srikanth Sivaraman, James Hyde, Jiro Nagatomi.
Department of Bioengineering, Clemson University, Clemson, SC 29634-0905

Statement of Purpose: The urinary bladder is one of the few organs that has been successfully engineered in-vitro using PGA based scaffolds and implanted in humans[1]. Although the initial clinical success of bladder tissue engineering demonstrated the feasibility of this technology, most polyester scaffolds possess several limitations such as inadequate compliance. Biological hydrogels derived from the extra-cellular matrix (ECM) such as collagen, offer desirable properties for tissue engineering including cell adhesion sites, but its low mechanical strength is not suitable for bladder tissue regeneration. In contrast, synthetic hydrogels such as PEG allow tuning of mechanical properties, but do not elicit protein adsorption or cell adhesion. For this reason, we are currently exploring the use of stiffer hydrogel blends composed of Tetronic (BASF) 1107-methacrylate (T1107-MA) in combination with ECM moieties, collagen and hyaluronic acid (HA) in this application. Specifically, the present study examined bladder smooth muscle cell response to this hydrogel system, as well as the time-course variation in mechanical properties of the cellular hydrogels constructs.

Methods: Bladder Smooth muscle cells (BSMC) were isolated from adult female Sprague- Dawley rats. Briefly, using an aseptic technique, the mucosal layer of the bladder was removed and the rest of the tissue was digested in a solution containing RPMI supplemented with 0.1% collagenase & 0.2% trypsin to dissociate cells from the extracellular matrix. The BSMC were collected by centrifugation of the tissue digest. The smooth muscle phenotype of these cells was confirmed by immuno-staining using primary antibodies for α- smooth muscle actin and smooth muscle myosin heavy chain (SM-MHC). T1107-MA was synthesized by addition reaction of T1107 with acryloyl chloride in the presence of Tetraethyl-amine HCL. The final product was precipitated in ether. BSMC (4x 10^6/mL) in suspension were mixed with the hybrid hydrogel composed of 5% T1107-MA, 0.5% collagen Type 1, 0.1-0.2% HA, and 0.1% irgacure, a photo-initiator. The gels (0.75mL) were cast in custom-made Teflon molds (3cmx1cmx0.5cm) and were polymerized by photo-initiated free radical polymerization under UV light for 12 min. The 3D BSMC constructs were cultured in RPMI + 10% FBS for 7 and 14 days. Acellular hydrogels (PBS instead of cells) were used as controls. At the end of the prescribed time periods, the BSMC in these 3D constructs were stained with rhodamine-phalloidin (f-actin) and DAPI (cell nuclei) and the cell morphology was examined using laser confocal microscopy (Nikon).The mechanical characterization of the hybrid hydrogels was performed by uniaxial tensile testing using MTS synergie 100 at the end of 7 and 14 days. The dog bone shaped hydrogel constructs were subjected to tension under hydrated conditions (PBS) at a rate of 5mm/min until rupture. The stress-stretch relation was analyzed using the Neo-Hookean, hyper-elastic model where stress (τ) was plotted against $\lambda - 1/\lambda^2$ (where λ is the stretch ratio of deformed to reference lengths) and the shear elastic modulus was calculated from the slope of the plot. Hydroxyproline collagen assay was performed on the hydrogel samples (acellular, cellular 7 and 14 days) to determine the concentration of collagen (μg) per mg of hydrogel sample.

Results: Based on the results of immuno-staining, cells below six passages consistently expressed smooth muscle phenotypic markers and were used in the experiments. Confocal images of the constructs showed that the cells were well distributed throughout hydrogel scaffolds and demonstrated an elongated and spindle shaped morphology. The initial results of the hydroxyproline assay indicated an increase in collagen concentration at successive time points in the cellular samples compared to acellular samples. Compared to the control (acellular) hydrogels, the mechanical properties (peak stress, peak strain and elastic modulus) of the cellular hydrogels were significantly greater. Moreover, the results of mechanical testing indicated nearly a 100 % increase in both ultimate tensile stress (4.2 kPa to 9.8 kPa) and elastic modulus (18.3 kPa to 34.4 kPa) in cellular hydrogels at the 14 day time point when compared to the 7 day time point.

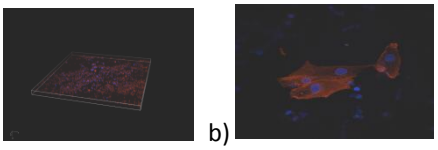

Figure 1: Viability of SMCs in hydrogel construct construct after 7 days of culture (a) 10X (b) 60X

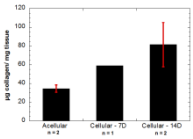

Figure 2: Collagen concentration in various samples of the hydrogel scaffold

Conclusions: The result of the present study demonstrated that the hybrid hydrogel system promoted BSMC spreading and growth. The improvement in stiffness and strength of the cellular constructs and increase in collagen concentration over time indicates the possibility of ECM deposition and formation of extensive cell networks. Further studies, however, are necessary to further quantify newly synthesized collagen and expression of SMC phenotype markers in the hybrid hydrogel tissue constructs.

References: (1) Atala A et al., Lancet 367:1241-6.

Humeral Torsion Measurements by Ultrasonographic Means

Thurston, Bryan, BS; Marionneaux, Alan; Wyslko, Ales; Harman, Melinda, PhD
Department of Bioengineering, Clemson University, Clemson SC

Statement of Purpose. Stresses placed on the arm can cause major morphological differences in the humerus bone. This study examines Humeral Torsion, which is the inherent twist that develops in the humerus bone as a result of these forces and can be measured as the angular difference between the axis of the humeral head and that of the epicondyles. Torsion in the arm is directional based on the force profile of daily activities over bone-growth periods, resulting in either internal rotation (antitorsion) or external rotation (retrotorsion) of the epicondyles in comparison to the head of the humerus. In throwing athletes, the magnitude of twist can become extreme and vary considerably from the dominate to non-dominate arm. To measure this humeral torsion, the benchmark process consists of a computed tomography (CT) scan to identify humeral anatomic landmarks. However, this introduces patients to ionizing radiation and is expensive. In comparison, measurement protocols using ultrasound have been introduced in clinical settings as a less invasive and relatively inexpensive alternative. The purpose of this study is to measure humeral torsion using CT scans and ultrasound and verify the accuracy of an ultrasound measurement protocol for future torsional studies.

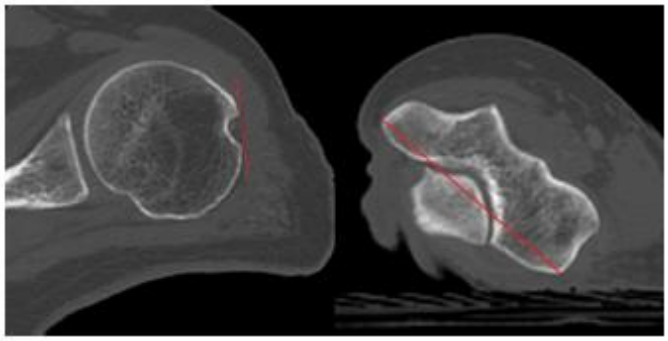

FIGURE 1: CT SCAN AXIS MEASURES.

Methods. This IRB-approved study includes 13 intact upper extremities acquired from nine cadavers obtained with donor consent. The donors included 6 males (3 bilateral) and 3 females (1 bilateral) with an average age of 67 (range, 40-89) years. Measurement of humeral torsion was accomplished on each extremity using two imaging methods, namely CT and ultrasonography. Each extremity was imaged using a CT scanner (Brilliance CT-64, Phillips) resulting in DICOM images of 2 mm thick slices. Two CT image slices were selected for each humerus based on identification of specific anatomic landmarks, namely the greater and lesser tuberosities surrounding the bicipital groove proximally and the medial and lateral epicondyles defining the distal humeral axis. Measurements of humeral torsion based on these landmarks were completed using a custom graphical user interface program (Matlab, Mathworks, Natick, MA). Two observers used the program to independently select slices and identify the anatomic landmarks, allowing calculation of the humeral torsion angle (Figure 1). Each observer repeated three measurement trials per humerus. Likewise, each extremity was imaged using ultrasonography (M Turbo, Sonocite) with simultaneous measurement of the forearm angle. One observer placed the ultrasound probe on the anterior surface of the shoulder while a second observer internally or externally rotated the forearm until the bicipital groove was fully visible in the sonograph with the greater and lesser tuberosities approximately level and parallel to the probe. A vertical drape was placed across the forearm to obscure observers at the shoulder from seeing the orientation of the forearm. An inclinometer placed against the ulna measured the rotation angle relative to vertical, which is considered the clinical measurement of humeral torsion. Two ultrasound observers and two inclinometer observers were used to create three sets of original data, with each observer pair completing three repeated measurement trials.

Results. Humeral torsion averaged 33.1 (SD 2.5) degrees and 32.3 (SD 1.1) for the CT scan and ultrasound measurement techniques, respectively. However, some limbs showed considerable variation between the two techniques, especially in the presence of advanced osteoarthritic changes in the gleno-humeral joint (4 shoulders) and limb abnormalities associated with humeral fracture (1 shoulder). The absolute difference between the techniques averaged 5.0 (range, 0.4 to 19.1) degrees when all shoulder were considered, but dropped to 2.8 (SD 2.4) degrees when limbs with the above pathologies were excluded, resulting in good correlation between the two techniques (linear regression, R^2=0.7). Intraobserver standard deviation among the three trials for observer 1 and observer 2 measuring the CT scan images were both less than 1 degree and interobserver standard deviation averaged 2.5 degrees. Similarly, for the three pair of observers completing the ultrasound assessments, the intraobserver standard deviation averaged 0.353 (pair 1), 0.402 (pair 2), and 1.357 (pair 3) degrees, with an interobserver standard deviation average of 1.1 degrees over all nine observations per arm.

Conclusions. Although considerable bone pathology was noted in several of these cadaver shoulders obtained from elderly subjects, there was good agreement between the humeral torsion measurements acquired from the CT scans and ultrasonography. Visual identification of the bicipital groove and tuberosity was challenging using either method in patients with bony pathology associated with osteoarthritis or trauma, resulting in approximately 5 to 20 degrees difference in humeral torsion measurements from the CT and ultrasound techniques in those subjects. In such cases, taking care to select images from the CT scan that clearly define the bicipital groove may prove useful for reducing the deviation between the two techniques.

Acknowledgements: Bailey, Lane, PT; Shanley, Ellen, PhD, PT; Thigpen, Chuck, PhD, PT

Chemical and Biological Warfare Agent Interactions with Environmental Surfaces: Basic Science Experimental Studies of Adsorbed Protein Structure & Bioactivity

_Aby A. Thyparambil[*], Yang Wei[*] and Latour R.A.[*]
[*]Bioengineering Department of Clemson University, Clemson, S.C., U.S.A

Statement of Purpose: Protein toxins represent an important class of biological warfare agent, the release of which will contaminate environmental surfaces that they come in contact with, leading to serious health risks. A molecular level understanding of protein-surface interactions (PSI) is required to formulate effective and efficient decontamination strategies to neutralize threats that may arise due to protein-toxin adsorption. The objective of the current study was therefore to develop experimental methods that can be used to quantitatively characterize the adsorbed protein orientation and conformation, and their influence on adsorbed-state protein bioactivity under various conditions.

Materials and Methods

Toxin simulants: Hen egg white lysozyme (HEWL) and bovine pancreatic ribonuclease-A (RNAse) were dissolved in potassium phosphate buffer (PPB, pH 7.4).

Environmental surface simulants: Fused silica glass (GLASS), high-density polyethylene (HDPE) & poly(methyl-methacrylate) (PMMA).

Protein Adsorption: Proteins were adsorbed onto each adsorbent material from a series of protein concentrations (0.03 mg/mL – 1 mg/ml) for 2 hours, after which surfaces were diluted under running water and incubated at room temperature for 24 hours in pure PPB to equilibrate the adsorbed proteins.

Determination of Solution Structure, Surface Density and Secondary Structural Shifts of Adsorbed Proteins Using circular dichroism (CD) Spectroscopy: The structure of HEWL in solution, the amount of protein adsorbed on each surface, and the subsequent adsorption-induced conformational changes on these proteins due to adsorption on various material surfaces were determined using CD spectropolarimetry. The CD spectra (consisting of the ellipticity and absorbance values over wavelengths ranging from 190 nm to 300 nm) were obtained at room temperature using a Jasco J-810 spectropolarimeter. The solution structure of the proteins was determined in quartz cuvettes (Starna Cells) while the structure of the adsorbed proteins was determined using a custom-designed cuvette that was previously described.[1]

Bioactivity Assays for solution and adsorbed state of proteins: Turbidometric assay to monitor the enzymatic activity of HEWL were carried out in the custom-designed cuvette that was previously described.[1] Bioactive substrates were prepared in PPB to a final concentration of 60 mg/liter Micrococcus lysodeikticus (Sigma M3770) and the assays to determine the enzymatic bioactivity were done at pH 7.4 for a time period of 10 min at 450 nm. Similarly, turbidometric assay were done with 0.5 mg/mL RNA (Sigma, R6750) in PPB (pH 7.4) for over a time period of 10 min at 300 nm. Prior to assay, all the samples were incubated with the bioactive substrate at room temperature for one minute before the decrease in respective spectrometric absorbances were recorded.

In situ differential modifications of HEWL: Experimental data on the adsorbed conformation and orientation of HEWL on each surface were investigated using a series of amino-acid side-chain (arginine, carboxyl groups, tryptophan) modification assays combined with mass spectrometry. In this study, we employed a chemical strategy to first label the amino acids in the adsorbed protein in an irreversible manner, after which the adsorbed proteins are desorbed, enzymatically digested and analyzed by ultra-performance liquid chromatography (UPLC) interfaced to a hybrid quadrupole, orthogonal acceleration time-of-flight mass spectrometer (Q-ToF MS).

Results and Discussion.

Role of protein-protein interactions (PPI) on the adsorption responses of protein: Adsorption-induced protein unfolding and bioactivity is greatly influenced by the interplay of PSI, PPI and bulk solution concentration. (Figure 1) On each of these surfaces, the adsorption behavior was seen to be strongly material-surface-type dependent, with PPI playing a critical role in the adsorption response of the protein.

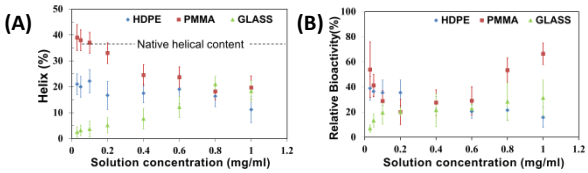

Figure 1: (A) Conformational shifts in adsorbed HEWL on different surfaces when adsorbed from varying solution concentrations as determined by CD. (B) Bioactivity of adsorbed HEWL on different surfaces when adsorbed from varying solution concentrations as determined by bioactivity assay. (n= 6, mean ± 95% CI).

Role of PSI on the adsorption responses of protein: In order to isolate surface-induced adsorption behavior from effects caused by PPI, adsorption conditions were established that minimized the influence of PPI on protein adsorption behavior. The conformation responses of HEWL under minimized PPI conditions (determined to be provided by 0.03 mg/ml bulk protein concentration) were found to be highly PSI-specific. The resulting conformational shifts in adsorbed proteins also lead to substantial decreases in its bioactivity. (Figure 2) Mass spectrometric analyses of the adsorbed HEWL on each of these surfaces have provided further insights into the tertiary and orientational state of the protein. (Figure 3)

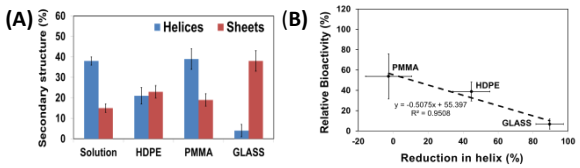

Figure 2: (A) Conformational shifts in adsorbed HEWL (adsorbed at 0.03 mg/mL) on three different surfaces (arranged in decreasing order of contact angle) as determined by CD. (B) Correlation between relative bioactivity of adsorbed HEWL and the loss in helix. (n = 6, mean ± 95% CI).

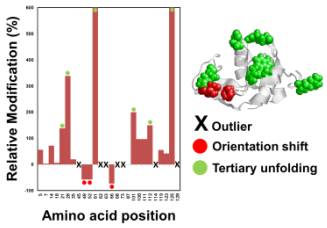

Figure 3: Determination of adsorbed structure by chemical labeling and mass spectrometry for HEWL adsorbed on GLASS.

Concluding Remarks. Protein adsorption behavior is shown to be highly protein-surface-system specific. The synergistic use of CD, bioactivity assays, and chemical labeling/mass spectrometry can provide molecular-level information on proteins adsorbed under minimized PPI conditions so as to gain a fundamental understanding of safe and effective means to design decontamination agents for biodefense applications.

Acknowledgement. This project received support from the Defense Threat Reduction Agency-Joint Science and Technology Office for Chemical and Biological Defense (Grant no. HDTRA1-10-1-0028).

References:

1. Sivaraman, B.; Fears, K. P.; Latour, R. A., Investigation of the Effects of Surface Chemistry and Solution Concentration on the Conformation of Adsorbed Proteins Using an Improved Circular Dichroism Method. *Langmuir* **2009,** 25, (5), 3050-3056

Antibacterial Coatings on Orthopedic Implants to Prevent Post-Operative Infections

Chengyi Tu and Alexey Vertegel
Department of Bioengineering, Clemson University, South Carolina, United States 29634

Introduction: Orthopedic implants associated infection rate is low but significant. Notably, bacteria growing within a biofilm on the surface of an implant are especially resistant to antibiotics and result in persistent infection and eventually cause implants failure. *Staphylococcus aureus* is a normal part of human skin flora and also a major pathogen involved in implants-associated infections. An easy and effective solution to this situation is to pre-coat the implants with lysostaphin, a glycylglycine endopeptidase which specifically cleaves the crosslinking pentaglycin bridges in the cell wall of *Staphylococcus aureus*. The result shows that lysostaphin coated hips implants were capable of inhibiting and killing *S.aureus in vitro* and may be promising way to prevent implants infections.

Methods: *Staphylococcus aureus* was and revived in tryptic soy broth and stored in 4℃ for antibacterial assay. Lysostaphin was labeled with Alex Fluor 594. Three different concentrations (0.05mg/ml, 0.1mg/ml and 0.2mg/ml) of lysostaphin solution were prepared in 3 ml PBS as coating solution. The titanium alloy hip implants were immersed in the solution and incubated in 37 ℃ for 1 hour and washed in 5 ml PBS 3 *5 min. Aliquots (200 ul) were taken before and after the coating to read the fluorescence(absorption at 590nm, emission at 610nm). The decrease in fluorescence is proportional to the drop of lysostaphin concentration in coating solution, so the amount of enzyme adsorbed to the implant can be calculated. For antibacterial assay, 3 ml of *S.aureus* suspension adjusted to approximately 5*10^8 CFU/ml was prepared in PBS and co-incubated with the coated implants in 37℃. Aliquots were taken at different time points and the optical density was read at 600nm with a plates-reader.

Result: The amount of lysostaphin adsorbed to the implant surface increases with concentration of the coating solution and reaches saturation at about 0.1mg/ml. And the coated implants showed effectively killed over 90% of *S.aureus* in PBS in as short as 3 hours.

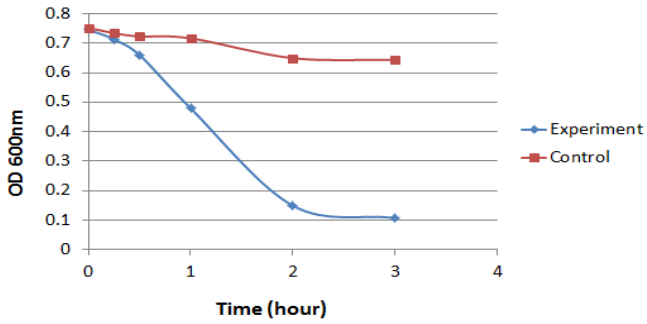

Fig 1 In vitro antibacterial assay with lysostaphin coated implants (blue) and plain implants as control (red).

Conclusion: Given the excellent in vitro activity of lysostaphin-coated implants against *S.aureus*, it might be an effective way to prevent infections after implants surgery. And the coating procedure is very easy and quick, taking no more than two hours, along with a relatively low cost.

Acknowledgement: Thanks to my advisor Dr Vertegel and Dr Melinda for providing the implants. Thanks to all my labmates.

Tension-Controlled Bioreactor for Soft Tissue Engineering Applications

James Turner, Benjamin Fleishman, Rachel Ostendorff, Jiro Nagatomi
Clemson University

Statement of Purpose: Our previous *in vitro* study demonstrated that when bladder smooth muscle cell-seeded collagen gels were exposed to sustained tension, the cells exhibited an elongated, spindle-like morphology and expression of phenotypic marker proteins α-SMA and SM22 was significantly greater than the free-floating group (Roby). However, to date, the exact magnitude of tension that triggered these responses in SMC and underlying mechanisms are not fully understood. The goal of the present study is to improve understanding of the relationship between bladder wall tissue tension and smooth muscle cell function. For this reason, we have developed an experimental setup which allows exposure of SMG in a three-dimensional collagen gel culture to controlled tension loading conditions that mimic the storage and voiding cycles of the normal bladder. The tension-controlled bioreactor may be used in bladder and other soft tissue engineering applications to facilitate cell growth and maintain phenotype.

Methods: The tension-controlled bioreactor contains two channels capable of linear stretch on a hydrogel construct with a stepper motor (Haydon Kerk Motion Solutions, Waterbury, CT) and load cell (LCL-113, Omega) on each end of both channels of the device. The stepper motor is controlled through a custom designed LabVIEW (National Instruments) program allowing for precise control of linear displacement, which simulates tension associated with bladder filling *in vivo*. The bioreactor is designed to operate in cell incubator conditions of 37°C and 5% CO_2 and device components can be sterilized by UV radiation. Bladder smooth muscle cells were isolated using methods developed in our lab and incorporated into the hybrid hydrogel construct. The hydrogel construct was created using a combination of modified Tetronic® T1107 acrylate compound (BASF Corporation), collagen type I, and hyaluronic acid. The T1107 compound is modified to crosslink using a photoinitiator compound (Irgacure, I-2959, BASF Corporation). Following exposure to controlled tension regimes, the cell-seeded hydrogels were fixed in paraformaldehyde at room temperature for 15 minutes, followed by quenching with 0.1 M glycine for 5 minutes. Permeabilization of the cellular membrane is performed using 0.1% Triton-X 100 (T9284, Sigma). Cells were exposed to the Rhodamine-Phalloidin solution (Invitrogen) for staining f-actin filaments followed by DAPI (Invitrogen) for cell nuclei at a 100X dilution in PBS according to protocol. The hydrogels were washed in PBS and images were taken using laser confocal microscopy (Nikon TI Eclipse) to analyze the cell morphology.

Results: Our custom LabVIEW program for the tension bioreactor uses a feedback loop mechanism that reads the force (converted into tension) value from the load cell while applying a linear displacement on the specimen to control the amount of stretch that matches the desired tension. The LabVIEW program is also capable of controlling the load rate and maximum tension, to mimic slow bladder filling and storage at sustained tension (Figure 1). Early work on the bioreactor show an elongated cell shape on rat bladder smooth muscle cells exposed to static tension (Figure 2) with a larger average aspect ratio than those not exposed to static tension (not pictured).

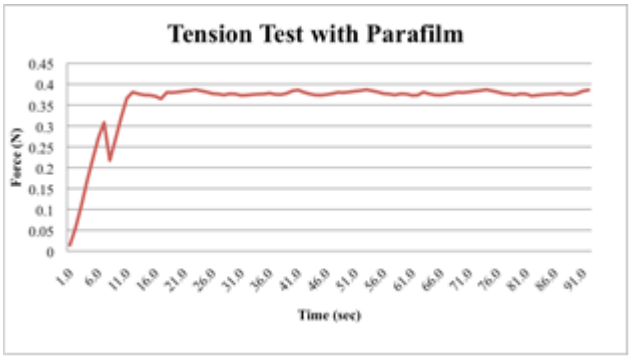

Figure 1. A proof of concept experiment conducted on parafilm shows the capabilities of the device to sustain a desired tension on the construct.

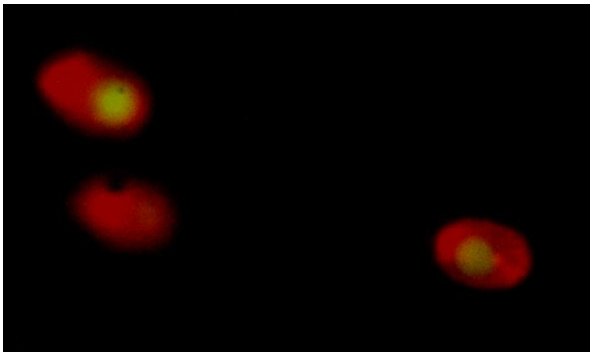

Figure 2. Morphology of rat bladder smooth muscle cells within the hydrogel construct after exposure to static tension at 2.5g of static tension

Conclusions: To date, the machine is calibrated to provide accurate linear displacement on a hydrogel sample and read voltage corresponding to force on the load cell. The novelty of the tension-controlled bioreactor device is the ability to subject 3D cell culture specimens to desired tension (N/cm) rather than stretches (% elongation) on elastomeric membranes. As shown in previous studies, bladder smooth muscle cells respond with a phenotypic shift to increased tension rather than length changes. Although the current usage lies in bladder smooth muscle cells in a hydrogel construct, the device contains the capabilities of being used in other soft tissue and hydrogel applications for linear cyclic or static tension loading.

References: Roby, T., Olsen, S. Nagatomi, J. Annals of Biomedical Engineering, Vol. 36, No. 10, October 2008 pp. 1744–1751

Effects of Polymeric Nanoparticle Surface Properties on Interaction with Brain Tumor Environment

Olga Uvarov[1], Thomas Willi[1], Laura Reese[1], Sam Pollard[1], Lauren O'Donnel[1], Devante Horne[1], Jhilmil Dhulekar[1], Bruce Frankel[2], Brandon Mattix[1], Frank Alexis[1]

[1]Clemson University, Dept. of Bioengineering, Clemson, SC.

[2]Medical University of South Carolina, Dept. of Neurosciences, Charleston, SC.

Statement of Purpose: The American Cancer Society predicts that in 2012 over 570,000 people will die due to cancer in the United States alone. Current cancer treatments include chemotherapy and radiotherapy, both possessing particular pros and cons in specific applications. One approach to improve the efficacy of cancer treatments is drug delivery to cancerous cells using nanocarriers. When injected into the body, the surface of the nanocarriers interacts with the biological environment, which controls the bioactivity of these drug delivery systems. However, there is a lack of understanding regarding how functional properties on the surface of nanocarriers control nanoparticle (NP) interactions with the ECM and cells. Nanomedicine for drug delivery is a promising area of research expected to improve cancer therapy by increasing drug dose, decreasing unintended drug side effects, controlling drug release, and targeting tumors.

Methods: As a proof-of-concept, we tested biocompatible and biodegradable poly(lactic acid) – poly(ethylene glycol) (PLA-PEG) NP's interactions with cellular uptake and drug delivery. Cellular internalization studies have been performed using two human brain cancer cell lines (U87 & U138) and four control cell lines (NCI-H460 human lung cancer cells, MCF-7 human breast cancer cells, HBMEC human brain micro-vascular endothelial cells, and HUVEC human umbilical vein endothelial cells). Additionally, qualitative verification of uptake was confirmed using confocal fluorescent microscopy. The effect of surface properties on NP drug delivery was analyzed using paclitaxel-loaded NPs, with studies analyzing the effects of surface properties, incubation time, and NP concentration on their drug delivery capabilities. Finally, Matrigel ECM solutions with varying amounts of collagen were used as a model ECM and used to determine the ability of NPs to cross an ECM membrane and deliver a drug payload.

Results: Cellular uptake results demonstrated that the internalization of NPs into cells varies between cell lines, with high uptake being noted in human brain cancer cells compared to non-cancerous human brain cells and other human cancer cell lines. Additionally, drug-loaded NPs are effective at inducing the desired toxic effects, with decreased viability occurring at concentrations as low as 0.0056 µg PTX (per well). Furthermore, it is noted that incubation time and time post-incubation are important factors for their use in drug delivery, as drugs are gradually released within the cell. Drug delivery across ECM studies were performed in order to model the ease with which NPs can diffuse through the extracellular matrix and deliver a desired payload to cells. Experiments were performed using matrigel as a model ECM and varying collagen content in order to determine the effect of collagen on the NP's motility, as collagen levels vary based on tissue type and grade of cancer. A NP's ability to diffuse through a tissue is essential for controlling its biodistribution

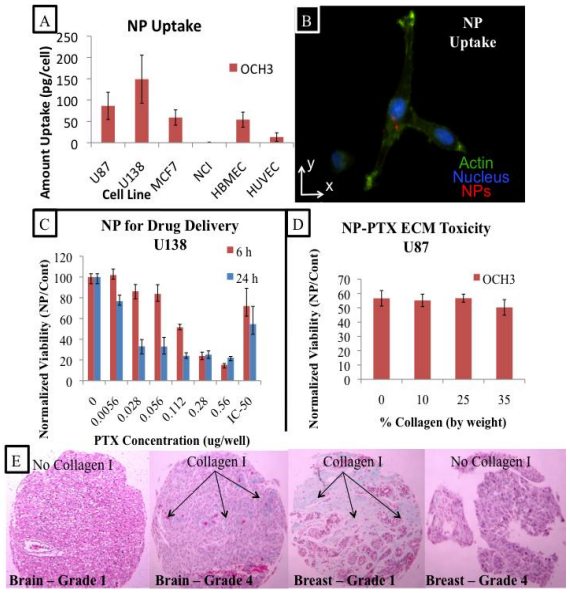

Fig 1. (A) NP Uptake was quantified and revealed that internalization of NPs into cells varied between cell lines. **(B)** To confirm that NPs were internalized, fluorescent confocal microscopy was performed using fluorescently labeled NPs **(C)** The ability of NPs to deliver drug was tested using U138 human brain cancer cells, with results showing that PTX-loaded NP could effectively deliver paclitaxel and induce desired toxic effects. **(D)** The ability of NPs to deliver drugs across an ECM was analyzed using U87 human brain cancer cells, revealing that NPs can effectively cross an ECM membrane and induce desired toxic effects regardless of ECM composition. **(E)** Collagen levels were varied for ECM toxicity studies because studies have shown that collagen levels vary between different tissues and grades of cancer.

Conclusions: Results for NP uptake and toxicity highlight the ability of these NPs to be used in drug delivery applications, confirming that NPs are internalized at different degrees in some cells and surface properties can be tuned for drug delivery applications. Understanding NP diffusion through ECM to deliver target payloads allows for proper dosing with different cancerous tissues, each containing varying amounts of collagen. These studies showed that multiple factors must be accounted for when developing a drug delivery system for a targeted approach, ultimately aiming to limit any adverse side effects related to use of the drug. Results suggest that one NP formulation is not suitable to treat all cancers and the surface properties must be addressed.

Nanomaterials for the Development of Rapid Immunoassays

Ryan Waddell[1], Vladimir Reukov[1], Chen-Chih Tsai[2], Konstantin Kornev[2], Alexey Vertegel[1]
[1]Department of Bioengineering, Clemson University, Clemson, SC 29634, United States,
[2]School of Materials Science and Engineering, Clemson University, Clemson, SC 29634, United States

Statement of Purpose: Currently, many over-the-counter diagnostic tests are based on an immunochromatography principle. For instance, human chorionic gonadotropin (hCG) is labeled with gold nanoparticles to detect pregnancy. In these tests, gold conjugates migrate along an immunochromatographic membrane [1]. This study will incorporate nanofiber yarns into an immunochromatographic assay. These yarns would allow the incorporation of immunochromatography into cheap, over-the-counter diagnostic tests, reducing the cost and time required for patient diagnosis. This will allow earlier treatment and decreased patient recovery time. These fibers would also benefit third world countries with limited availability of funds and medical care. The goal of this study is to demonstrate the viability bionanomaterials in immunochromatography assays.

Methods: Mouse anti-fluorescein isothiocyanate antibody (MaFITC) was labeled with gold nanoparticles via physical adsorption. Immunoassay fibers were produced by immobilizing antibody on nanofiber polymer yarns prepared by electrospinning. Bovine anti-Mouse IgG (BaM) was labeled by Alexa Fluor 488 to serve as a control line on the yarn, and MaFITC antibody was labeled with Alexa Fluor 594 to serve as the test line on the yarn. The labeled antibody was covalently cross-linked to the fiber surface by UV-sensitive Sulfo-NHS-LC-Diazirine cross-linker (Sigma). A mask placed over the yarn allowed localization of antibody immobilization by blocking UV exposure to the non-specific regions of the yarn. The yarn was then washed with 1% ethanolamine blocking solution to prevent non-specific binding of Au-MaFITC conjugates. The immunochromatographic assay was conducted by incubating the gold conjugates with the antigen, FITC labeled bovine serum albumin (FITC-BSA), for reaction and then wicking the nanoparticle conjugates along the yarn with immobilized antibody. The yarn was then flushed with PBS buffer to further migrate nanoparticles along the yarn.

Results: Fluorescence microscopy confirmed the localized immobilization of the antibodies. Results are shown below in *figure 1*. The immunochromatographic assay showed specific accumulation of gold conjugates at the site of antibody immobilization, as shown below in *figure 2*.

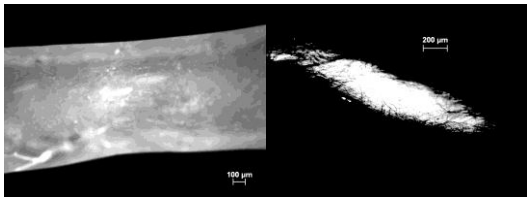

FIGURE 1. Fluorescence of the polymer yarn after antibody immobilization. The control region of Alexa Fluor 488 labeled bovine anti-mouse immobilization (right) and the test region of Alexa Fluor 594 labeled mouse anti-FITC antibody (left).

FIGURE 2. Polymer nanofiber yarn after performing immunoasasy. A) Non-specific accumulation of nanoparticles at end of yarn, B) nanoparticle accumulation at the MaFITC (test) line, and C) nanoparticle accumulation at the BaM (control) line.

Conclusions: The fluorescence images of the localized immobilization (*figure 1)* show that polymeric nanofiber yarns are a viable material for antibody immobilization, and the method for antibody immobilization allows for localized antibody immobilization on the yarns. The result of the immunoassay (*figure 2)* shows that gold conjugates not reacted with BSA-FITC can bind specifically to control (BaM) antibodies and test (MaFITC) lines when the antigen (BSA-FITC) is present. Further, the immunoassay shows that the 1% ethanolamine blocking method is a viable method for blocking non-specific binding of the gold conjugates to regions of the fiber where no antibody is immobilized. Future work will be done to clarify the immunoassay and eliminate excess nanoparticle accumulation at the ends of the yarns. The binding efficiency of the antibodies to the polymer fibers needs to be quantified, as well as the optimal quantity of gold-antibody conjugates loaded on the fiber. Future work will also focus on developing a biosensor for detection of specific conditions.

Acknowledgement: This research was funded by National Science Foundation, Grant No. EFRI 0937985.

References:

[1] Rojanathanes, R, et al. Taiwan J Obstet Gynecol 2008:147(3): 296-299.

Quantifying the Wear Rate of Enamel After Whitening Treatments

J. Willis[1], B. Schultz[1], R. Wilson[1], D. Dean[1], M. Kennedy[2]
[1]Department of Bioengineering, Clemson, SC 29634
[2]Department Materials Science and Engineering, Clemson, SC 29634

Statement of Purpose: Despite remarkable improvement in the nation's oral health over the years, record numbers of restorative procedures to repair damaged enamel and dentin are being performed. Unlike bone, dental mineralized tissue has no mechanism for repair after damage and synthetic materials are often used to repair the damage to the enamel by coating the enamel, filling holes in the enamel/dentin or replacing the entire tooth structure. In addition to procedures to repair damaged enamel, tooth whitening is becoming a common practice in American dental practices. These whiteners typically dilute solutions of carbamide peroxide gel (10%, 16%, 22%, etc.) that react with water to form hydrogen peroxide. The oxidizing agent then diffuses through the rod-like crystals of enamel to reach and remove any stains that may have accumulated in the dentin layer. To better understand the extent to which external factors may influence enamel degradation, many groups have focused developing characterization methods to determine both the wear mechanisms and rates of homogenous enamel. ***This study explores how the wear rate of enamel changes as a function of enamel whitening and the inclusion of restorative materials such as zirconia.***

Methods: After obtaining IBC approval (IBC #2012-07), teeth were obtained from the MUSC Dental School. Teeth were selected for analysis based on mottled amount and location. One half of the tooth was treated with Crest Whitestrip™, which contains 10% hydrogen peroxide. The teeth were then embedded in Caroplastic™ and cuts were made to exposed regions of parallel and perpendicular enamel-rod orientations. Roughness was measured using a white light interferometer and Dektak3. Next, nanoindentation is performed using a Hysitron™ quasi-static transducer with a modified Veeco Multimode™ AFM. The nanoindentation is performed in a straight line across the exposed enamel at a constant loading rate of 1200 µN/sec (9500 µN) with a 10 µm spacing between loads. Scratch testing was performed using a CETR with both zirconia and stainless steel pins.

Results: Teeth whitened with Crest Whitestrips™ were nanoindented across the DEJ. The data showed a distinct decline in hardness and elastic modulus across the junction (going from enamel into dentin). The hardness dropped from 2.86 ± 0.14 to 0.76 ± 0.06 and the modulus dropped from 46.79 ± 7.99 GPa to 5.64 ± 2.06 GPa from enamel to dentin. These values were similar to trends in Zimmerman[2] and Angker[3].

The wear rate in enamel was quantified for both a 440C stainless steel and zirconia counterface. The post-scratch roughness for the stainless steel ball was rougher than the zirconia, 114.77 ± 29.68 nm and 66.37 ± 14.99 nm respectively, but the post-scratch roughness for the zirconia scratch was rougher than the stainless steel scratch, 364.27 ± 54.45 nm and 308.59 ± 55.22 respectively. Figure 1 shows the depth profile for the zirconia and stainless steel scratches. The zirconia scratch has a depth of 20.3 µm and has a wear rate of 2.1×10^{-12} Pa^{-1} and the stainless steel scratch has a depth of 9.4 µm and has a wear rate of 6.2×10^{-13} Pa^{-1}. Similar test parameters shows that the coefficient of friction for the stainless steel ball bearing on the tooth is 0.45 while at the same test time, the zirconia ball bearing never reached steady state and was continuing to increase until the test ended at 0.8.

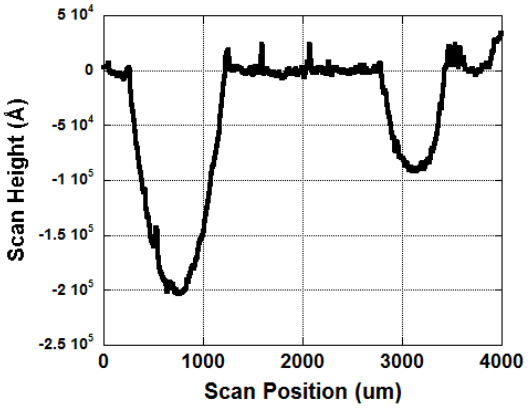

Figure 4-Comparison of enamel wear when sliding is caused by a zirconia (left) or stainless steel (right) counter surface.

Conclusions: Teeth treated with Crest Whitening strips showed hardness and modulus values that were similar to literature reports[2,3]. The wear rate of enamel was shown to be a function of the counter surface material, as well as the normal load and velocity. The lower relative wear rate of enamel with stainless steel found in this work is opposite of other groups.[4] Additional tests will be needed to elucidate the cause of these wear rate alterations.

References:

1. Garrido MA, Giraldez I, Ceballos L, del Rio MTG and Rodriguez J. Nanotribological behaviour of tooth enamel rod affected by bleaching treatment. Wear 2011;271(9-10):2334-9.

2. B. Zimmerman *et al.* J. Mechanical Behavious of Biomedical Materials. Alteration of dentin–enamel mechanical properties due to dental whitening treatments 3 (2010) 339- 346.

3. Angker, L., Swain, M.V., 2003. Micro°©mechanical characterizationof the properties of primary tooth dentine. J. Dent. 31, 261-267.

4. V. Preis *et al.* Dental Materials. Wear performance of substructure ceramics and veneering porcelins. 27 (2011) 796-804.

Acknowledgements: The authors gratefully acknowledge funding from the Clemson University Creative Inquiry program (1550364) and the Clemson University URGC.

Engineering Enzyme Mediate Release from Bioactive Hydrogel for Actuated Drug Delivery

A. Nolan Wilson[1,2] and Anthony Guiseppi-Elie[1,2,4,5,6,*]

[1]*Center for Bioelectronics, Biosensors and Biochips (C3B), Clemson University Advanced Materials Center 100 Technology Drive, Anderson, South Carolina 29625, USA*

[2]*Department of Chemical and Biomolecular Engineering,* [4]*Department of Bioengineering,* [5]*Department of Electrical and Computer Engineering, Clemson University, Clemson, South Carolina 29634, USA*

[6]*ABTECH Scientific, Inc., Biotechnology Research Park, 800 East Leigh Street, Richmond, Virginia 23219, USA.*

Introduction: Hydrogels have been extensively used as a biocompatible scaffold material for drug delivery, sensors, and regenerative medicine. The complexity of these systems has increased dramatically as the responsive nature of the polymers has been leveraged to produce systems which can sense and respond to the local environment. Functionalization of hydrogels with bio-specific moieties has conferred such properties as biomimicry, biocompatibility, and biomolecular recognition to these polymeric systems. To further the evolution of bioresponsive hydrogels, enzymatically actuated hydrogels are being explored as drug delivery platforms. One approach to creating such a system is to covalently link therapeutic molecules via protease cleavable peptides to the hydrogel. When the peptide-drug bond is cleaved by the protease, it releases the drug at a targeted location in metabolically regulated rates and doses. Here, two biomimetic poly(HEMA)-based bioresponsive hydrogel were synthesized and sensitivity to trypsin and chymotrypsin was conferred to the polymer via a acrylate-peptide conjugate. A surrogate drug molecule, p-nitroaniline, was released upon incubation in protease solutions. Release rates and release amounts were controlled by varying monomer composition and transport properties via cross-link density. The results subsequently analyzed using a tortuosity model.

Materials and Methods: A bioresponsive hydrogel based on 2-hydroxyethyl methacraylate (HEMA) was formulated, cast, and hydrated in TRIS buffer. The cross-link density was controlled (1-12 mol% tetraethyleneglycol diacrylate (TEGDA)) and the payload of cleavable peptide controlled by varying the mol% of 2-aminoethyl methacrylate (-NH_2) or by mol% of peptide-drug conjugate in the monomer cocktail. Kinetic assays and a Hill (Lineweaver-Burk) analysis was performed for protease triggered release monitored using UV-Vis Spectroscopy (Synergy MX). A Thiele modulus analysis established the diffusivity constants of the enzyme within the hydrogel and a mass balance established the efficiency of loading and release.

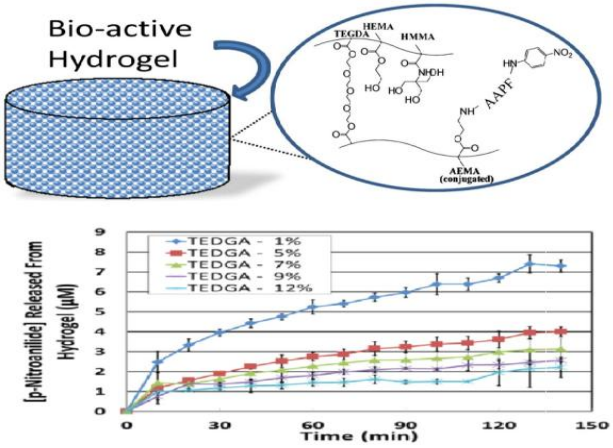

Results and Discussion: Controlled, triggered release of the chromophore, p-nitroaniline, from the hydrogel was shown to be dependent on cross-link density as well as on substrate loading. The ability to accurately control the amount as well as the rate of release of a drug is vitally important in maintaining the therapeutic window for drug efficacy. Here, it is demonstrated how varying the cross-link density to alter the effective diffusivity constants of the protease ($0.1\times10^{-8} \leq D_{eff} \leq 6.9\times10^{-8}$) and varying the conjugate concentration within the hydrogel can be used to achieve a controlled release rate and dose..

Conclusions: An integrated feedback control modulates protease activity to various levels is being experimentally explored *in vitro*. This system represents a viable method for more accurately controlling dosage levels of protease inhibitor drugs based on protease activity. It offers a model system from which further investigation into the dynamics of inhibitory bioresponsive hydrogels can be studied and developed for therapeutic applications.

Acknowledgements: US DoD PRMRP grant DAMD17-03-1-0172 and the C3B.

References: Wilson, A.N., R. Salas, and A. Guiseppi-Elie, Bioactive hydrogels demonstrate mediated release of a chromophore by chymotrypsin. Journal of Controlled Release, 2012. 160(1): p. 41-47

Tetronic® T904 as a Pharmaceutical Excipient for Enhanced Polyplex Gene Delivery

Jeremy Zhang, Sooneon Bae, Jeoung Soo Lee, Ken Webb
Clemson University

Statement of Purpose: Gene therapy offers the potential to stimulate tissue regeneration and treat disease through the overexpression or silencing of target genes. Nonviral vectors are generally safer, less immunogenic, and more suitable for scale-up/manufacturing than viral vectors; however, their transfection efficiency is much lower. The Pluronics® surfactants are a family of linear, amphiphilic triblock copolymers of poly(ethylene oxide) (PEO) and poly(propylene oxide) (PPO). Previous studies have demonstrated that several Pluronics® are capable of significantly increasing endocytosis, nuclear entry, and transcriptional activity of polyplex vectors. [1] In this study, we investigated the effects of a related family of a four-arm PEO/PPO amphiphilic block copolymers (Tetronics®/poloxamines) on the transfection efficiency of polyethlyenimine (PEI)-based polyplex vectors.

Materials and Methods: Plasmid DNA encoding the Monster Green Fluorescent Protein (pGFP, Promega) was used as a reporter gene for transfection efficiency. PEI/pGFP polyplexes at N:P ratios (PEI nitrogen : DNA phosphate) of 5:1 and 7.5:1 were prepared in water and incubated 30 minutes at 37 °C. To evaluate the effect of varying polymeric excipients, Pluronics® F127, F68, P123, P85 and Tetronics® T304, T904, T1107, and T90R4 at final concentrations of 5 µM were added to polyplex solutions immediately prior to transfection. After screening of varying polymeric excipients effect on transfection, we evaluated the dose-response of T904 (1 to 10 µM of final concentration) on the transfection efficiency of PEI/pGFP complexes at N/P ratios of 5/1 and 7.5/1. All transfections were performed in medium containing 5% serum in 12 well plates using 2 µg of pGFP per well on C6 glioma cells at 70% confluency. After addition of polyplexes with varying excipients, medium was exchanged at 24 hours and transfection efficiency was analyzed after an additional 24 hours. GFP expression was measured using fluorimetry and normalized to total protein determined by BCA assay (Pierce). The % cell transfection was also evaluated by flow cytometry. Cytotoxicity of varying polymeric excipients as well as varying concentrations of T904 was determined by MTT assay.

Results: Among the various polymer excipients tested, P123 and T904 both significantly increased GFP expression at 5 µM final concentration. When tested at varying concentrations, addition of T904 increased GFP expression in a dose-dependent manner (Figure 1). Although GFP expression was higher at 7.5:1

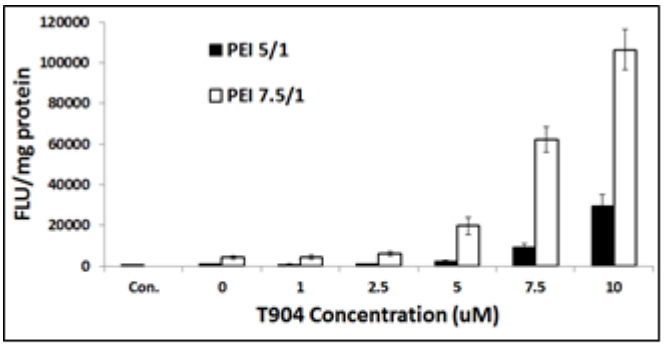

Figure 1. Transfection efficiency in C6 cells measured by fluorimetry with PEI/pGFP at N/P ratios of 5/1 and 7.5/1 and T904 excipient concentrations from 0-10 µM.

N:P ratio than that of 5:1 N/P ratio for all conditions, 10 µM T904 increased GFP expression approximately 25 times relative to PEI alone (0 T904) at both N:P ratios. Using flow cytometry, we found that PEI/pGFP at N/P ratio 7.5/1 without T904 transfected 12.3±2.9% cells. Addition of T904 at final concentrations of 5 and 10 µM resulted in 23.4±3.1% and 79.5±1.7% transfection, respectively. Overall, the magnitude of increase between 0 and 10 µM T904 measured by fluorimetry was larger than that measured by flow cytometry, suggesting that T904 increases both the number of transfected cells and the level of gene expression in each transfected cell. Average cell viability was 90% of non-transfected control after transfection with PEI/pGFP alone. When T904 was included, cell viabilities averaged 84, 82, and 76% at 5, 7.5, and 10 µM concentrations, respectively.

Conclusions: Addition of T904 offers a simple method to substantially increase the effectiveness of nonviral gene delivery. Hydrogels prepared from or including T904 may be particularly attractive candidates for localized gene delivery for tissue engineering. Current studies are exploring vector/copolymer uptake and intracellular trafficking to gain further insight into the underlying mechanism.

Acknowledgments: SC Center of Biomaterials for Tissue Regeneration and NIH grant #P20RR021949-03 and 8P20GM103444-04.

References: [1] Yang, Z. Bioconjugate Chem, 2008: 19 (1987-1994).

Unknown author

Sensors based upon surface-enhanced Raman spectroscopy (SERS) are attractive because they have narrow, vibrationally specific spectral peaks that can be excited using red and near-infrared light which avoids photobleaching, penetrates tissue, and reduces autofluorescence. Several groups have fabricated pH nanosensors by functionalizing silver or gold nanoparticle surfaces with an acidic molecule and measuring the ratio of protonated to deprotonated Raman bands. However, a limitation of these sensors is that macromolecules in biological systems can adsorb onto the nanoparticle surface and interfere with measurements. To overcome this interference, we encapsulated pH SERS sensors in a 30 nm thick silica layer with small pores which prevented BSA molecules from interacting with the pH-indicating 4-mercaptobenzoic acid (4-MBA) on the silver surfaces, but preserved the pH-sensitivity. Encapsulation also improved colloidal stability and sensor reliability. The noise level corresponded to less than 0.1 pH units from pH 3 to 6. The silica-encapsulated functionalized silver nanoparticles (Ag-MBA@SiO_2) were taken up by J774A.1 macrophage cells and measured a decrease in local pH during endocytosis. These nanosensors could be further introduced to detect endosomal pH variation during apoptosis.

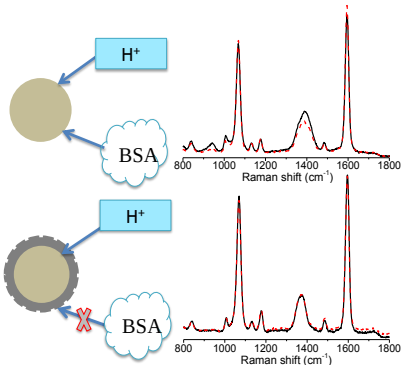

The addition of BSA influences the pH detection of Ag-MBA, while addition does not influence the pH detection for Ag-MBA@SiO_2.

Nanoparticle mediated targeted drug delivery for abdominal aortic aneurysm treatment

Unkown author

Introduction: Abdominal aortic aneurysm (AAA) is a degenerative disease of the artery characterized by severe protease-mediated degradation of extracellular matrix, especially elastin, causing dilatation of the aortic wall leading to rupture and death. However, systemic delivery of anti-aneurysm drugs like statins, β-blockers, ACE inhibitors, tetracyclines and anti-inflammatory agents have undesirable side-effects and reduced effectiveness in treating aneurysms. Our research goal is to develop a novel biodegradable nanoparticle system that recognizes the site of aneurysm; attaches and delivers the drug locally to the site of aneurysm. We tested luminal targeting of drug by the delivery of Polylactic acid (PLA) nanoparticles decorated with elastin-specific antibodies on to the surface of the particles. This minimally invasive technique can mitigate the undesirable effects of drugs and increase drug efficiency.

Materials and methods: For the preparation of nanoparticles, poly-lactic acid (PLA) and DSPE-PEG-Maleimide (4:1) were dissolved in acetone. A lipophilic near infra-red fluorescent tracer dye- 1,1′ -dioctadecyl-3,3,3′ ,3′ -tetramethylindotricarbocyanine iodide (DIR), was added to the polymer solution. The mixture was added drop-wise to water and sonicated for 1 hour in a bath sonicator. Simultaneously, rabbit-anti-rat-elastin/IgG antibodies were thiolated using Traut's Reagent. 4 µg of antibody was used for 1 mg of polymer. The thiolation was conducted for an hour at room temperature. The thiolated antibodies were added to the nanoparticles and left under mild shaking overnight at room temperature. Purified ENPs and IgGNPs (with control IgG antibody on the surface) were injected either systemically or locally in a clinically relevant rat model of AAA.

Results: ENPs were sized ~250nm by dynamic light scattering, atomic force microscopy and TEM. ~80% of the nanoparticles are metabolized by the liver within 24 hours. Five times greater total fluorescence was recorded in the AAA of the ENP group when compared to the IgGNP group after systemic delivery of particles (Fig 1). However, direct local perfusion of ENP into site of aneurysm shows ~20 fold greater attachment when compared to IgGNP controls. Furthermore, local ENP perfusion is ~21 times more efficient in binding to damaged elastin when compared to systemic ENP delivery (Fig 2).

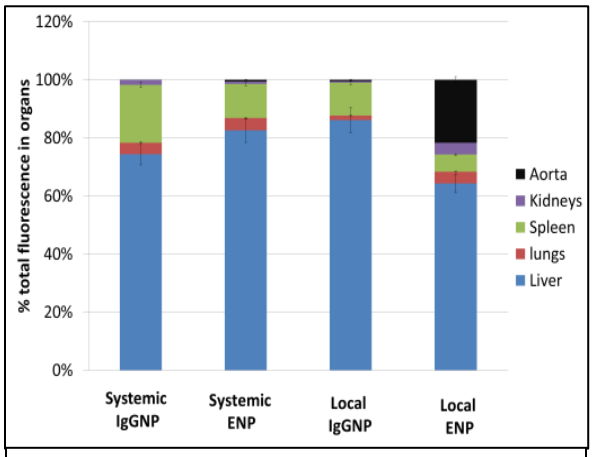

Fig 1: Bio-distribution of nanoparticles

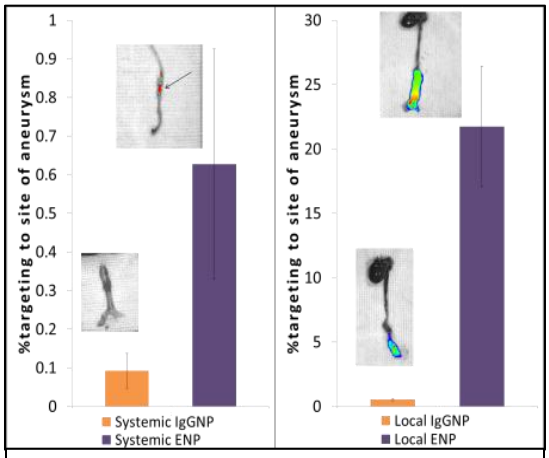

Fig 2: percentage targeting in systemic Vs local nanoparticle delivery local

Conclusion: In conclusion, anti-aneurysm drug/gene releasing nanoparticles, coated with elastin antibody could prove to be a useful minimally invasive targeted drug delivery option for aneurysm repair. These particles can either be delivered systemically (for early aneurysms) or locally (late-stage aneurysms) as an adjunct to endovascular aneurysm repair.

References: [1] Robert W Thompson, MD, Patrick J Geraghty, MD, Jason K Lee, MD, "Abdominal Aortic Aneurysms: Basic Mechanisms and Clinical Implications", Current problems in Surgery, Vol 39, Issue 2, February 2002, 110–230

Acknowledgements:

We thank the Society For Biomaterials for funding the SFB-CU Biomaterials Day 2012. We thank the SFB-Tissue Engineering SIG for funding two additional awards for graduate and undergraduate student presentations. We thank the Department of Bioengineering for additional financial support.

We thank keynote speakers and technology panel speakers to accept the invitation to participate to the SFB-CU Biomaterials Day 2012.

We thank all the graduate students involved in the preparation and organization of the SFB-CU Biomaterials Day. In particular, we thank Jonathan Shaul, Allison Kennamer, Brandon Mattix, Olsen Horton, and Harleigh Warner.

We thank Terry Bruce, JoAn Hudson, Tony Guiseppi-Elie, Martine Laberge, Duong Nguyen, Christian Kotanen, Maria Torres, Leigh Humphries, Jenny Bourne, and Sherri Morrison to assist the organization and CU tours.